LA-10006-PR
Progress Report

Los Alamos National Laboratory is operated by the University of California for the United States Department of Energy under contract W-7405-ENG-36.

Research and Development Related to the Nevada Nuclear Waste Storage Investigations

July 1—September 30, 1983

Los Alamos
Los Alamos National Laboratory
Los Alamos, New Mexico 87545

The four most recent reports in this series, unclassified, are LA-9577-PR, LA-9666-PR, LA-9793-PR, and LA-9846-PR.

This report was prepared by the Los Alamos National Laboratory as part of the Nevada Nuclear Waste Storage Investigations managed by the Nevada Operations Office of the US Department of Energy. Based upon their applicability to the investigations, some results from the Radionuclide Migration Project, managed by the Nevada Operations Office of the US Department of Energy, are included in this report.

Edited by Jody H. Heiken, INC Division

LA-10006-PR
Progress Report

UC-70
Issued: July 1984

Research and Development Related to the Nevada Nuclear Waste Storage Investigations

July 1—September 30, 1983

Compiled by

E. A. Bryant
D. T. Vaniman

Los Alamos National Laboratory
Los Alamos, New Mexico 87545

CONTENTS

RESEARCH AND DEVELOPMENT RELATED TO THE NEVADA NUCLEAR WASTE STORAGE INVESTIGATIONS

July 1--September 30, 1983

Compiled by

E. A. Bryant and D. T. Vaniman

Contributors

B. P. Bayhurst
D. L. Bish
J. D. Blacic
N. Bower
D. E. Broxton
F. M. Byers, Jr.
F. A. Caporuscio
B. A. Carlos
M. R. Cisneros
T. L. Cook
B. M. Crowe
D. B. Curtis
C. J. Duffy
R. R. Geoffrion
L. E. Hersman
S. W. Hodson
J. F. Kerrisk
S. D. Knight
F. O. Lawrence
S. S. Levy
A. J. Mitchell
E. J. Mroz
C. W. Myers
D. C. Nelson
T. W. Newton
H. E. Nuttall
A. E. Ogard
J. C. Rowley
D. M. Roy
V. L. Rundberg
R. S. Rundberg
K. W. Thomas
B. J. Travis
D. T. Vaniman
R. J. Vidale
P. L. Wanek
K. Wolfsberg
D. A. York

ABSTRACT

This report summarizes the contribution of the Los Alamos National Laboratory to the Nevada Nuclear Waste Storage Investigations for the fourth quarter of 1983.

EXECUTIVE SUMMARY

This report summarizes some of the technical contributions from the Los Alamos National Laboratory to the Nevada Nuclear Waste Storage Investigations (NNWSI) project managed by the Nevada Operations Office of the US Department of Energy (DOE) from July 1 through September 30, 1983. The report is not a detailed technical document but does indicate the status of many investigations being performed at Los Alamos.

Water Chemistry

Water from Well UE-25p#1 was pumped and sampled at two depths as the well was being drilled. Water from the lower depth (the Paleozoic) had more calcium, magnesium, sodium, potassium, chloride, sulfate, and especially bicarbonate than is normally found in Yucca Mountain groundwater. This water is being used as one of the bounds on groundwater compositional effects in some sorption experiments.

Additional samples of Well J-13 water from Yucca Mountain have been analyzed following contact with various tuffs. Using this type of experiment, it should be possible to estimate changes in groundwater that could occur in the groundwater along the flowpath to the accessible environment.

Sorption and Precipitation

Batch sorption measurements provide important information about the sorption properties of Yucca Mountain tuff. Samples from Drill Hole USW GU-3 from the unsaturated zone of Yucca Mountain are still being measured; these tuffs are similar to those in the proposed repository unit. Studies were also initiated with samples from Drill Hole USW G-4 from the tuff of Calico Hills, which underlies the proposed repository zone. As observed in previous reports, sorption ratios for strontium, cesium, barium, and europium on tuff samples that contain mainly glass and alkali feldspars in the absence of zeolites are low to moderate, whereas technetium does not sorb. The ratios measured for neptunium and plutonium were as expected for the tuffs studied.

Experiments have been undertaken to measure the effect of time on sorption ratios. The effects of short contact time for americium and plutonium were measured beginning at 1 hour and continuing to 6 weeks. The sorption ratios increase with time but change very little between 3 and 6

weeks. The effect of long contact time is being investigated for neptunium and technetium, both of which sorb very little, if at all, during contact times up to 6 weeks. Contact times of up to 15 months will be studied.

Because groundwater composition may vary between the repository and the accessible environment, the effects of different groundwater compositions on sorption ratios are being studied. Water from Well J-13 in Jackass Flats has been used in most batch sorption measurements to date. The sorption measurements now under way use water pumped from Well UE-25p#1. This water has a much higher concentration of magnesium, strontium, barium, calcium, sodium, and bicarbonate than does the J-13 water.

Although it is not specifically listed by the EPA in 40CFR191 as a primary hazardous waste element, thorium is important because ^{230}Th is the long-lived parent of ^{226}Ra, which is considered a hazardous nuclide. Because its parent is so long-lived (half-life = 7.5×10^4 year), radium may be transported in the form of the parent thorium isotope. It is important, therefore, to study the sorption behavior of thorium on tuff of Yucca Mountain. Preliminary studies of thorium solubility and sorption have been started. Thorium appears to have very low solubility at pH values between 7.5 and 8.5, and a tentative R_d of 580 mℓ/g has been measured at pH 6.8.

Oxygen up-take and aerobic growth rates were measured for several bacteria that are capable of using drilling detergent, which is currently employed at Yucca Mountain, as a nutrient source. The oxygen consumed and by-products formed by microbial growth could cause (1) a significant reduction in the Eh of the repository site and (2) changes in groundwater pH if sufficient quantities of nutrients were present in the repository.

The effects of drilling polymer, detergent, complexing agents, and bacteria on sorption are being investigated. The presence of drilling polymer in concentrations from 7.5×10^4 to 750 ppm appears to have little effect on the sorption of plutonium and only a very slight effect (at higher concentrations) on strontium sorption. The same is true for EDTA, a complexing agent present in the drilling polymer. The effects of detergent and of bacteria on sorption are still being evaluated.

Solubility Measurements and Calculations

The EQ3/6 chemical equilibrium computer program is being used for chemical modeling of waste elements, local minerals, and groundwater at Yucca

Mountain. A new version of EQ3/6, from Lawrence Livermore National Laboratory, includes additional thermodynamic data for uranium, plutonium, and fluorine.

A thermodynamic data file for americium is being compiled. The two primary uncertainties in the calculation of americium solubilities are (1) thermodynamic data for its complexes with carbonate, and (2) the identity and thermodynamic data of americium solids that will control solubility in Yucca Mountain water. Collecting and evaluating americium thermodynamic data will help reduce these uncertainties.

Solubility, a geochemical process that limits the transport of radionuclides, will exert its primary influence in the vicinity of the waste form, where it can limit the concentration of radionuclides dissolved in the water that leaves the repository. Initial radionuclide concentrations or release rates will act as source terms for the transport calculations.

Two simple solubility models have been developed to determine the importance of parameters such as waste-element solubility and water flow rate in controlling the release rates of radionuclides. The first is a saturation-limited dissolution model, in which the flow rate of water through the repository area is assumed to be saturated with each waste element. The second model is a diffusion-limited model in which waste-element saturation is assumed at the waste/water interface, and dissolution is limited by diffusion of the element into water flowing past the waste. Results of calculations for 10 elements indicate that for spent fuel as a waste form, plutonium, uranium, and tin would have solubility-limited dissolution rates for the gross solubility model, and that plutonium, uranium, tin, and americium would have solubility-limited dissolution rates for the diffusion-limited solubility model. With high-level waste, 99.5% of the uranium and plutonium would be removed during reprocessing. For this waste form, only tin would have a solubility-limited dissolution rate for the saturation-limited dissolution model, whereas tin, plutonium, and americium would have solubility-limited dissolution rates for the diffusion-limited solubility model.

These calculations will provide (1) information on the importance of solubility in controlling element concentrations in the vicinity of the repository and (2) estimates of the concentrations, which can be used as source terms for transport calculations.

Plutonium Chemistry in Near-Neutral Solutions

The rates of disproportionation and the first steps of polymerization of Pu(IV) have been studied in very dilute solutions ($\sim 10^{-6}$ M Pu and pH 3). The reaction rates were found to be predominantly second order in unreacted Pu(IV) and were studied as a function of pH in the range from 2.9 to 4.1.

Plutonium chemistry in water characteristic of Yucca Mountain is being studied to determine the effect of the carbonate content of the water on the solubility of hydrous PuO_2.

Tentative conclusions from these studies are that (1) many days are required for $PuO_2 \cdot nH_2O$, forming in bicarbonate solutions at room temperature, to reach centrifugable size ($>\sim 50$Å); (2) 0.01 M HCO_3^- enhances the solubility of $PuO_2 \cdot nH_2O$ by as much as a factor of 13 at pH 8; and (3) the use of $^{238}PuO_2$ appears to give solubilities that are too large near pH 8.

Hydrothermal Geochemistry

The stability of zeolites in Yucca Mountain is of particular importance to the NNWSI program because of the sorptive properties of these minerals. In the past, temperature has often been considered the principal control on zeolite stability. The rather complex distribution of zeolites has been taken as an indication that equilibrium modeling is of limited value for understanding the present mineral distribution: it is assumed that the mountain is mineralogically out of equilibrium.

To test these assumptions and to examine other parameters that might affect zeolite stability, a thermodynamic model has been constructed for analcime. When tested against field observations reported in the literature, the model agrees with the observed compositional variation in natural analcimes and is consistent with observed thermal stability. It explains the observed compositions of analcime in the Green River formation, Wyoming, as well as the reaction relationships observed there. It also accounts for the fact that analcime and quartz reactions to albite appear to have taken place at temperatures not exceeding 40 to 70°C.

The model suggests that, in addition to temperature, the following are important parameters that can affect the stability of analcime: the activity of H_2O, the activity of albite, the state-of-order of albite, the difference between lithostatic pressure and fluid pressure, and the activity of aqueous silica. When the model is applied to Yucca Mountain, it appears that the

concentration of aqueous silica, and therefore, the persistence of metastable silica phases is particularly important in determining the stability of analcime. The comparison of model predictions with field observation also suggests that there is considerable equilibration of analcime at temperatures well below 100°C.

Hot Spring Analogues

Nine hot spring occurances in felsic rock were examined to study the effect of heated groundwater on the physical and chemical properties of the rock. There have been changes that may prove important in the near-field environment of a radioactive waste repository: (1) the rocks that had been exposed to hot water over long periods of time were much more porous and friable than their unexposed counterparts; (2) silica sinter, smectite clays, and zeolites had precipitated near hot springs of neutral pH; and (3) highly acid systems had been formed by many of the springs at some stage in their evolution.

Further work to define the observed changes is recommended, including laboratory investigations of the effect of percolating heated groundwater on rock properties and additional studies of cores taken at depth in hot spring systems.

Flow and Transport Modeling

During this reporting period, the initial report on flow and transport in Yucca Mountain was completed. Water flow and radionuclide transport in partially saturated, fractured rock were computed for a range of rock property values.

Several conclusions can be drawn. (1) Significant fracture flow can occur, but only through large cracks (several 100 μm) or in a low-permeability, nearly saturated formation. (2) Diffusion, adsorption, and matrix suction have a profound effect on transport. For most of the important radionuclides, the time required for migration to the water table is large--at least 10 000 years. (3) Heat load in partially saturated tuff can result in a dried out, steam-filled region that extends several meters above and below a repository with recharge during the cool-down phase. These conclusions are based on various assumptions and simplifications made in this preliminary analysis.

Mineralogy-Petrology of Tuff

Existing quantitative x-ray diffraction data for five drill holes and new data for three drill holes were examined for mineralogic variability within the potential repository host rock in the lower part of the Topopah Spring Member, Paintbrush Tuff. The host rock includes the interval below the zone of abundant (>15%) lithophysal cavities in the upper part of the member and above the basal vitrophyre of the member. Aside from sparse phenocrysts (<2%) and fracture-filling minerals, over 98% of the mineralogic content of the host rock can be ascribed to quartz, cristobalite, and alkali feldspars. Within the exploration block, the abundances of these minerals vary by no more than 1 std dev from their average abundances, with the exception of a low cristobalite abundance in USW GU-3. North of the exploration block in Drill Hole Wash, the host rock mineralogy is much more variable.

The thickness, distribution, and mineralogic variability of the strata beneath the exploration block were also examined. Nine petrologic zones of different lithology are recognized. Internally, these zones are sufficiently similar to contrast markedly with neighboring petrologic zones. However, the thickness and mineralogy within individual zones can be quite variable. All or part of the nine petrologic zones intercede between the repository horizon and the static water level at the southern end of the exploration block. Only five of the petrologic zones appear above the water table in the northeast part of the exploration block.

Geopetal opal and zeolite deposits in zeolitized tuffs within the exploration block preserve evidence of structural tilting during and after zeolitization. Textural information, drill hole data, and geologic study results suggest that zeolitization at Yucca Mountain preceded the cessation of major tilting around or before 11.3 Myr. The alternative theory of major zeolitization during the Pleistocene is limited by the results from earlier studies of Nevada Test Site (NTS) geology.

Heating experiments at 20 to 300°C have been performed on sodium, calcium, and potassium cation-exchanged clinoptilolites. Contraction varied from 8.5 to 1.6% at 300°C, varying as Na >> Ca > K in clinoptilolite. In all cases, a reduction in b cell dimension is primarily responsible for contraction, indicating collapse of channels parallel to c and a.

Volcanism

Volcanism studies have included revisions of the Site Characterization Plan (SCP) and efforts focused on resolving identified areas of uncertainty in the SCP. Geochemical data reported previously show that the basalt cycles of the NTS region have varying degrees of enrichment in incompatible elements. Newly obtained data for the basalts of the silicic episodes show a moderate degree of incompatible element enrichment in comparison to that of the younger rift basalts. The younger rift basalts are unusual, therefore, only in the degree of trace-element enrichment. This suggests that the geochemical process or processes that enriched the basalts are not unique in time or space. These data and the low volumes and eruption rates of the younger rift basalts indicate that the occurrence of trace-element enriched basalts in the Yucca Mountain region is not a significant licensing issue. The question of past bimodal (basalt-rhyolite) volcanism in the Crater Flat area has been resolved. Drill Hole USW VH-2 penetrated a reversely magnetized, 11-Myr basalt flow that is correlative with exposed, reversely magnetized lavas at the south end of Crater Flat. These lavas, which underlie much of Crater Flat, are probably responsible for the previously discussed aeromagnetic anomalies of Crater Flat.

The potential hazards of future hydrovolcanic activities at Yucca Mountain have been identified as a new area of concern in volcanism studies. This is based on recently published geologic literature and present research concerning hydrovolcanic explosions and the physics of fuel-coolant explosions in simulated reactor accidents.

Major-element chemical analyses for basalts of NTS region have been entered into a data base management system on a VAX 11/780. This system provides quality assurance documentation and efficient access to basalt geochemical data. Geochemical procedures were developed and 70 basalt samples were analyzed for nickel, chromium, strontium, and rubidium.

Rock Physics

Long-term creep tests are still being run on zeolitized tuff of Calico Hills (from USW G-4) to study borehole sealing and other applications. Tests ranged from ~5 to 30 days. During these tests, steady-strain rates as low as 6×10^{-10}/second were measured. Several interesting and unexpected phenomena have been observed in these preliminary tests.

(1) Unexpectedly long pore saturation times range up to 5 weeks, and they appear to be the result of continued high porosity and low permeability, typically 25% and 0.5 μdarcy, respectively. This implies that equilibrium pore pressure of effective stress conditions in large volumes of tuff characterized by combined high porosity and low permeability will be difficult to achieve in any reasonable time. This problem could impact interpretation of the heated block or other in situ tests.

(2) In one experiment at low deviatoric stress, the sample slowly lengthened against the stress; apparently this is the result of slow swelling during rehydration of the sample. This implies that stresses at least as high as 20 MPa might result from changes in hydration of zeolitized tuff. These effects could occur in the altered vitrophyre layer below the candidate host rock zone in the Topopah Spring. The induced stresses could be either compressive or tensile, depending on whether the zeolites were hydrating or dehydrating, respectively, and therefore could alter rock mass permeability during postclosure or could cause other changes. Further research will determine if the net effect of the change would be favorable.

Shaft and Borehole Sealing

A variety of experiments have been completed on CL-40 CON-14 concrete; these experiments represent different end-member conditions that might arise in an unsaturated repository environment. Reactions have been accelerated by temperature to substitute for long exposure time. Those samples exposed to a vapor phase at 200°C showed similar but less intense alteration than those exposed to liquid. Calcium sulfate crystallized in the experiments, probably as a result of the breakdown of ettringite. Formation of smectite was observed as the solution became saturated. Extensive alteration of glass was also observed. Vitric tuff aggregates were much more reactive than densely welded tuff aggregate.

With completion of studies on CON-14, studies will concentrate on evaluating the behavior of the silica-rich cementitious mixture PSU/MRL #82-22 and tuff from the Topopah Spring Member. During experiments completed in this system, all solids that remained in the reaction products developed scale. However, the vapor-phase experiments showed less scale development than did similar experiments with CON-14. In experiments on powders, the scale appeared to act as a cement binding the powders into a rigid mass. The

observed pH values of 6.5 are considerably higher than those of 4.5 observed with CON-14. This value is also much closer to values observed in groundwaters in Yucca Mountain.

Exploratory Shaft

Design

The Title II design of the Exploratory Shaft (ES) surface and subsurface facilities was completed and approved by Los Alamos. The DOE has approved some, but not all of the design. There are several items that were not included in the Title II design because of incomplete criteria. The final criteria will not be available until after the ES Test Plan has been reviewed by the Technical Project Officers (TPOs), DOE, Waste Management Project Office (WMPO), and peers.

Test Plan

The Exploratory Shaft Test Plan (ESTP) activity continued at a very high level this quarter. The final draft of about 75% of the test plan was prepared; however, it was apparent at the end of the quarter that a complete draft of the ESTP could not be delivered to the WMPO by September 30, 1983, as originally planned. In the revised schedule, the ESTP will be delivered at the TPO meeting November 30-December 1, 1983.

Quality Assurance

Los Alamos

A records survey estimates about 10 000 records are on hand and approximately 2000 more documents are expected. A new procedure for NNWSI records has been drafted.

An archive for basalt rock samples for volcanism studies was established.

A review was completed of the Pennsylvania State University quality assurance program for geochemistry of shaft and borehole sealing materials.

USGS

Audits were performed at Fluke Manufacturing, Inc. and the Colorado Department of Agriculture to qualify calibration services supplied to the US Geological Survey (USGS).

Five USGS ES test plans were reviewed and comments were written. Surveillance activities were performed on the insertion of heat dissipation probes and psychrometers at Well UZ-1.

R. R. Geoffrion, P. L. Bussolini, and J. Willmon made work commitments for incomplete USGS quality assurance activities for the next 6 months.

I. INTRODUCTION

This report summarizes some of the technical contributions from the Los Alamos National Laboratory to the NNWSI project managed by the Nevada Operations Office of the US DOE during the period from July 1 through September 30, 1983. The report is not a detailed technical document but does indicate the status of many investigations being performed at Los Alamos.

II. WATER CHEMISTRY (A. E. Ogard)

Water from Well UE-25p#1 was pumped and sampled at two different total depths as the well was being drilled. The first sample (analysis given in Table I) was of water pumped from between the standing water level at 400-m (1300-ft) and 1198-m (3894-ft) depth. The well had been drilled somewhat deeper but was cemented below this level because the 1198-m depth was within the tertiary zone. The well was also sampled between 1298 and 1792 m (4218 to 4824 ft) to obtain water representative of the Paleozoic carbonate rocks (Table I). The composition of the latter sample is typical of water pumped from the carbonate aquifer at the NTS. Composition[1] of water pumped from a carbonate aquifer in Well C is also shown on Table I.

Water from the Paleozoic is being used at Los Alamos in sorption experiments because it is representative of one of the extreme compositions of water that might be encountered between the repository and the accessible environment. The main effect of this water should be noticed in changes in sorption and solubility of some of the actinides as a result of increased HCO_3^- content.

Crushed tuffs from drill cores have been used to pretreat waters for sorption experiments. In this series, cores from the following samples were used:

- GU-3-855 (263 m; 50 to 90% alkali feldspar, 5 to 10% cristobalite, 15 to 25% quartz, and 2 to 3% smectite)
- GU-3-916 (282 m; 60 to 70% alkali feldspar, 20 to 30% cristobalite)
- GU-3-1436 (442 m; 30 to 70% alkali feldspar, 20 to 60% glass and small amounts of cristobalite, quartz, and mica)
- GU-3-1531 (471 m; 20 to 60% alkali feldspar, 10 to 50% glass, 15 to 25% quartz, 3 to 9% cristobalite, and 3 to 7% mica)
- G-4-1502 (462 m; a highly zeolitized tuff from the Calico Hills).

TABLE I

COMPOSITION OF NTS WELL WATERS

Well No.	pH	Concentration (mg/ℓ) Ca	Mg	Na	K	Li	Fe	Mn	Al	Si
UE-25p#1 (400-1198 m)	6.7	30.6	8.4	82	6.5	0.276	0.103	0.028	0.135	20.1
UE-25p#1 (1298-1792 m)	6.7	87.8	31.9	171	13.4	0.720	0.045	0.103	0.139	17.4
Well C (carbonate aquifer)	7.3	75	30	125	14	0.32	<0.1	<0.1	0.1	30

	Concentration (mg/ℓ) F^-	Cl^-	SO_4^{2-}	HCO_3^-	NO_3^-	$CO_2(g)$
UE-25p#1 (400-1198 m)	2.8	12.6	40	323	2.4	--
UE-25p#1 (1298-1792 m)	3.5	37	129	698	<0.1	242
Well C (carbonate aquifer)	1.0	34	65	580	<0.1	—

Results for pretreated Well J-13 water, shown in Table II, are similar to results shown in the last quarterly report.[2] Eventually, this information will be used in equilibrium codes to model the change in composition of water along possible migration pathways through various tuff strata.

In addition, some of the tuffs were used in experiments with distilled water. During the first thousand years of a repository's life, the temperatures are expected to be above 100°C, and water contacting the tuff at the edge of this heated zone would be essentially distilled water. Results for 2-week contact periods are shown in Table III.

TABLE II

COMPOSITION OF GROUNDWATER PRETREATED WITH TUFF

Tuff	Concentration (mg/ℓ)										
	Ca	Mg	Na	K	Fe	Mn	Si	F^-	Cl^-	SO_4^{2-}	HCO_3^-
GU-3-855	9.3	2.14	37.5	7.8	0.010	0.014	24.1	3.5	8.7	21.0	120
916	9.0	2.15	37.8	9.4	0.018	0.003	23.4	2.7	8.8	20.1	131
1436	11.1	1.45	37.8	4.2	0.017	0.022	26.2	2.6	9.3	20.2	163
1531	13.4	0.87	36.9	2.4	<0.002	0.010	26.0	2.7	8.7	19.9	203
G-4-1502	0.24	0.016	50.9	3.1	0.016	0.001	23.0	2.6	8.4	19.8	127

Based on a comparison between the limited results in Table III and those in Table II, it appears that manganese, iron, and fluoride come from minerals in the tuff that dissolve rapidly, whereas the magnesium, calcium, and sodium came from minerals that are much slower to dissolve. Silicon's rate of change is between these two groups. There is insufficient data to discuss the impact of these differences in dissolution rates.

III. SORPTION AND PRECIPITATION

Geochemical and petrological data from the NNWSI geochemistry program have been entered into the DATATRIEVE data base management system on the VAX 11/780. Data have been entered under four domains: an x-ray diffraction (XRD) listing of mineral abundance data for core samples, sorption-desorption results and experimental conditions for batch sorption experiments, water-chemistry data, and field and petrological data for core samples used in the batch sorption studies. This work has several major goals: (1) multivariant statistical analyses of sorption, mineralogical, and water-chemistry data to identify the most important parameter correlations and (2) formatting of data through search and sorting routines to include in reports and in a preferred data set for Sandia National Laboratories to use in studies of performance assessment. The existing statistical codes have been examined; those that were chosen are best suited to run analyses of data distribution, preferred statistical descriptors, and multivariate analyses of all data entered into the data base. The first data run will use the SAS and ARTHUR codes.

TABLE III

COMPOSITION OF DISTILLED WATER PRETREATED WITH TUFF

Tuff	Concentration (mg/ℓ)										
	Ca	Mg	Na	K	Fe	Mn	Si	F^-	Cl^-	SO_4^{2-}	HCO_3^-
GU-3-1436	0.85	0.12	2.5	0.50	0.000	0.006	3.0	2.7	1.1	--	8.8
GU-3-1531	0.66	0.035	6.7	0.73	0.049	0.019	12.5	1.9	1.0	--	10.6

A. Batch Sorption Experiments of Sorption and Precipitation (B. P. Bayhurst, S. D. Knight, F. O. Lawrence, M. R. Cisneros, and K. W. Thomas)

The investigation of the sorptive behavior of Yucca Mountain tuffs continued. Sorption ratios for tuff sample GU-3-1203* (~45% alkali feldspar, ~40% glass, no zeolites; from the Topopah Spring vitrophyre) were measured for strontium, cesium, barium, europium, and technetium. The behavior of plutonium and neptunium on tuffs USW GU-3-916 and USW G-4-1502 was also investigated. Sample USW GU-3-916 is from the Topopah Spring unit and consists of 60 to 70% alkali feldspar and 25 to 30% cristobalite. Sample USW G-4-1502 is a highly zeolitized tuff from the Calico Hills unit. The XRD analysis of this tuff is not yet available. Table IV lists the sorption ratios measured this quarter.

The sorption ratios reported for strontium, cesium, barium, europium, and technetium on GU-3-1203 were in the expected range, based on previous measurements.[3-6] That is, sorption ratios for the first four elements on tuff samples containing mainly glass and alkali feldspars in the absence of zeolites are low to intermediate in value, and technetium does not sorb. Likewise, the sorption values reported for neptunium and plutonium on the low-glass tuff USW GU-3-916 and the highly zeolitized tuff USW G-4-1502 lie in the same ranges as previous measurements.[3-6] Neptunium ratios are less than 10 and plutonium ratios range from ~50 to several hundred.

Although thorium is not specifically listed by the US Environmental Protection Agency (EPA) in 40CFR191 as a primary hazardous waste element, the sorption of thorium is important because ^{230}Th is the long-lived parent of

*Identified in previous quarterly[2] as GU-3-1227 or GU-3-vitrophyre.

TABLE IV

BATCH SORPTION RATIOS

Core[a]	Element	Tracer pH[b]	Tracer[c] Concentration of the Elements (M)	Sorption Ratio[d] (mℓ/g)			Desorption Ratio[d] (mℓ/g)		
				pH[e]	Experimental	Average[f]	pH[e]	Experimental	Average[f]
GU-3-1203[g]	Sr	8.60	1×10^{-6}	8.56	43	42(1)	8.45	48	47(1)
				8.52	42		8.47	46	
	Cs	8.60	4×10^{-9}	8.56	380	350(30)	8.45	450	340(10)
				8.52	330		8.47	330	
	Ba	8.60	4×10^{-8}	8.56	0.02	640(40)	8.45	750	720(30)
				8.52	600		8.47	700	
	Eu	8.60	9×10^{-8}	8.56	190	190(2)	8.45	610	650(50)
				8.52	192		8.47	700	
	Tc	8.60	1×10^{-11}	8.56	0.02	0	Not Applicable		
				8.52	-0.03				
GU-3-916	Np	NA[h]	6×10^{-11}	8.8	4.8	4.9(0.1)	In Progress		
				8.7	4.9				
	Pu	8.4	1×10^{-7}	8.7	270	240(25)	In Progress		
				8.7	220				

TABLE IV (cont)

Core[a]	Element	Tracer pH[b]	Tracer[c] Concentration of the Elements (M)	Sorption Ratio[d] (mℓ/g) pH[e]	Sorption Ratio[d] (mℓ/g) Experimental	Sorption Ratio[d] (mℓ/g) Average[f]	Desorption Ratio[d] (mℓ/g) pH[e]	Desorption Ratio[d] (mℓ/g) Experimental	Desorption Ratio[d] (mℓ/g) Average[f]
	Tc			In Progress					
GU-4-1502	Np	8.7	1×10^{-10}	8.3	4.6	4.0(0.5)		In Progress	
				8.3	3.5				
	Pu	8.7	2×10^{-7}	8.7	53	57(3)		In Progress	
				8.7	60				
	Tc			In Progress					

[a]All crushed rock fractions were 75- to 500-μm particle size.

[b]pH of tracer feed solution before contact with the crushed rock.

[c]Contact times for sorption and desorption were 6 weeks.

[d]pH values measured after separation from the rock.

[e]Numbers in parentheses are standard deviations of the means.

[f]In earlier reports, this core was mistakenly identified as GU-3-1227.

[g]Not measured because of a lack of sufficient feed solution.

^{226}Ra, which is considered a hazardous nuclide. Because its parent is so long-lived (half-life = 7.5×10^4 year), radium may be transported in the form of the parent thorium isotope. It is important, therefore, to characterize the sorption properties of thorium as well as radium.

Studies conducted this quarter have shown that thorium will not go into solution to any extent in Well J-13 groundwater at a thorium concentration of 5×10^{-6} M and at final pH values between ~7.5 and ~8.5. The tracer used for these studies is the alpha emitter ^{230}Th, which is commercially available in 1 M nitric acid solution. At pH <7.5, the thorium tracer solution can be filtered through 0.05-μm Nuclepore membranes with a 68% recovery of the tracer. Above pH 8.3, thorium solubility also increases. At pH 8.3, 12% of the tracer was recovered after filtering, and at pH 8.6, 21% was recovered. In these experiments, 50 mℓ of tracer (in 1 M HNO_3) was added to 20 mℓ of J-13 groundwater (pH 7.6), which results in a solution of pH 3. The pH was adjusted using dilute NH_4OH, and the samples were shaken for 4 days before being filtered. The pH values increased 1 to 2 pH units during the shaking period.

One preliminary sorption measurement for thorium has been made. The thorium tracer solution was prepared as above; the initial pH was 2.9, and no further pH adjustment was made. The tuff studied was G-1-1292, a high-glass tuff (80 to 90%) from the Topopah Spring unit. Contact time was 11 days and the final pH measured 6.8. An R_d of ~580 mℓ/g was calculated.

Future thorium sorption measurements will not be made in the pH range of 7.5 to 8.5, our normal sorption range, because of the very low solubility of thorium at this pH. Because the pH of Yucca Mountain groundwater is typically less than 7.5 (Ref. 1), future thorium sorption experiments will be performed in a controlled-atmosphere box in which the CO_2 content will be regulated to maintain a constant groundwater pH of approximately 7. This method of controlling the pH is preferred to neutralizing because it eliminates the possibility of locally, very basic (albeit temporary) regions being created in the groundwater during neutralization. These highly basic regions may cause unwanted behavior in the tracer, such as polymerization or precipitation.

B. Long-Term Sorption Experiments on Technetium and Neptunium (S. D. Knight, F. O. Lawrence, M. R. Cisneros, and K. W. Thomas)

Sorption ratios for technetium on tuff samples studied to date are zero or nearly zero at contact times of 3 to 6 weeks.[3,5] Neptunium sorption ratios are greater than zero but typically less than 10 (Refs. 2, 3, and 5). Long-term experiments have been undertaken to determine if the measured sorption ratios for these two elements increase or, in the case of neptunium, change over periods of time longer than 6 weeks.

Three tuff samples are being studied. Contact times are scheduled for 6 weeks and 3, 6, 9, 12, and 15 months. Samples USW GU-3-916 and G-4-1502 are described above. Sample USW GU-3-1301 is a nonwelded, ~40% glass, ~35% alkali feldspar tuff from the Topopah Spring unit. The 6-week data for neptunium are given in Table IV for GU-3-916 and G-4-1502. The data for GU-3-1301 and the technetium data will be reported in the next quarterly. No observations can be made at this point other than that the neptunium 6-week sorption ratios are in the expected range for Yucca Mountain tuff.

C. Short-Term Sorption Experiments on Americium and Plutonium (F. O. Lawrence, M. R. Cisneros, and K. W. Thomas)

Short-term (beginning with 1-hour contact time) batch sorption experiments were performed with americium and plutonium on tuff sample G-4-1502, a nonwelded, highly zeolitized tuff from the Calico Hills unit of Yucca Mountain strata. The purpose of this study was to measure time-dependent effects on sorption ratios for comparison with flowing column experiments. Contact time in flowing column studies is much less than the usual 6-week time used for batch sorption measurements. Short-contact-time batch data are necessary for comparison of the two methods.

Sorption contact times ranged from 1 hour to 6 weeks. Table V gives the measured sorption ratios. It appears that the americium sorption ratios peak at 1 week, whereas the plutonium ratios do not change between 2 days and 3 weeks. For contact times on the order of hours to 1 day, the americium ratios steadily climb; however, over the same period, the plutonium ratios increase very little (Table VI).

These short-term experiments have demonstrated that, on the order of 1 hour to 1 day, the measured sorption ratios for americium increase by over a factor of 2, which indicates that kinetics or some phenomenon affecting

TABLE V

AMERICIUM AND PLUTONIUM SHORT-TERM SORPTION RATIOS ON USW G-4-1502 CRUSHED ROCK[a]

Sorption Time	Am[b] pH Values		Am[b] R_d (mℓ/g)		Pu[c] pH Values		Pu[c] R_d (mℓ/g)	
	Feed[d]	Sample	Individual	Average[e]	Feed[d]	Sample	Individual	Average[e]
1 hour	8.5	8.3	470	490(20)	8.4	8.4	19	19(1)
		8.3	510			8.2	20	
4 hours	8.5	8.4	720	715(5)	8.4	8.2	24	22(1.2)
		8.4	710			8.1	21	
1 day	8.5	8.3	1000	1100(60)	8.4	8.3	26	27(1)
		8.4	1200			8.3	28	
2 days	8.5	8.4	1200	1200(5)	8.4	8.3	36	34(2.3)
		8.4	1200			8.3	31	
3 days	8.5	8.3	1500	1450(50)	8.4	8.4	31	34(2.9)
		8.3	1400			8.4	38	

TABLE V (cont)

Sorption Time	Am[b] pH Values Feed[d]	Am[b] pH Values Sample	Am[b] R_d (mℓ/g) Individual	Am[b] R_d (mℓ/g) Average[e]	Pu[c] pH Values Feed[d]	Pu[c] pH Values Sample	Pu[c] R_d (mℓ/g) Individual	Pu[c] R_d (mℓ/g) Average[e]
1 week	8.5	8.5	1800	1900(20)	8.4	8.3	36	36(1)
		8.4	2000			8.3	37	
3 weeks	8.5	8.5	1600	1550(10)	8.4	8.5	34	34(1)
		8.5	1500			8.5	34	
6 weeks	8.5	8.7	1400	1400(5)	8.4	8.6	44	43(1)
		8.7	1400			8.6	43	

[a]The rock particle size was 75 to 500 μm.

[b]Americium concentration was 1.3×10^{-8} M.

[c]Plutontium concentration was 3.1×10^{-8} M.

[d]Aliquots of the same americium or plutonium feed solutions were used for all these experiments.

[e]The values in parentheses are the standard deviation of the means.

TABLE VI

THE 3- AND 6-WEEK SORPTION MEASUREMENTS FOR PLUTONIUM AND AMERICIUM[a]

Core	Core Sorption[c] Category	Sorption Time (Weeks)	Pu[b] R_d (mℓ/g)	Pu[b] 6-week R_d / 3-week R_d	Am R_d (mℓ/g)	Am 6-week R_d / 3-week R_d
JA-37	Devitrified, smectite	3	*300	1.63	18 000	2.06
		6	*490		37 000	
YM-22	Devitrified	3	37	1.73	1500	0.73
		6	64		1100	
YM-38	Zeolitized	3	58	2.07	6100	0.85
		6	120		5200	
YM-49	Zeolite and Glass	3	140	1.29	2900	0.97
		6	*180		2800	
YM-54	Devitrified	3	52	1.56	150	1.07
		6	81		160	
G-1-1292	Glass	3	*160	3.31	Not Measured	
		6	*530			
G-1-1883	Devitrified	3	*51	1.41	4200	1.07
		6	*72		4500	
G-4-1502[d]	Zeolitized[e]	3	34(1)[f]	1.26	1550(10)[f]	0.90
		6	43(1)[f]		1400(5)	

[a]Reference 3, Appendix A.

[b]The asterisk indicates values from nonduplicate samples on the same type of rock; otherwise, the results are from single measurements.

[c]Reference 3, Appendix B.

[d]This work.

[e]Preliminary analysis.

[f]Duplicate samples; parentheses represent standard deviations of the means.

kinetics plays an important role. The sorption ratio for plutonium, on the other hand, changed only by a factor of 1.4 for this time period and only by approximately a factor of 2 from 1 hour to 6 weeks.

D. Effect of Groundwater Composition on the Sorptive Properties of Tuff (S. D. Knight and K. W. Thomas)

Because groundwater composition may vary between the repository and the accessible environment, studies are being carried out to determine what effect several different groundwater compositions have on the measured R_d values. Most previous sorption experiments were performed using groundwater from Well J-13, located in Jackass Flats. The water was pretreated by contact for several weeks with samples of the crushed tuff of interest and then was used with fresh tuff samples for the R_d measurements. Table VII lists the composition of J-13 well water before contact with tuff.[3] Previous reports[2,3] discuss changes observed in the J-13 water composition after contact with a variety of tuff samples. Similar experiments are now under way using a second groundwater.

The water P-1, pumped from Well UE-25p#1, is now being studied; its composition is given in Table I. This water was selected for study because of its relatively high magnesium, strontium, barium, calcium, and sodium content compared to that of Well J-13 water. Sorption measurements are in progress for ^{85}Sr, ^{137}Cs, ^{133}Ba, and ^{152}Eu on tuff samples GU-3-1301, a nonzeolitized tuff from the Topopah Spring unit, and G-1-2233, a zeolitized tuff from the Bullfrog unit.

Future investigations will concentrate on additional elements, a tuff sample from the Calico Hills unit, and a third water composition. Comparisons will be made against the R_d values obtained for J-13 water and samples of the same tuffs.

E. Microbiological Activity at Yucca Mountain (L. E. Hersman, F. O. Lawrence, S. D. Knight, M. R. Cisneros, and K. W. Thomas)

The organisms that were first isolated on detergent or drilling polymer media used at Yucca Mountain are still being studied. The growth characteristics of such organisms are important because a growing microbial population can result in a change in soil pH and Eh, thereby possibly affecting radionuclide movement. It is further suspected that soil microorganisms provide

TABLE VII

COMPOSITION OF WELL J-13 GROUNDWATER[a]

Element	Concentration[b] (mg/ℓ)
Magnesium	2.17 (0.22)
Manganese	0.16 (0.02)
Silicon	30.7 (2.3)
Iron	0.001 (0.020)
Strontium	0.09 (0.06)
Barium	0.021 (0.014)
Vanadium	0.023 (0.016)
Titanium	0.000 (0.013)
Calcium	12.2 (1.2)
Lithium	0.16 (0.16)
Potassium	6.8 (2.0)
Aluminum	0.003 (0.011)
Sodium	51.7 (3.5)

[a]From Ref. 3.

[b]Mean of seven measurements made over a 6-month period. Values in parentheses are the standard deviations of the means.

chelating agents that may also affect the behavior of radionuclides through complexation or precipitation mechanisms. The organisms studied were characterized in an earlier progress report[6] and are referred to in this report by species number.

Aerobic growth rates of species Nos. 1, 5, 6, and 8 have been determined photometrically, and oxygen consumption rates of all but species No. 6 have been analyzed. These species were all originally grown on detergent medium.[6] For the photometric analysis, 3 mℓ of 3-day-old cultures and 25 mℓ of fresh detergent medium were placed in 300-mℓ side-arm flasks. The flasks were placed in a bench-top shaker (100 rpm) and incubated at room temperature. Using a Klett-Summerson photometer, unscattered, transmitted light was measured every 24 hours for 1 week. An earlier report[2] describes the method

used to determine oxygen consumption rates. Preliminary data suggest that organism Nos. 1, 5, and 8 grew well in detergent medium. In addition, these results further illustrate that many microbial species can use detergent or drilling fluid as an energy source.

Several experiments have been initiated to determine the effect of drilling polymer, detergent, and bacteria on the sorptive properties of tuff. The first series of studies were conducted with drilling polymer alone to determine if its presence affects sorption (perhaps because of the small concentration of EDTA it contains[2]). The second series contained EDTA alone, and the third used detergent alone. Bacteria have been introduced into two additional tuff experiments. One experiment contains bacteria in the presence of detergent and polymer media, and the second involves bacteria suspended only in water.

The tuff used in these experiments is G-4-1502, a highly zeolitized tuff from the Calico Hills. The elements currently being studied are strontium and plutonium. Standard procedures are followed in pretreating the crushed tuff and Well J-13 groundwater and in performing the sorption measurements. For samples where sterility is required, the tuff, water, filters, containers, and other equipment used in the procedures are autoclaved for 15 minutes at 121°C and 15 lbs pressure; sterile handling techniques are used in preparing the samples. The tracer solutions are not autoclaved but are prepared with sterile water. Each experiment has a sterile and a nonsterile control that do not contain any polymer, EDTA, detergent, or added bacteria. The nonsterile control, which is simply a standard sorption experiment, serves as a direct comparison point for the sterile experiments. The sterile control shows the effect of the sterilization process on the measured sorption ratios and is the comparison point for the substance-added experiments.

Results from the polymer-added experiment are given in Table VIII. In this experiment, 1 mℓ of 1.0, 10^{-2}, 10^{-4}, or 10^{-6} dilutions of polymer growth medium[6] was added to 19 mℓ of sterile, pretreated J-13 water that contained the ^{239}Pu and ^{85}Sr tracers and 1 g of pretreated crushed tuff. Contact time was 3 weeks, and sterile and nonsterile controls were used. All measurements were made in duplicate.

The most noticeable result was the difference between the sterile and nonsterile controls for plutonium. The strontium sorption ratios in both

TABLE VIII

SORPTION RATIOS FOR PLUTONIUM AND STRONTIUM IN THE PRESENCE OF DRILLING POLYMER ON TUFF SAMPLE G-4-1502[a]

Drilling Polymer Concentration (ppm)	Environment	Plutonium R_d (mℓ/g) Measured Ratio at (pH)		Plutonium R_d (mℓ/g) Average[b]	Strontium R_d (mℓ/g) Measured Ratio at (pH)		Strontium R_d (mℓ/g) Average[b]
0	Nonsterile	80 (8.29)	100 (8.33)	90(11)	>80 000 (8.29)	>80 000 (8.33)	>80 000
0	Sterile	30 (8.34)	30 (8.32)	30(1)	>80 000 (8.34)	>80 000 (8.32)	>80 000
750	Sterile	32 (8.33)	31 (8.35)	31(1)	16 500 (8.35)	19 500 (8.33)	18 000(1500)
7.5	Sterile	34 (8.35)	34 (8.33)	34(1)	>80 000 (8.35)	>80 000 (8.33)	>80 000
7.5×10^{-2}	Sterile	39 (8.37)	36 (8.38)	37(1)	>80 000 (8.37)	>80 000 (8.38)	>80 000
7.5×10^{-4}	Sterile	35 (8.39)	33 (8.40)	34(1)	>80 000 (8.39)	>80 000 (8.40)	>80 000

[a]Crushed tuff was 75 to 500 μm. Sorption time was 3 weeks. Concentration of plutonium was 1.5×10^{-6} M, and strontium was 5×10^{-7} M.

[b]Numbers in parentheses are standard deviations of the means.

cases were so large that only lower limits to the R_d are reported. The sorption ratio for the nonsterile plutonium control was 90, compared to 30 for the sterile control. Autoclaving may increase the amount of plutonium that stays in solution by removing bacteria that are naturally present in sorption experiments or by altering the morphology of the crushed rock.

Autoclaved crushed-tuff samples have been submitted for XRD analysis to determine if gross changes have occurred in mineral composition. If, however, only the very surface of the tuff has been altered, such as by slight annealing, this would not be seen by x-ray analysis. Plans are being made to sterilize the tuff with gamma radiation and to compare those R_d results with autoclaved tuff data.

A routine streak plate isolation test has demonstrated that several species of bacteria were present in the nonsterile control, whereas no bacterial contaminants were present in any of the autoclaved samples. Bacteria often serve as a surface to which metals attach. Because bacteria can be removed from solution by centrifugation, any attachment of plutonium to bacteria would enhance the removal of plutonium from solution and thereby increase the measured sorption ratio. At polymer concentrations <750 ppm, the sorption ratios are independent of polymer concentration for both plutonium and strontium, although they may be slightly enhanced compared to the sterile control. At the highest polymer concentration investigated, the plutonium sorption ratio matched the sterile control, whereas strontium sorption was decreased. This strontium ratio, however, is still extremely large.

To further investigate the effect bacteria may have on plutonium sorption, bacteria suspended only in water have been added to sterilized tuff following the procedure outlined above. Because there is no growth medium present, the cells should not be actively reproducing, and the measurement should reflect the influence of the bacterial cells rather than their by-products. Experiments to obtain more information about the effects of microbial by-products on plutonium sorption have also been initiated. Detergent and polymer media containing 1-week-old cultures of bacteria have been added to sterile tuff. These data will be compared to the cell-alone, polymer-alone, and other data to give more detailed information regarding the effects of bacteria on sorption.

Preliminary data from the EDTA-alone experiments follow the same trend as those from the polymer-alone studies. Concentrations of EDTA were chosen to bracket the 7.5×10^{-7} M concentration of plutonium tracer, and various dilutions were studied. Again, the nonsterile plutonium sorption ratio is higher than the sterile, whereas the strontium ratios are so high (>60 000) that no effect is observed. The sorption ratios for plutonium show a very slight enhancement (~10%) over the sterile controls at EDTA concentrations less than 3.7×10^{-7} M. At EDTA concentrations around 4×10^{-6} M, the strontium sorption ratio is decreased but still exceeds 30 000, and the plutonium ratio is the same as the sterile control.

The detergent-alone experiments are in progress and a more detailed comparison of the polymer, EDTA, and detergent experiments will be made in the next quarterly report. Further investigations will involve other radionuclides and a variety of tuff samples that have, for example, much lower sorption ratios for strontium.

IV. SOLUBILITY MEASUREMENTS AND CALCULATIONS (T. W. Newton, V. L. Rundberg, and J. F. Kerrisk)

A. Chemical Modeling

The EQ3/6 chemical equilibrium computer program is being used for chemical modeling of waste elements, local minerals, and groundwater at Yucca Mountain. A new version of EQ3/6 and its associated thermodynamic treatment programs (version 3230) has been received from Lawrence Livermore National Laboratory and is now running at Los Alamos. The new version includes additional thermodynamic data for uranium, plutonium, and fluorine. Input formats for EQ3, EQ6, and the thermodynamic data programs MCRT and EQTL have been changed; existing input files are being converted to the new formats.

B. Americium Thermodynamic Data

Work has started on a thermodynamic data file for americium. Data are being collected in the same format used for the manganese and strontium data files that were recently described.[2] At this time, data have been found or estimated for 26 aqueous species and 2 solids. Most of the data are for 25°C only. Data for complexes with fluoride, chloride, sulfate, phosphate, and nitrate were generally consistent in the species proposed and in the

formation constants for these species. Data for hydroxyl complexes showed some variation in the reported formation constants: complexes of composition $Am(OH)^{2+}$, $Am(OH)_2^+$, $Am(OH)_3$, and $Am(OH)_4^-$ have been proposed; however, there is little evidence for the last complex. Two sources of data for complexes with carbonate were found. Bidoglio has proposed four complexes with carbonate and bicarbonate [$Am(CO_3)_2^-$, $Am(OH)(CO_3)_2^{2-}$, $AmHCO_3^{2+}$, and $Am(HCO_3)_2^+$] (Ref. 7). Lundqvist proposed two complexes [$Am(CO_3)^+$ and $Am(CO_3)_2^-$] under similar conditions.[8] The two sets of data lead to different predictions of what species would predominate in water at Yucca Mountain. This conflict must be resolved before americium solubility can be modeled.

Thermodynamic data for two solids were found [$Am(OH)_3(c)$ and $Am_2(CO_3)_3$]. The existance of the hydroxide is well established: the sesquicarbonate was inferred from the solubility measurements of Shiloh et al. in K_2CO_3 and its formation under other conditions.[9,10] Two measurements of americium solubility have been reported without a determination of the solid phase. Edelstein et al.[11] reported solubilities of 10^{-5} to 10^{-8} in neutral to basic solutions; Rai et al.[12] reported solubilities of 10^{-8} to 10^{-12} in acidic to neutral solutions in contact with contaminated soil.

The two primary uncertainties in the calculation of americium solubilities are (1) thermodynamic data for americium complexes with carbonate and (2) the identity and thermodynamic data of americium solids that will control solubility in Yucca Mountain water. Work on the collection and evaluation of americium thermodynamic data is continuing in an attempt to reduce these uncertainties.

C. Solubility Limits on Radionuclide Dissolution

Solubility is one of the geochemical processes that will help limit the transport of radionuclides along water flow paths from a repository toward the accessible environment. Solubility will exert its primary influence in the vicinity of the waste form, where it can limit the concentration of radionuclides dissolved in the water leaving the repository. To calculate the rate at which radionuclides are transported along water flow paths, it will be necessary to define the mechanisms that control the concentrations of waste elements in water near the waste. These initial radionuclide concentrations or release rates will act as source terms for the transport calculations.

Two simple dissolution models have been developed in an attempt to better understand the importance of parameters such as waste-element solubility and water flow rate in controlling the release rates of radionuclides. The first is a saturation-limited dissolution model, in which it is assumed that the water flowing through the repository area is saturated with each waste element. This is a very conservative model because it would be highly unlikely that adequate contact between the water and waste (enough to saturate all the water) could be obtained. The second model is a diffusion-limited dissolution model, in which waste-element saturation is assumed at the waste/water interface and dissolution is limited by diffusion of the element into water flowing past the waste.[13] This model requires assumptions about waste containers, water flow characteristics and velocity, and element diffusivities; thus, it is subject to more uncertainty at this time. Neither model accounts for the effects of other parts of the engineered barrier system in limiting radionuclide dissolution. Both models require that an upper limit be placed on the dissolution rate of soluble elements; this upper limit represents a dissolution rate that is controlled by the bulk waste form dissolution. If the solubility-limited dissolution rate is less than the bulk waste dissolution rate, the element release rate will be controlled by solubility. If the solubility-limited dissolution rate is greater than the bulk waste dissolution rate, bulk waste dissolution will control the element release rate. This assumes that radionuclides are uniformly distributed throughout the bulk waste and that solid-state diffusion can be neglected. Calculations that identify which waste elements will have solubility-limited release rates and which elements will be released at the bulk waste form dissolution rate are useful for defining the importance of solubility in limiting the transport of radionuclides.

Calculations of dissolution rates were done for 10 waste elements. Table IX lists the solubilities estimated for the elements in Well J-13 water under oxidizing conditions (Eh = 700 mV). Oxidizing conditions were assumed because present indications are that water in the unsaturated zone and upper levels of the saturated zone may be oxidizing. Three of the elements (carbon, cesium, and technetium) were assumed to have solubilities so large that they would not limit dissolution. Three other elements (uranium, strontium, and neptunium) also have relatively high solubilities; solubility of uranium and neptunium are high because of the oxidizing conditions. Water

TABLE IX

SOLUBILITIES OF WASTE ELEMENTS

Element	Solubility (moles/ℓ)
Americium	1.0×10^{-8}
Plutonium	1.8×10^{-6}
Uranium	2.1×10^{-4}
Strontium	9.4×10^{-4}
Carbon	large
Cesium	large
Technetium	large
Neptunium	3.0×10^{-3}
Radium	1.0×10^{-7}
Tin	1.0×10^{-9}

flow through the repository was taken as 910 ℓ/MTHM year (1 MTHM = waste containing 1000 kg of heavy metal). This value was calculated by assuming a water recharge rate of 8 mm/year and a waste loading limit to 10 W/m^2. The fractional dissolution rate of the bulk waste form was taken as 1×10^{-4}/year. For the diffusion-limited model, the waste forms were taken to be cylinders of 0.25-m radius and 4.5-m length that contain 3 MTHM (for spent fuel waste) and cylinders of 0.16-m radius and 3.0-m length that contain 2 MTHM (for high-level waste). The apparent diffusion coefficient of species in the water surrounding the waste was assumed to be 1×10^{-10} m^2/second; this value includes corrections for connectivity and tortuosity of the surrounding rock, which has a porosity of 10%. Results of the calculations indicate that for spent fuel as a waste form, plutonium, uranium, and tin would have solubility-limited dissolution rates for the saturation-limited dissolution model, and that plutonium, uranium, tin, and americium would have a solubility-limited dissolution rate for the saturation-limited dissolution model, whereas tin, plutonium, and americium would have solubility-limited dissolution rates for the diffusion-limited dissolution model. Of the other waste elements studied, cesium, technetium, and carbon were not considered to have solubility limits (see Table IX), and the solubilities of strontium and

neptunium were large enough that they did not exhibit solubility-limited dissolution under the assumptions used here. Radium has a relatively low solubility but is present in such small quantities that solubility does not limit its dissolution rate. The saturation-limited dissolution model and the diffusion-limited dissolution model will be used to test the influence of parameters such as element solubility and water flow rate on the dissolution rates of waste elements. These calculations will provide information on the importance of solubility in controlling element concentrations in the vicinity of the repository and will provide estimates of the concentrations that can be used as source terms for transport calculations.

D. Plutonium Chemistry in Near-Neutral Solutions

The rates of disproportionation and the first steps of polymerization of Pu(IV) have been studied in very dilute solutions ($\sim 10^{-6}$ M plutonium and pH 3). These studies are part of a program to understand the chemistry of Pu(IV) in near-neutral solutions. Previous work has developed the techniques necessary to analyze the reaction products.[2] Reaction rates for disproportionation are reported here.

The reacting solutions were analyzed spectrophotometrically using Os(II) complexes and Ce(IV) as reagents. Disproportionation products Pu(III) and Pu(V) were identified by using their elution behavior from zirconium phosphate ion exchange columns. The reaction rates were predominantly second order in unreacted Pu(IV) and were studied as a function of pH in the range from 2.9 to 4.1. The logarithm of the second-order rate constant, expressed in M^{-1} min^{-1}, increased from about 4 at pH 2.9 to about 7 at pH 4.1. The slope of log k vs pH is about 1.9 at pH 3 and about 2.9 at pH 4. An interpretation of the pH dependence that would allow reliable extrapolation to higher values will require more accurate values for the higher hydrolysis quotients of Pu(IV) than are now available.

Another aspect of plutonium chemistry in water that is characteristic of Yucca Mountain is the effect of the carbonate content of the water on the solubility of hydrous PuO_2. Both the identity and stability of Pu(IV) carbonate complexes are uncertain at this time. If Pu(IV) in 1 M Na_2CO_3 is heated to about 80°C, hydrous PuO_2 is precipitated nearly quantitatively.[14] Heating is not necessary and precipitation will occur if bicarbonate

solutions of Pu(IV) are merely diluted with water at room temperature. The XRD patterns of solids formed in this way show PuO_2 lines.

The Pu(IV) appears to be stable in 0.4 M NH_4HCO_3; the concentration of a 4×10^{-4} M Pu(IV) solution remained constant after a total of 4 hours of centrifugation at 16 000 G (12 000 rpm, 10 cm) and standing for 4 days. However, dilution with an equal volume of water caused the formation of material that can be removed by centrifugation as described above. A series of experiments was done in which the Pu(IV)/HCO_3^- ratio was held constant at about 1000, but the concentration of HCO_3^- was varied from 0.2 M down to 0.005 M. Values for pH ranged from about 8.0 for the most dilute solution up to about 8.7 for the most concentrated. The concentrations of plutonium remaining in solution or suspension were determined by alpha counting after centrifugation at 16 000 G for at least 2 hours. The resulting data show considerable scatter but a definite downward trend. Log (concentration) varied from >-4.7 in 0.2 M NH_4HCO_3 down to >-7.2 in 0.04 M NH_4HCO_3. The values for HCO_3^- concentrations <0.03 M were anomalously high, so an additional series of experiments was done using 0.01 M ammonium bicarbonate and five initial Pu(IV) concentrations, $(1.1 \text{ to } 5.5) \times 10^{-5}$ M. During 5 days at room temperature, no plutonium was lost to the walls or by settling, but centrifugation at 16 000 G brought the log concentration values down to -6.9 ± 0.2, where the indicated uncertainty is the mean deviation. There was no detectable trend in the values with initial Pu(IV) concentration. After an additional 5 days at room temperature and recentrifugation at 16 000 G, the average value was -7.4.

Related spectrophotometric experiments show that the conversion of the Pu(IV)-carbonate complex to hydrous PuO_2 is rather slow. Successive dilutions from 0.4 M HCO_3^- to about 0.05 M gave solutions that showed the Pu(IV)-carbonate spectrum for at least 1 or 2 hours, even though $PuO_2 \cdot nH_2O$ could be centrifuged out later. However, when Pu(IV) was left in 0.094 M HCO_3^- for 16 hours, the spectrum changed to one resembling that of the Pu(IV) polymer or colloid.

The rough solubility limits we have obtained for Pu(IV) in HCO_3^- may be compared with the observations of Kim et al.[15] for $^{238}PuO_2$. At pH 8 and 10^{-3} M $HCO_3^- + CO_3^{2-}$, these authors found log (solubility) was about -5.8; this should be compared with our upper limit of -7.4. The solubility of polymeric

Pu(IV) in the absence of carbonate reported by Rai and Swanson[16] and extrapolated to pH 8 is about -8.5.

V. WATER FLOW AND TRANSPORT: FRACTURE FLOW EXPERIMENTS (R. S. Rundberg, E. J. Mroz, and A. J. Mitchell)

The movement of radionuclides through fractures in welded tuff will be impeded by the diffusion of ions and molecules into the porous tuff matrix. Laboratory experiments with the migration of radionuclides through natural tuff fractures are being performed to provide evidence that this phenomenon will occur in the field and to determine the effective diffusion coefficients in tuff. The first of this series of experiments was performed using tritiated water. Figures 1 through 7 show the results of these experiments and the calculated elution curves.

The model used to fit the elution data has a one-dimensional flow field with diffusion perpendicular to the direction of flow. The model applied had no dispersion or channeling. The data, however, indicated a fairly nondispersed flow field, so that dispersion was not necessary in the model.

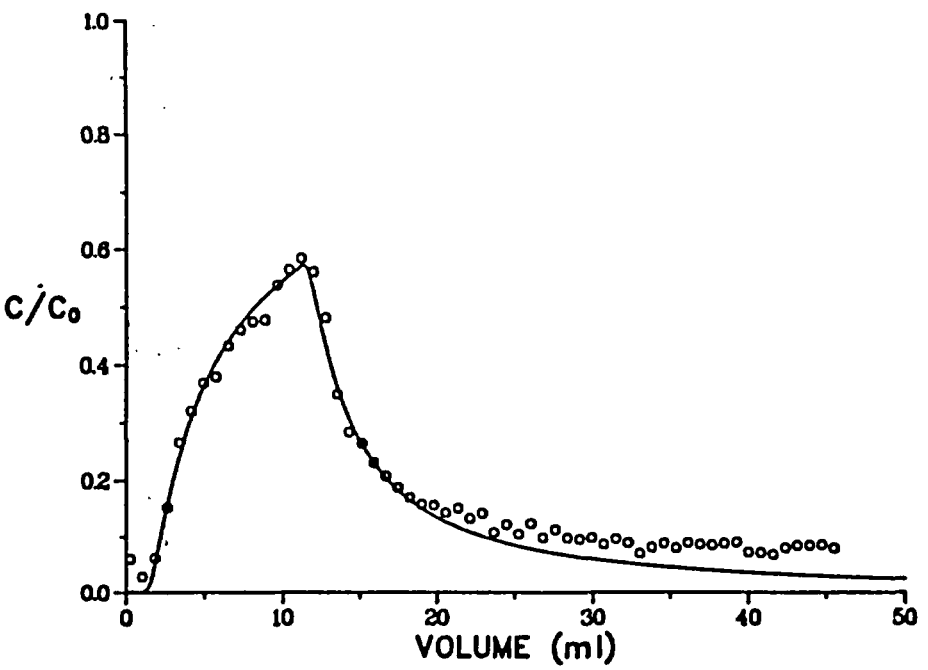

Fig. 1. The elution of tritiated water through a fracture in sample G-1-743. Circles are the experimental points, and the solid line is the fitted curve.

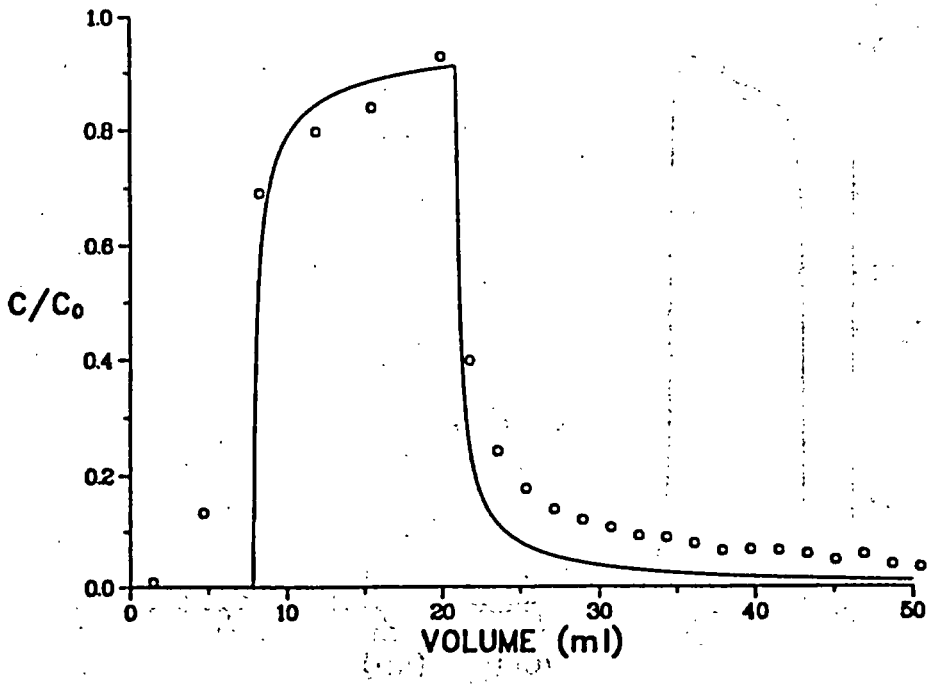

Fig. 2. The elution of tritiated water through a fracture in sample G-1-1221. Circles are the experimental points, and the solid line is the fitted curve.

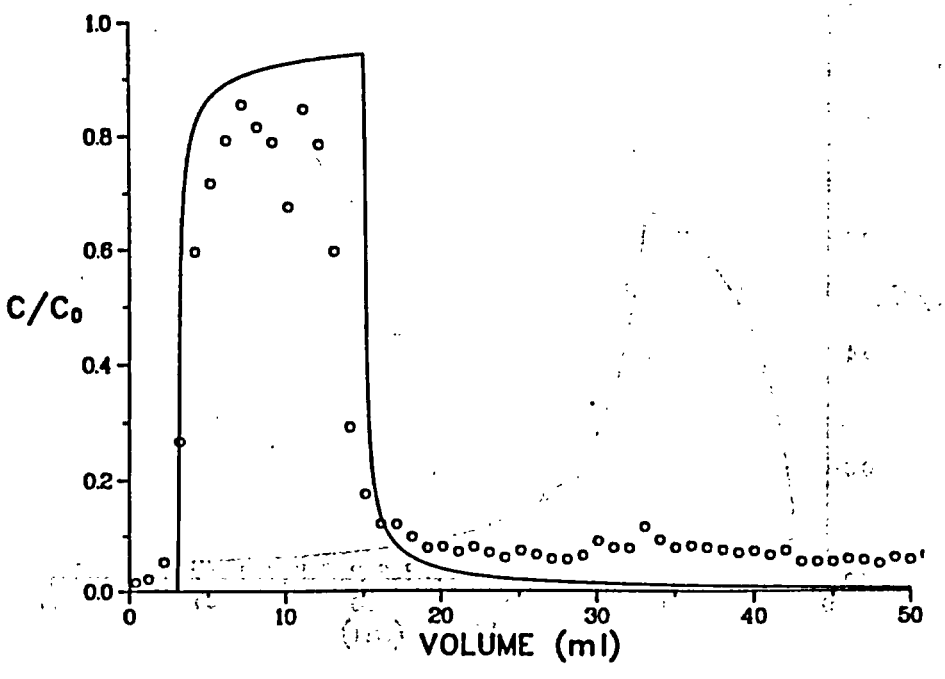

Fig. 3. The elution of tritiated water through a fracture in sample GU-3-104. Circles are the experimental points, and the solid line is the fitted curve.

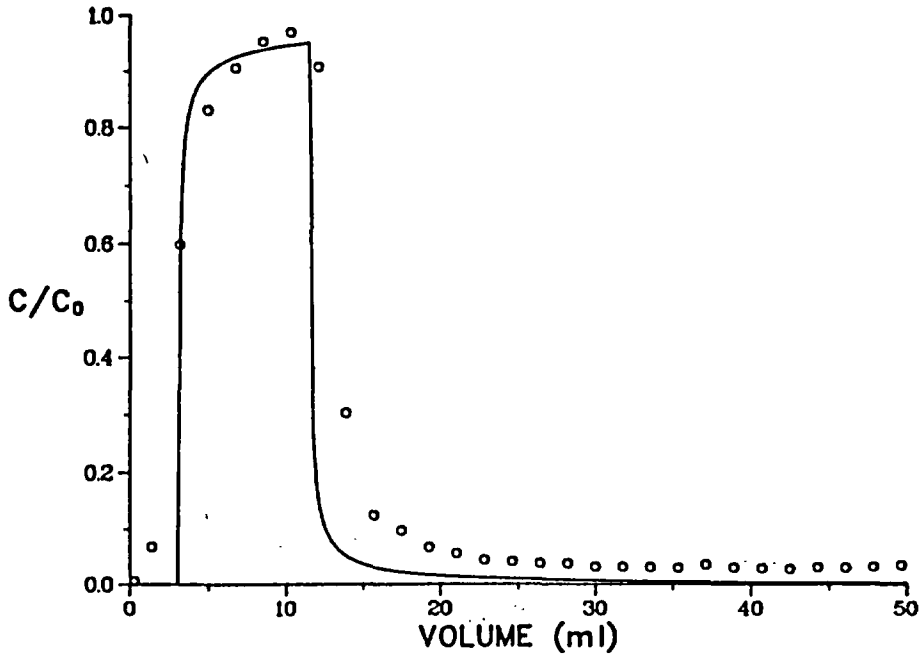

Fig. 4. The elution of tritiated water through a fracture in sample GU-3-104. Circles are the experimental points, and the solid line is the fitted curve.

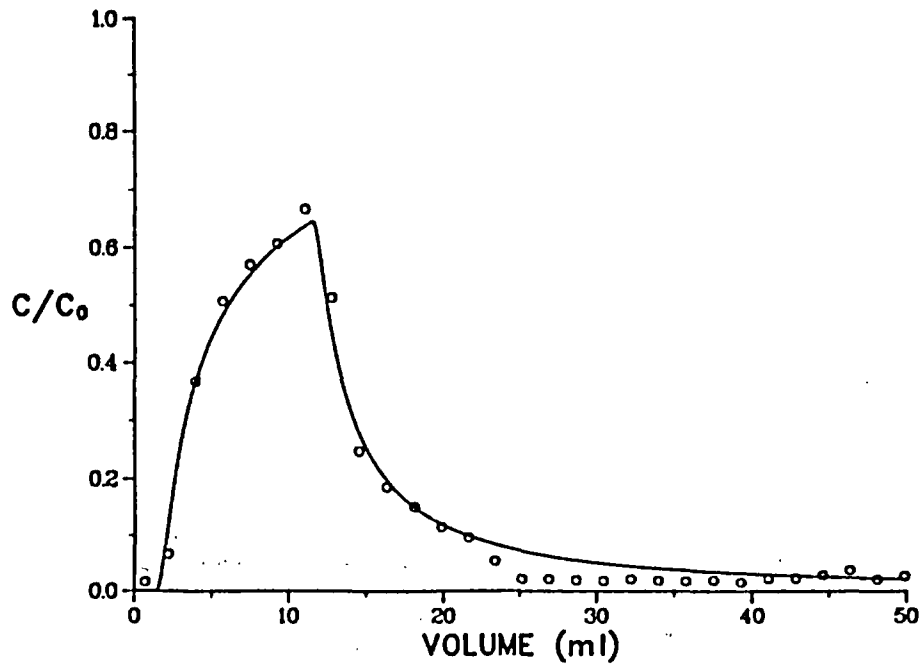

Fig. 5. The elution of tritiated water through a fracture in sample GU-3-2114. Circles are the experimental points, and the solid line is the fitted curve.

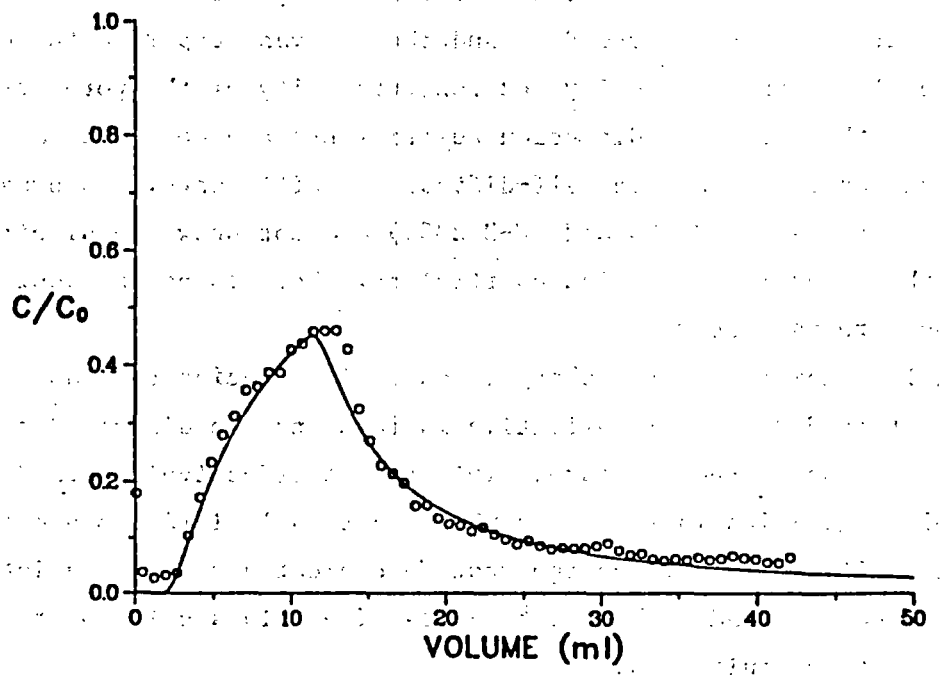

Fig. 6. The elution of tritiated water through a fracture in sample GU-3-2359. Circles are the experimental points, and the solid line is the fitted curve.

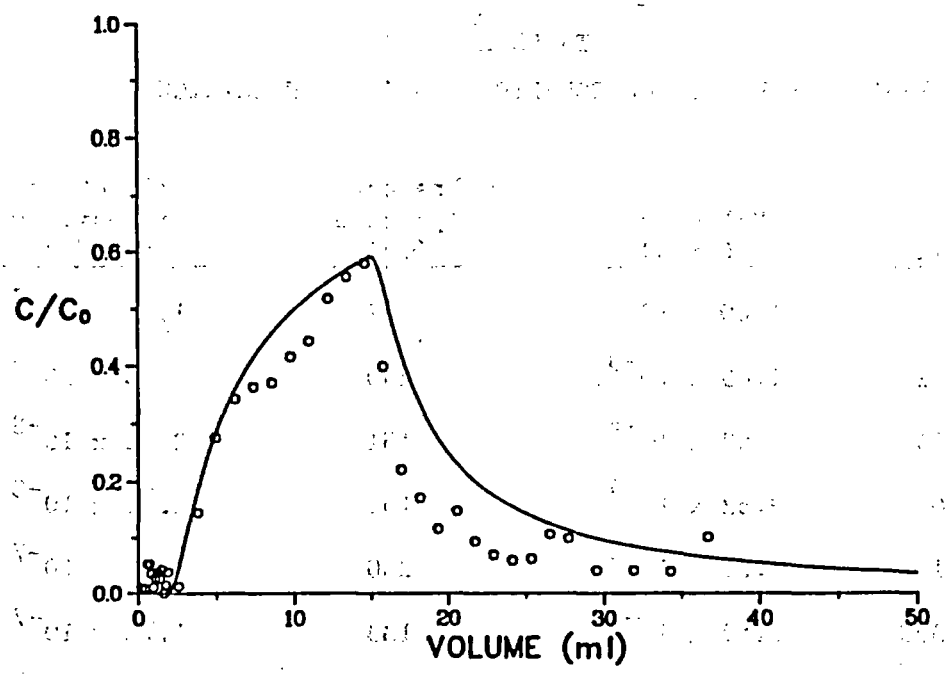

Fig. 7. The elution of tritiated water through a fracture in sample GU-3-2359. Circles are the experimental points, and the solid line is the fitted curve.

The details of this model are described in previous reports. Table X lists both the parameters used to fit the data and the relevant experimental conditions. As a result of the tortuosity and constrictivity of the pore structure in the tuff, the effective diffusion coefficients are more than an order of magnitude smaller than the free self-diffusion coefficients. Columns run at different flow rates (GU-3-104 and GU-3-2359) did not show any significant difference in the effective diffusion coefficient. This is as one would expect for a nonsorbing tracer.

These results show that for uncharged nonsorbing species such as tritiated water, matrix diffusion is effective in removing the dissolved species from the water flowing in the fracture. This effect effectively retards the movement of soluble species in fractures when the travel distances and times are longer. The effect of ionic charge must be evaluated before predictions for pertechnetate can be made. The next series of elutions using pertechnetate tracer are being initiated.

TABLE X

EFFECTIVE DIFFUSION COEFFICIENTS IN TUFF MATRICES

Tuff Sample	Water Velocity (cm/s)	Fracture Aperture (μm)	Effective Diffusivity (cm^2/s)
G-1-743	1.00×10^{-3}	57	1.26×10^{-7}
G-1-1221	1.05×10^{-3}	250	5.08×10^{-8}
GU-3-104	4.82×10^{-4}	151	2.52×10^{-8}
GU-3-104	8.62×10^{-4}	151	2.52×10^{-8}
GU-3-2114	7.29×10^{-4}	250	3.78×10^{-7}
GU-3-2359	5.52×10^{-4}	133	1.72×10^{-7}
GU-3-2359	8.99×10^{-4}	133	1.82×10^{-7}

VI. HYDROTHERMAL GEOCHEMISTRY: A THERMODYNAMIC MODEL FOR ANALCIME

(C. J. Duffy)

A. The Model

Zeolites are an important class of sorptive mineral in Yucca Mountain. However, to predict the effect of zeolites on the movement of waste elements in Yucca Mountain, the present distribution and future stability of the zeolite minerals must be understood. The important zeolites in Yucca Mountain are clinoptilolite-heulandite, mordenite, and analcime. Of these, analcime is the most studied.

To begin examining the parameters that affect the stability of zeolites, a thermodynamic model has been constructed for analcime. The analcimes in Yucca Mountain are more silica rich than $NaAlSi_2O_6 \cdot H_2O$, which is the formula commonly used for analcime. The model, therefore, represents analcime as an ideal solid solution between $NaAlSi_2O_6 \cdot H_2O$ and $Si_3O_6 \cdot 1.5H_2O$. This covers the compositional range of most naturally occurring analcimes, with the exception of some samples occurring in silica-undersaturated environments.[17] This model does not apply to analcime less silica rich than $NaAlSi_2O_6 \cdot H_2O$.

The model is based on calorimetric data,[18] on solubility data for silica in equilibrium with albite and analcime,[19] and on the compositions of analcimes coexisting with quartz in Yucca Mountain. Other thermodynamic data used in the calculations have been taken from Refs. 20 to 22.

To test the model, its predictions have been compared to field observations. The parameters that affect analcime stability are, however, seldom all measured. The model indicates that the following parameters have a significant effect on the stability of analcime: the activity of water (a_{H_2O}), the activity of albite (a_{Ab}), temperature (T), the difference of the lithostatic pressure and the fluid pressure ($P_T - P_{H_2O}$), the activity of aqueous silica [$^{m}SiO_2(aq)$], and the state of order of the albite. The Z-order parameter[20] has been used here as the measure of the state of order of albite. For completely ordered albite, Z is equal to 1 and is equal to 0 for completely disordered albite.

Figure 8 shows the temperatures and total pressures where albite, quartz, and analcime coexist for several combinations of Z, a_{H_2O}, a_{Ab}, and $P_T - P_{H_2O}$. The positions of these curves are rather insensitive to total pressure. This information is in agreement with data from the Niigata oil field, Japan,[23]

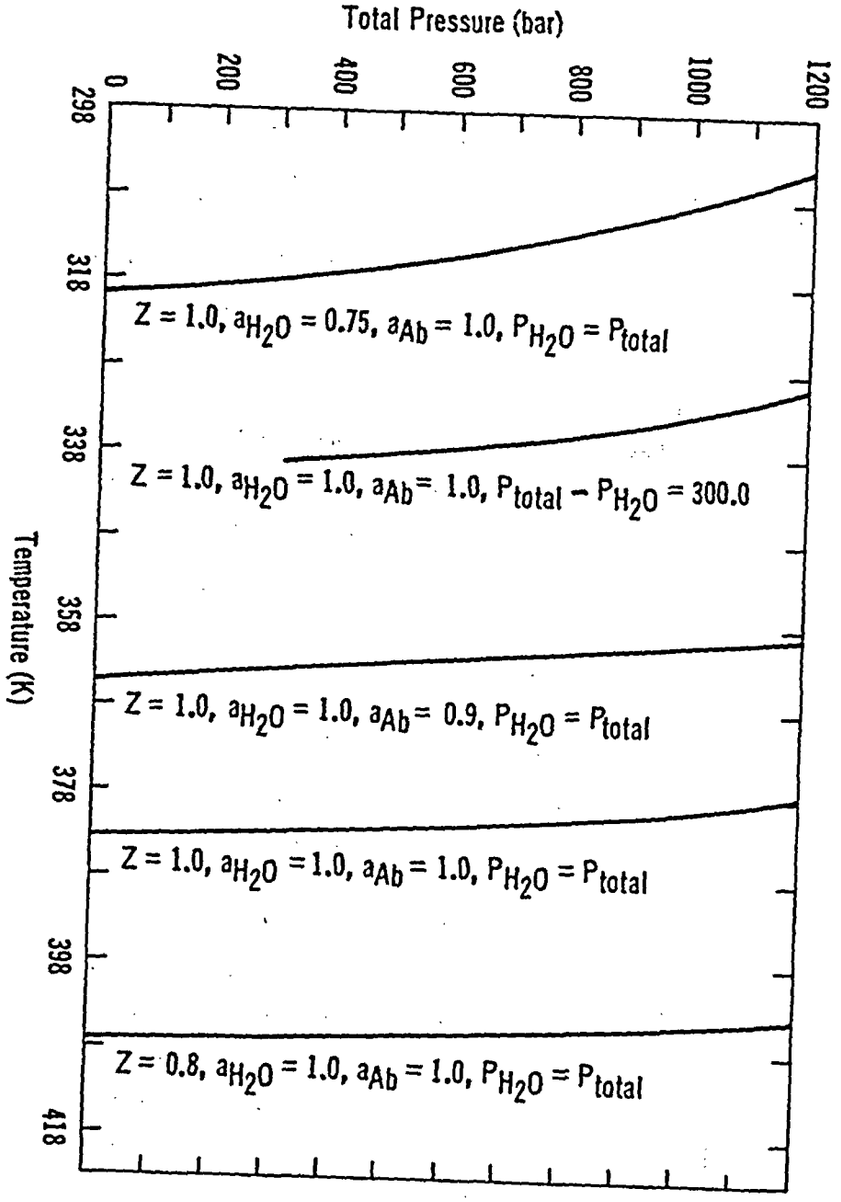

Fig. 8. The position of the univariant curve for the assemblage albite, analcime, quartz is shown for various combinations of the Z-order parameter and activity (a_{Ab}) of albite, the activity of water (a_{H_2O}), and the difference between the lithostatic pressure and the pressure of the fluid phase. Analcime plus quartz is stable below the curve; albite is stable above the curve.

where the first appearance of authigenic albite forming from analcime is at 393 K. This is consistent with the model, but it would require that P_{H_2O} be near P_{Total} and that Z be somewhat less than 0.8. Field evidence exists for the former, but no information is given on the state of order of the albite.

Most natural analcimes coexisting with quartz have compositions falling in the range of X = 0.97 to 0.77 (Refs. 17 and 24), where X is the mole fraction of $NaAlSi_2O_6 \cdot H_2O$. Compositions calculated from the model range from 0.97 to 0.72, but the very high silica values require the unlikely combination of temperatures near 298 K and pressures of several hundred bars or more. The observed and predicted compositional range are in almost perfect agreement.

Analcime in tuffs from the Green River formation, Wyoming, has a bimodal compositional distribution.[24] Analcimes coexisting with authigenic albite have compositions near X = 0.94, whereas those without authigenic albite are near X = 0.8. These minerals probably reached a maximum temperature in the range of 313 to 343 K, with pressures that did not exceed 400 bar. This is generally below the temperature thought to lead to the breakdown of analcime plus quartz to albite; however, the authigenic feldspars "are largely restricted to the saline facies, deposited in a sodium carbonate-bicarbonate-chloride brine, from which trona and halite precipitated."[24]

As illustrated in Fig. 9, lowering of a_{H_2O}, which takes place in a brine, substantially decreases the upper temperature stability of analcime. Lowering P_{H_2O} appreciably below P_{Total} also decreases the stability of analcime. However, it can be seen from Figs. 10 and 11 that as $P_T - P_{H_2O}$ increases, the maximum silica content of the analcime decreases. Therefore, unless P_{H_2O} was greater in the saline facies than elsewhere, P_{H_2O} was generally near P_{Total}. The model appears to provide a good explanation for the observations in the Green River formation. The high-silica analcimes have compositions consistent with the conclusion that they formed in relatively fresh water. As the salinity increased in parts of the deposit, it caused the analcime to react to albite and less silica rich analcime. The activities of water needed seem reasonable because that in a sodium chloride solution saturated with respect to halite is about 0.75. Certainly other ions were present in these brines that would have further reduced a_{H_2O}.

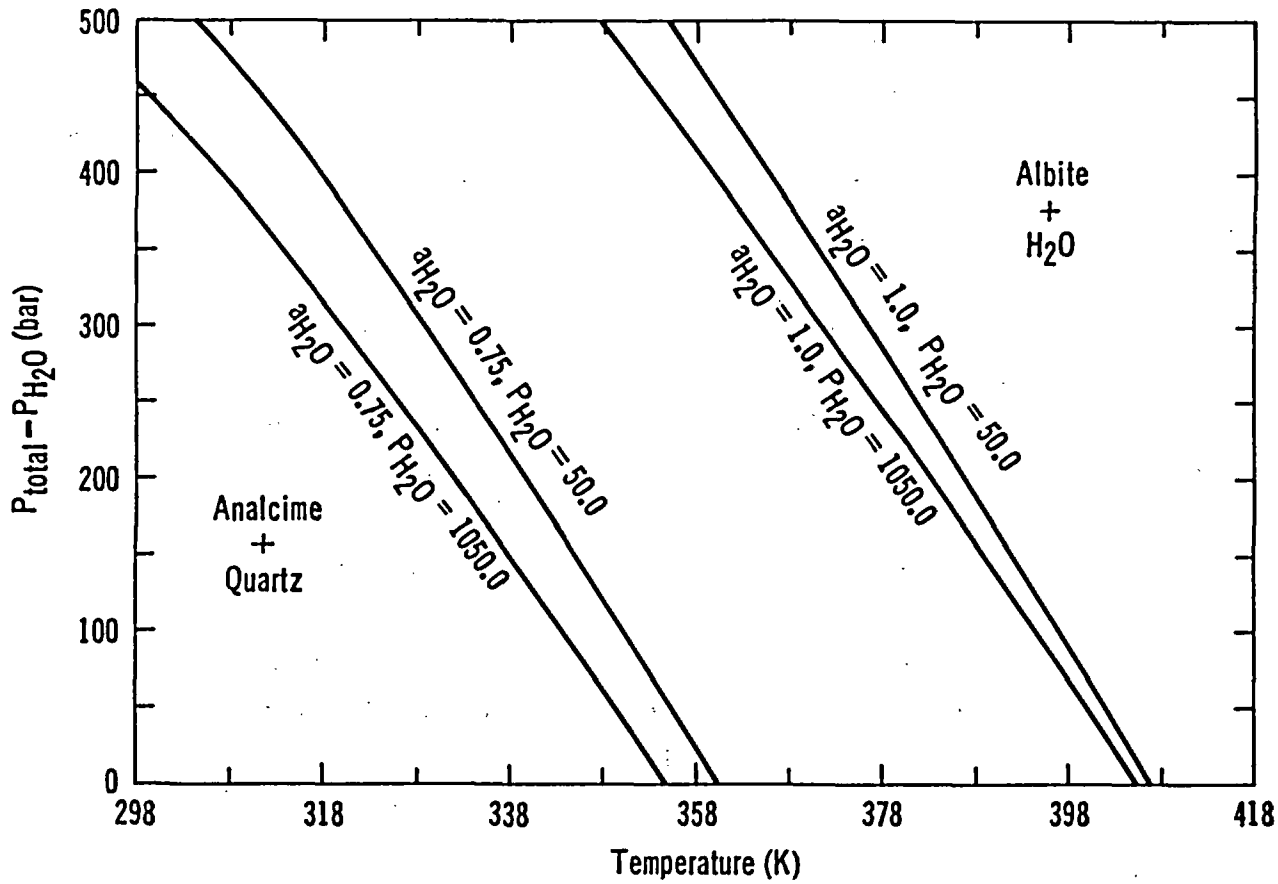

Fig. 9. The curves shown are equilibrium conditions for the assemblage albite, analcime, quartz as a function of temperature and lithostatic pressure minus fluid pressure. Labels on the curves are the activity of water and the fluid pressure. Analcime plus quartz is stable below the curves; albite is stable above the curves.

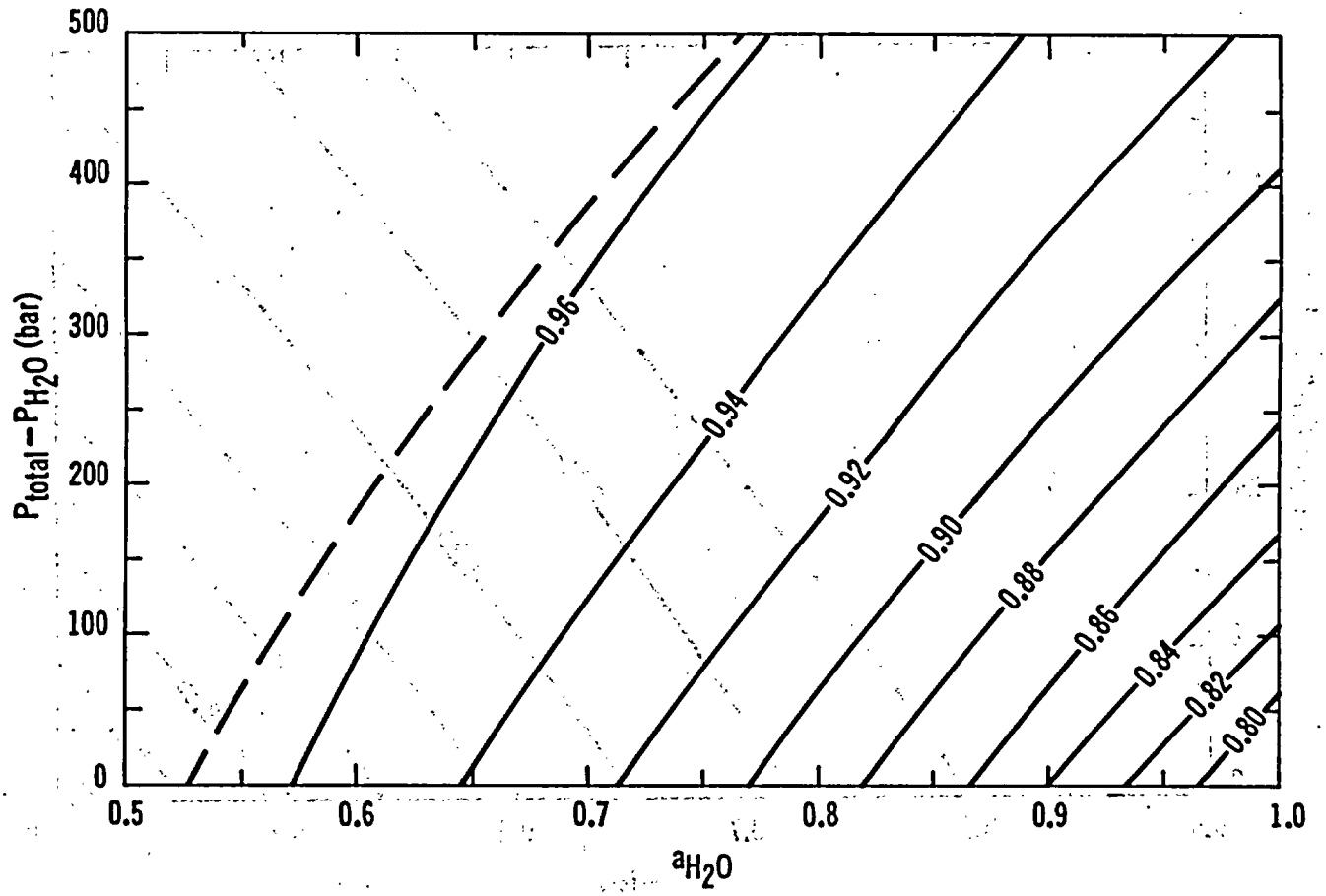

Fig. 10. The dashed curve is the equilibrium curve for albite, analcime, quartz. The analcime plus quartz field is contoured in mole fraction of $NaAlSi_2O_6 \cdot H_2O$ in the equilibrium analcime. Temperature is 308.15 K, and fluid pressure is 50 bar. The albite has a Z of 0.8 and an activity of 1.

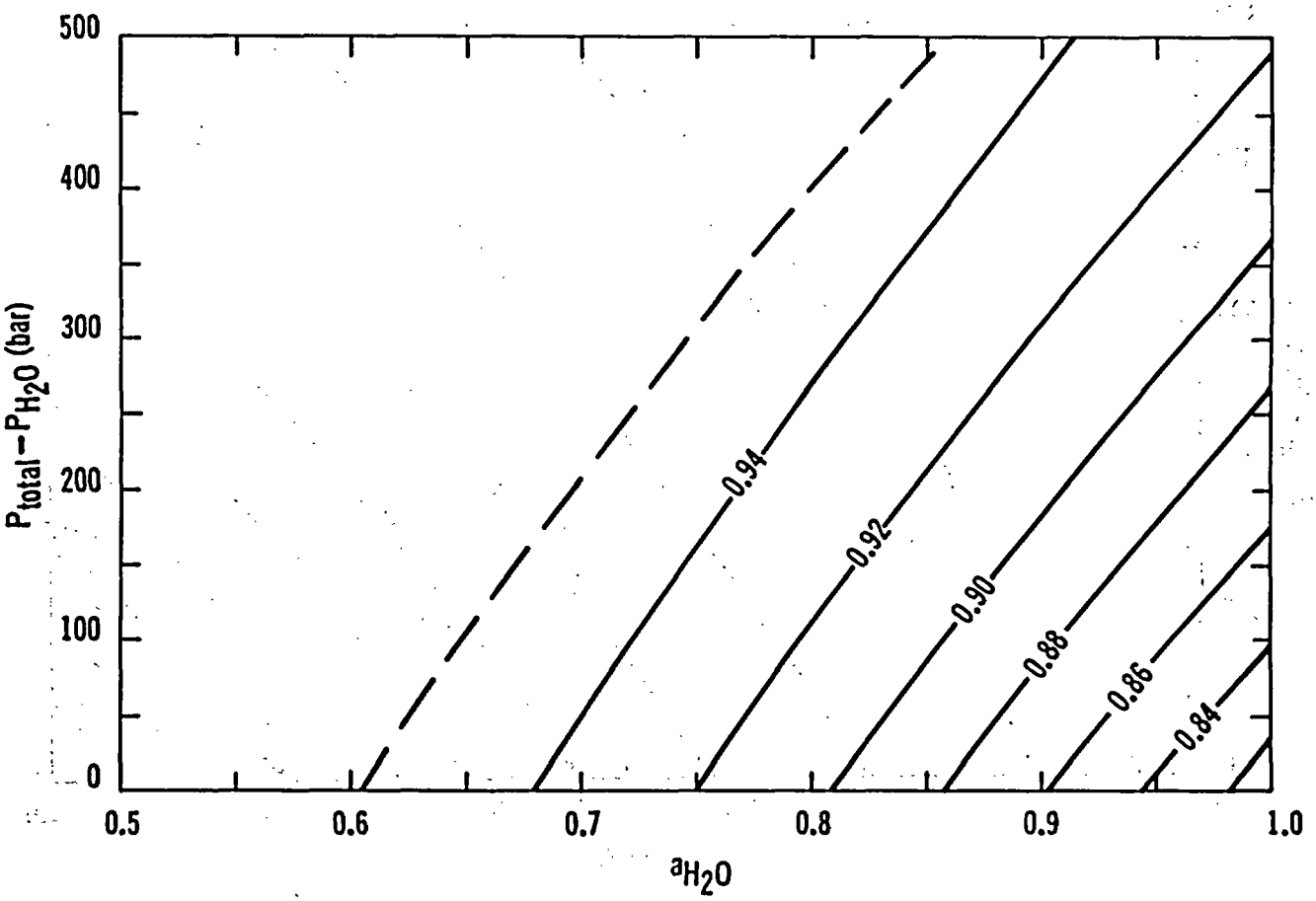

Fig. 11. The dashed curve is the equilibrium curve for albite, analcime, quartz. The analcime plus quartz field is contoured in mole fraction of $NaAlSi_2O_6 \cdot H_2O$ in the equilibrium analcime. Temperature is 328.15 K, and fluid pressure is 50 bar. The albite has a Z of 0.8 and an activity of 1.

B. Application to Yucca Mountain

Comparison of Figs. 10 and 11 suggests that the temperature of equilibration in the Green River formation may have been quite low (310 to 320 K). This suggests that at least some reactions may be at equilibrium in Yucca Mountain. Before this hypothesis can be examined, as many variables as possible should be fixed. Water analyses from Yucca Mountain indicate that the waters are quite dilute. Therefore, unlike that in the Green River formation, the activity of water at Yucca Mountain is probably not an important variable and can be set equal to 1. P_{H_2O} is probably well represented as that because of the hydrostatic head. The lithostatic pressure will be approximated by the lithostatic load if an average rock density of 2 g/cm^3 is assumed. This may require refinement as a result of the nonisotropic stress environment in Yucca Mountain.

Figure 12 shows the temperature/depth relationship for the reaction analcime plus quartz to albite for various albites; it also shows the approximate geothermal gradient in the USW G-1 drill hole. The standing water table is assumed to be at 580 m. The P_{H_2O} is taken as 1 bar above the water table and (depth minus 580)/10 bar below the water table. The lithostatic pressure is depth/5 bar. To determine if analcime plus quartz is stable, it is necessary to know composition and state of order of the albite. Probe analyses indicate that the authigenic albite in Yucca Mountain is usually quite pure, so that a_{Ab} is probably quite close to 1 for much of the authigenic albite in Yucca Mountain. Its state of order is not yet known, but it is unlikely to be more ordered than Z = 0.8. Therefore, analcime would appear to be stable with respect to albite in much of Yucca Mountain.

One of the reasons that albite persists in Yucca Mountain is illustrated in Fig. 13. If the concentration of aqueous silica in solution is much above that in equilibrium with quartz, analcime is no longer stable. Although analcime is not now present in the Topopah Spring Member, if repository heating were to cause the cristobalite now present to transform to the more stable quartz, it might also lead to the transformation of albite to analcime.

In view of field observations that vitric tuffs often devitrify to clinoptilolite and mordenite (which later transforms to analcime), it seems likely that the activity of aqueous silica may also be important in equilibria involving clinoptilolite and mordenite. Developing detailed

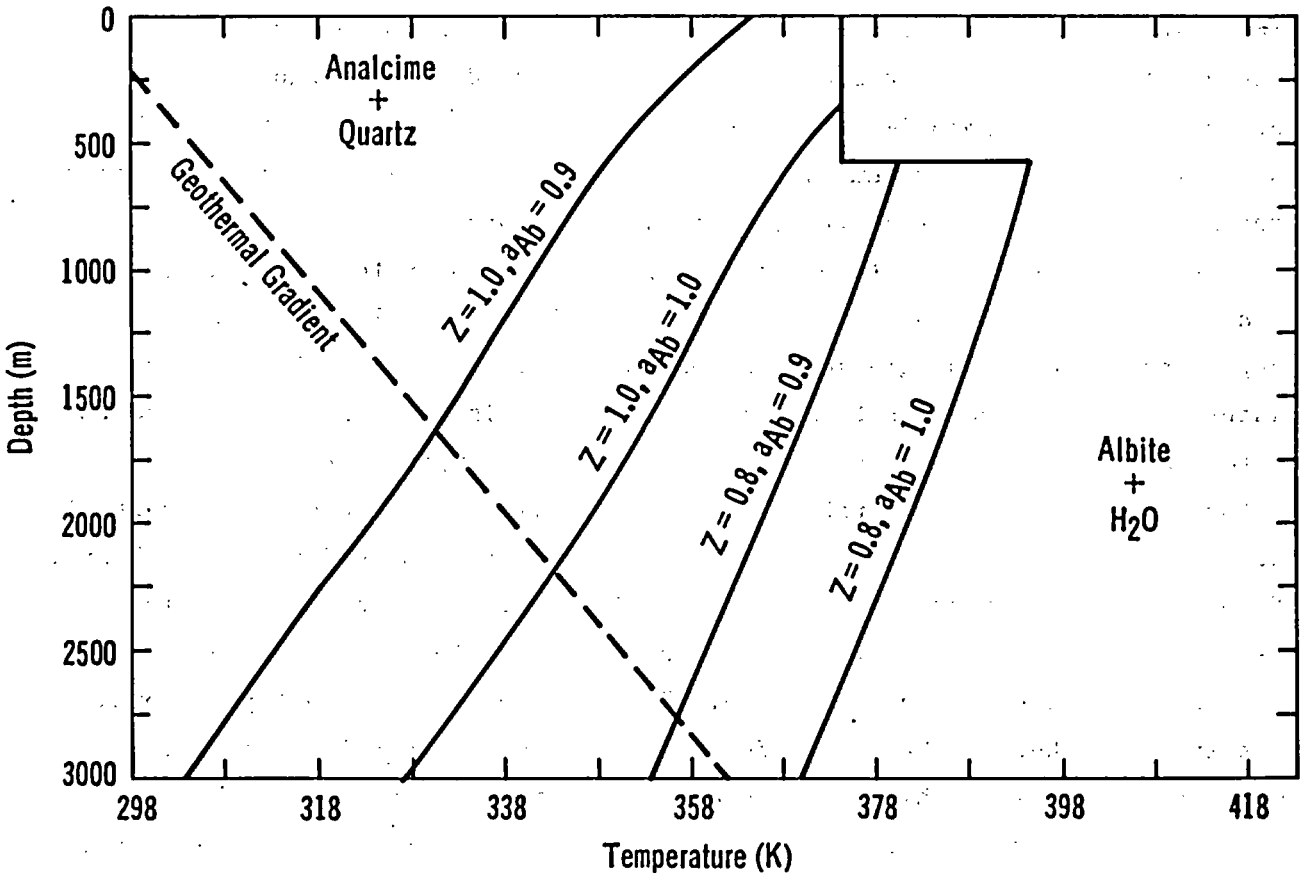

Fig. 12. Solid curves are equilibrium lines for albite, analcime, quartz for albites of different Z and activity. The dashed line is the approximate geothermal gradient in USW G-1. The relationships between lithostatic pressure, fluid pressure, and depth are given in the text. Analcime plus quartz is stable to the upper left, albite to the lower right.

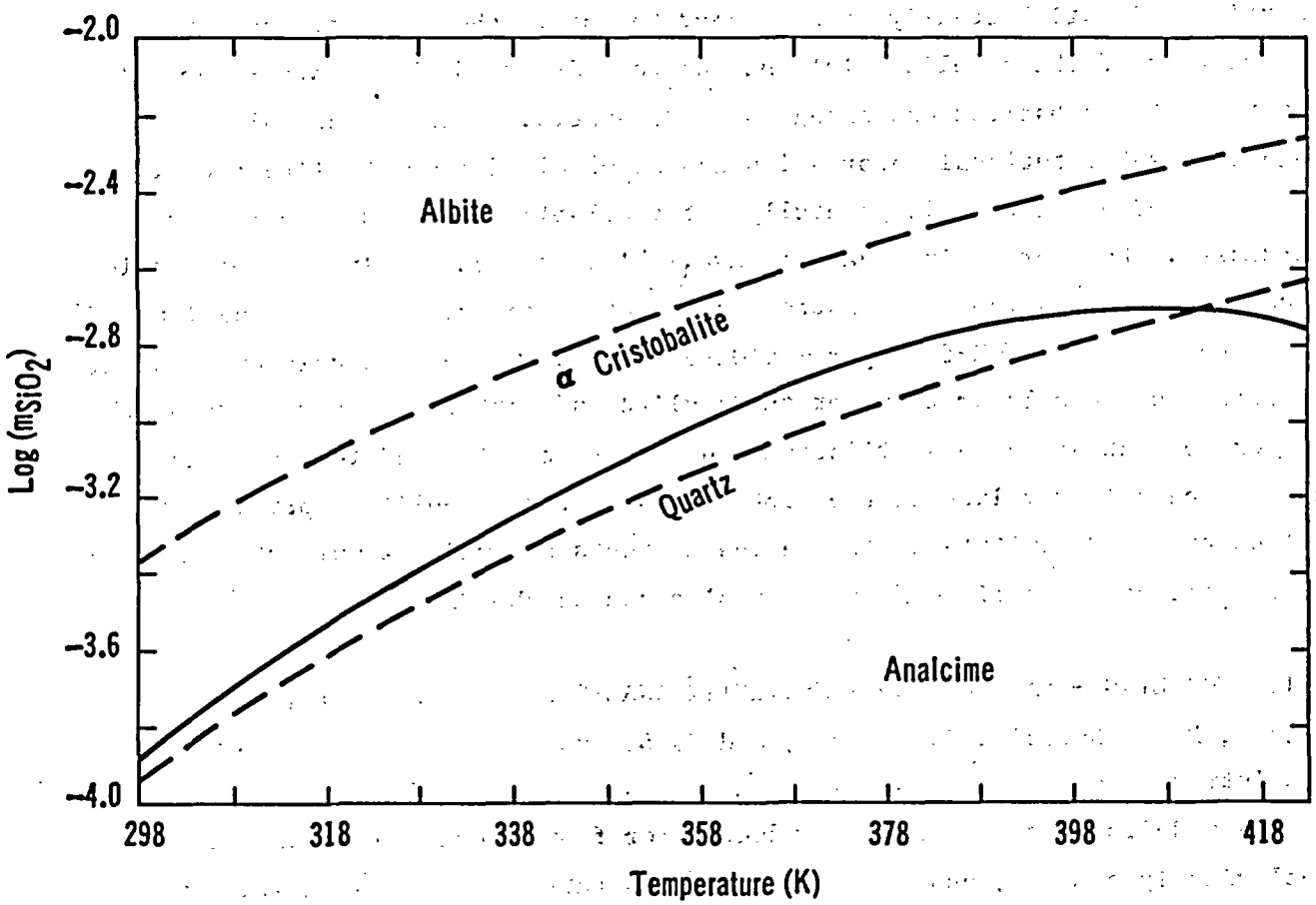

Fig. 13. The solid curve shows the concentration of aqueous silica in equilibrium with analcime plus albite as a function of temperature. The dashed curves show the concentration of aqueous silica in equilibrium with quartz and α-cristobalite.

models for these phases similar to the models for analcime will provide more insight into the roles of equilibrium and kinetic controls on the mineralogy of Yucca Mountain. At present, it appears that the most important nonequilibrium factor at Yucca Mountain is the metastably high silica activity present in large portions of the mountain.

To calculate phase equilibria involving clinoptilolite and mordenite, it will be necessary to obtain values for the Gibbs energy, entropy, heat capacity, and volume of these minerals. Because these minerals are also solid solutions, it will actually be necessary to obtain these quantities for the end members of these solid solutions and to understand the crystal-chemical nature of the substitutions among the end members. Much, if not all, necessary substitutional information can be obtained from the literature.

Thermodynamic data is generally not available for clinoptilolite or mordenite. However, volume data is available, and reasonably good estimation techniques are available for entropy and heat capacity. Because equations of the type M-zeolite $\rightarrow$ M-feldspar + SiO_2(eq) + H_2O (where M is calcium, sodium, or potassium) can be written for the zeolite end members, measurements of the silica concentration in equilibrium end members zeolite and feldspar can be used to calculate values of the Gibbs energy for the zeolites, provided no silica phase precipitates. If the measurements are made at multiple temperatures, the heat capacity and entropy also can be checked.

VII. MODELING - PATHWAY AND SENSITIVITY ANALYSIS (B. J. Travis, S. W. Hodson, H. E. Nuttall, T. L. Cook, and R. S. Rundberg)

A. Introduction

A modeling study is being conducted for flow and transport in the geologically complex, unsaturated, fractured tuff of Yucca Mountain. Two numerical models of mass and heat flow in conjunction with analytical solutions are being used for sensitivity and pathway analysis studies and to help design and interpret laboratory and field flow and transport tests in tuff. Figure 14 is a schematic diagram of the Yucca Mountain geologic formations and shows the underground location of the proposed repository. The potential repository site lies in a highly fractured, densely welded, low-porosity, ash-flow tuff named the Topopah Spring Member. This unsaturated formation is located about 300 m below the ground surface and

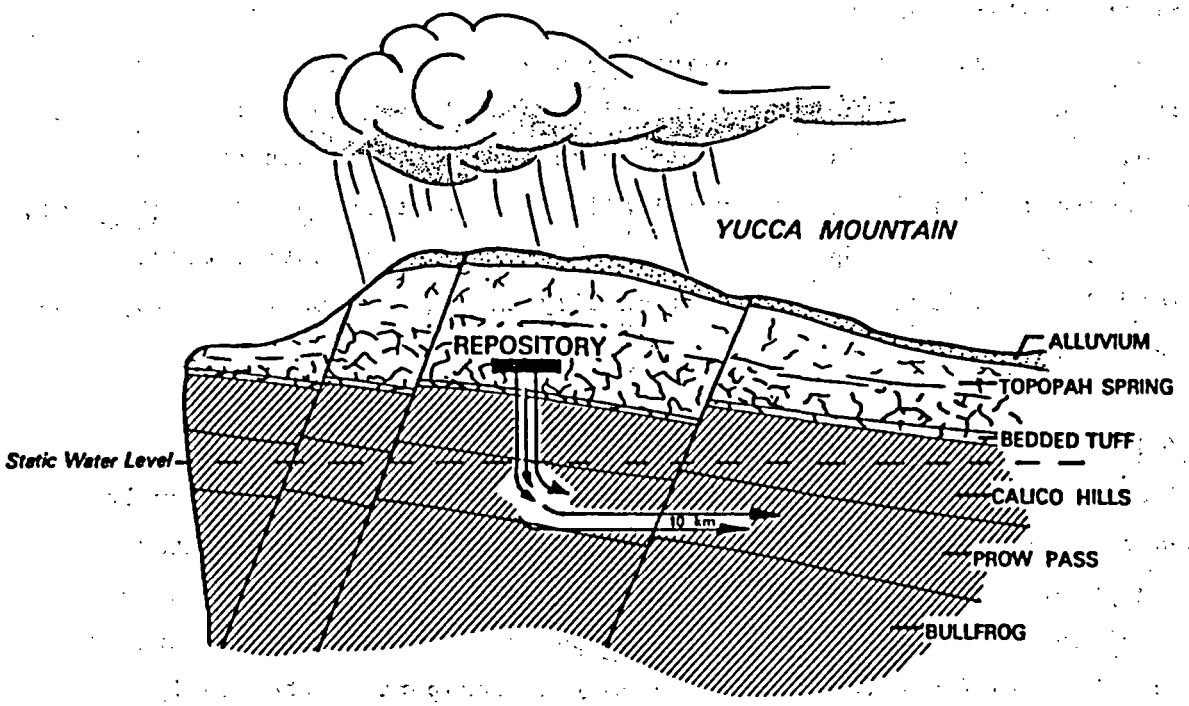

Fig. 14. Conceptual radionuclide transport path for the proposed Yucca Mountain radioactive-waste repository.

200 m above the water table. The tuff of Calico Hills and the Prow Pass and Bullfrog Members that lie below the proposed repository site consist of relatively unfractured, nonwelded, highly porous argillic and zeolitic bedded and ash-flow tuffs.

A major factor in approving a proposed site is the ability of the geological formation to retard the movement of radionuclides that might leak from waste canisters through the boundaries of the repository. It is assumed that if radionuclides were released from the repository, they would first pass downward through the unsaturated welded tuff and then would travel horizontally through the porous, nonwelded tuff, as illustrated in Fig. 14. The fundamental question is: How long will it be before any of the waste

traverses this 10-km path and reaches the "accessible" environment? The potential radionuclide transport path is geologically and geochemically complex, and a definitive answer may not be possible at present because of a lack of data. However, reasonable transport time estimates can be made and sensitivity analyses can be performed.

Analytical and numerical modeling are used to examine the effects of lithology and fractures on water flow and radionuclide transport within Yucca Mountain. The following is a preliminary sensitivity analysis of transport along a one-dimensional pathway, vertically downward through the unsaturated, highly fractured Topopah Spring Member and the relatively unfractured, nonwelded Calico Hills, and then horizontally through the Calico Hills, Prow Pass, and Bullfrog tuffs.

B. Modeling Approach

Both analytical and numerical models are used. A great deal can be learned from simple models and dimensional analysis. More complicated modeling problems require numerical solutions. Numerical codes used in this study include TRACR3D (Ref. 25), which computes saturated and unsaturated two-phase flow in fractured/porous media with transport of chemically retarded radionuclides, and the WAFE code,[26] which computes water, air, vapor, and energy movement in porous media. Analytic solutions were used for problems of steady water flow with transport of sorptive species down single or parallel fractures.[27-30]

C. Sensitivity Analysis

Various analyses were performed to assess the sensitivity of both water flow and radionuclide transport to characteristics of the proposed repository site, such as fracture width and spacing, matrix potential, saturation, permeability, diffusion, and adsorption. The following questions were considered in the preliminary site analysis:

(1) How far down can surface water created during episodic desert storms penetrate through the unsaturated fractured tuff?
(2) How well do the fractured and nonfractured tuff layers retard radionuclide transport?
(3) What is the effect of repository heat load on hydrology?

1. Flow in Fractures. Fractures can accelerate the movement of groundwater and the transport of radionuclides. Several analyses were performed[31] to assess the rate and distance that groundwater would flow in the fractured Topopah Spring formation. The schematic diagram used in modeling both flow and radionuclide transport through a fractured medium is presented in Fig. 15.

Episodic surface water is assumed to run down fractures as a slug of height H, where $H = hL/W$ and L is fracture spacing, W is fracture width, and h is the surface water depth. As a water slug moves down a fracture, it gradually shrinks because of suction of water into the surrounding tuff. In the rock matrix, it is assumed that water saturation σ is governed by $\partial_t \sigma = -\nabla\cdot(k/\varepsilon\mu\ \nabla P_c) = \nabla\cdot(bK_0P_0/\varepsilon\mu)\sigma^c\nabla\sigma = \nabla\cdot(A\sigma^c\nabla\sigma)$. The coefficient A combines all the important material properties, such as permeability (K_0), porosity (ε), and matrix suction (b and P_0). The depth a water slug will reach before being completely drawn into the tuff has been calculated for a range of A values, fracture widths, and initial matrix saturations. Figure 16 is an example of depth reached vs crack width for 70% matrix saturation.

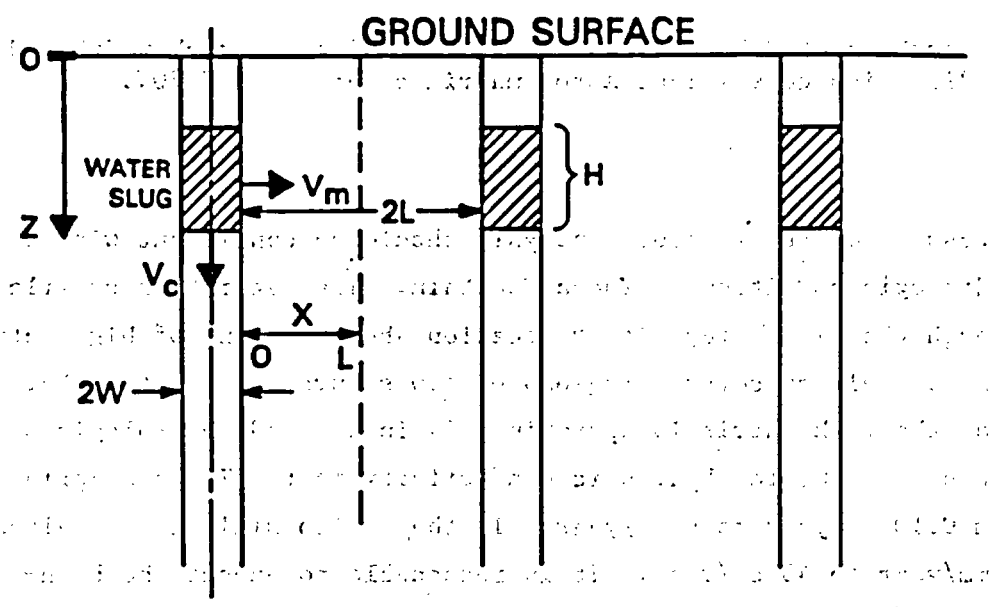

Fig. 15. Scenario used for fracture flow analysis.

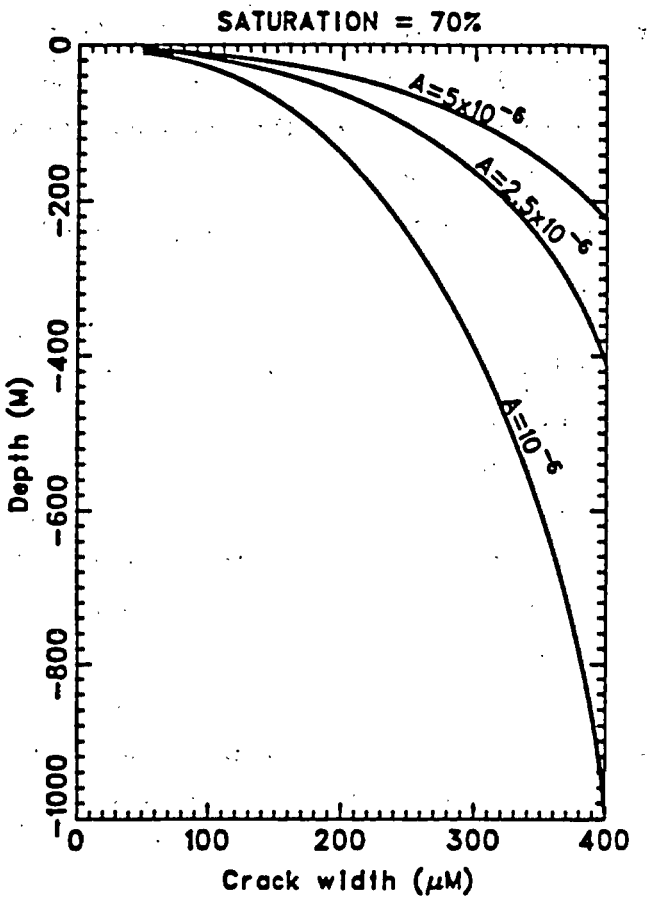

Fig. 16. Depth reached by water slug as a function of crack width and diffusion coefficient A for matrix saturation of 70%.

The results of the fracture analysis should be consistent with the actual hydrologic condition of Yucca Mountain. The saturation profile vs depth through the likely repository location shows regions of high saturation (80 to 90%) as well as several regions of low saturation (30 to 40%). It is likely that the rock matrix is approximately in a steady hydrologic state. Measurements of saturated hydraulic conductivity in the Topopah Spring tuff range from 0.10 mm/year to 6 cm/year. In the Calico Hills tuff, values range from 1.2 mm/year to 45 cm/year. It is reasonable to expect the high-saturation regions to correspond to low-permeability values (these regions cannot drain very easily) and the low-saturation regions to correspond to high-permeability values (these regions can rapidly drain off the 8 mm or so of recharge per year). Mass must be conserved. If 8 mm of water enters per

year, then 8 mm must leave if steady state is to be maintained. The simplest explanation for getting this recharge through the low-permeability regions (whose matrix permeability is too low to allow 8 mm/year of recharge) is to allow fracture flow. This is consistent with the analytical and numerical modeling.[31] In the high-permeability, low-saturation regions, water will be drawn out of fractures. The flow will be primarily porous flow. In the low-permeability, high-saturation regions, flow is primarily through fractures. If this interpretation is correct, there are alternating layers of porous flow and fracture flow from the surface down to the water table. Experiments that use tracers could help to validate this interpretation.

There are other inferences in this interpretation. Water in the high-saturation regions would be older than that in the low-saturation regions. Also, water travel time from the repository to the water table (50 to 100 m below) would be approximately the travel time through the porous flow layers (roughly 5000 years).

Very little data are available on fracture aperture distributions. However, from saturated permeability tests of the Topopah Spring Member, average fracture widths can be estimated. The measured fracture conductivity[32] is about 230 m/year (see Sec. 2 below). This corresponds to a permeability of 0.74 darcy. If a fracture spacing of 6 cm is used, the average fracture aperture is about 81 μm.

2. Radionuclide Transport. Although fractures are capable of transporting water to considerable depths, the transport of radionuclides is quite different. The reason for this disparity is the effect of chemical adsorption and molecular diffusion. Extensive preliminary calculations[31] were performed to estimate radionuclide transport times. The transport pathway being considered extends from the repository site to the water table (50 m of Topopah Spring tuff, about 15 m of bedded tuff, and 135 m of Calico Hills tuff) and then laterally for 10 km in the saturated region (see Fig. 14).

Analytical solutions[27-30] were used to estimate migration times through each of the four geologic formations. Ten radionuclides were studied: ^{141}Ce (an analogue for ^{151}Sm), ^{135}Cs, ^{90}Sr, ^{99}Tc, ^{238}U, ^{237}Np, ^{239}Pu, ^{243}Am, ^{152}Eu (an analogue for ^{151}Sm), and ^{133}Ba (an analogue for ^{226}Ra). In these simulations, flow and transport occur in a set of vertical, equidistant, parallel fractures (Fig. 15). Episodic flow is approximated by an average

flow rate of 200 m/year in fractures, and 10.0 cm/year in porous-flow-only layers. Radionuclides diffuse rapidly out of fractures into the porous tuff. Retardation factors for these nuclides range from 2 for ^{99}Tc up to 700 000 for ^{226}Ra. Half-lives also show great variation, ranging from 28 years for ^{90}Sr to 4.5 billion years for ^{238}U. No retardation was used in the fractures. Figure 17 shows the results for the 50-m-thick Topopah Spring layer with a 5-cm-fracture spacing. Relative concentration curves at the bottom of the layers are shown. Radionuclides not shown either took longer than 100 000 years to move through or decayed away before breakthrough could occur. Figure 18 shows similar curves for transport through the tuff of Calico Hills. Here, porous flow only is assumed because of the much lower fracture frequency in the tuff of Calico Hills. Transit times are much greater; of the 10 radionuclides considered, only ^{99}Tc can reach the water table in less than 10,000 years. Given the assumptions made in this study, diffusion, chemical adsorption, and radioactive decay prevent any of the other nine key radionuclides from reaching the accessible environment. Space is not available here for presentation of all results, but details of these calculations are presented in the report by Travis et al.[31]

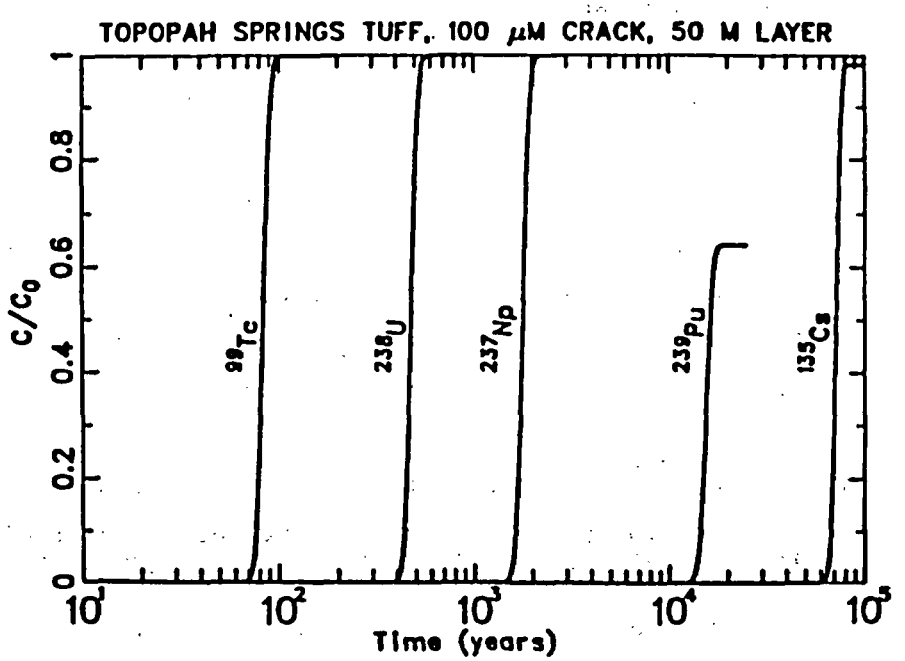

Fig. 17. Concentration histories at the bottom of a 50-m layer of Topopah Springs tuff.

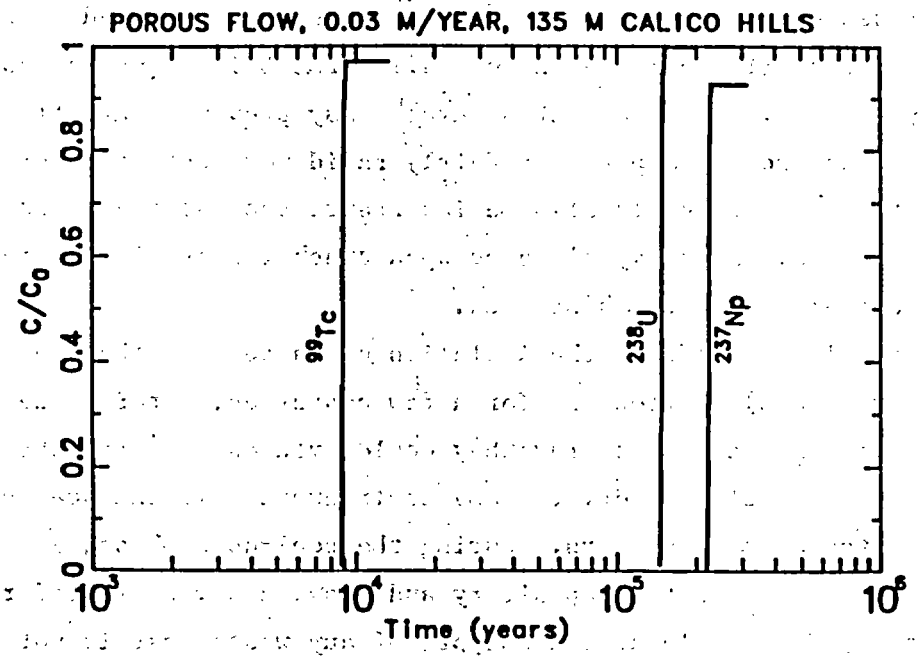

Fig. 18. Concentration histories for ^{99}Tc, ^{238}U, and ^{237}Np at the bottom of the Calico Hills layer (assuming porous flow only).

3. Heat Load Effect. The thermal energy released from radioactive decay of the implanted waste could have a significant effect on the surrounding environment. The heat load estimated for a high-level waste repository in Yucca Mountain is about 50 kW/acre and is expected to persist for several hundred years. The local hydrology surrounding the repository will impact upon the resulting thermal flux. Near the repository, water will boil off and then move outwards to condense in cooler regions. The more or less uniform ambient saturation field may change to a dried out region near the repository and a virtually saturated region some distance away. Convective or circulating flow patterns may develop if the effective Rayleigh number is large enough. This behavior will be reduced if the repository is

kept well ventilated. Later, when the radionuclides have decayed and the region cools, the fully saturated regions above the repository will tend to flow fairly rapidly down to and through the repository.

The presence of fractures can alter the thermally induced flow patterns. Many small cracks will increase the overall permeability, making convection more likely. A few large, conducting cracks may prevent convective circulation but would provide a path for fairly rapid movement of water, vapor, and air. Other factors could also be important, such as the thermomechanical behavior of cracks. Heat may close or open cracks, depending on the mechanical properties of the host rock.

How does all this affect the isolation of waste? If the heat load can provide a dry (steam) environment for a few centuries, water-borne species certainly cannot migrate (assuming they could even escape from the canisters). In addition, a dry (steam) environment will enhance the integrity of the waste canisters. During the cool-down phase, a pulse of water could move through the repository and provide a vehicle (of relatively short duration) for accelerated transport of any waste that is not contained. Also, the geochemical properties of the surrounding tuff may be altered by large temperature and saturation changes.

Heat loading in Topopah Spring tuff was calculated to estimate the induced flow field. The material properties used for tuff are those listed in Table XI. A cylindrical region 35 m in radius and 150 m high was considered. The horizontal cross-sectional area is about 1 acre. A heat load of 50 kW/acre was positioned at a depth of 250 m. The power rating is assumed to decay linearly to zero in 200 years. Calculations were made with the WAFE numerical code, which computes one- or two-dimensional transient two-phase (air, vapor, and water) flow with heat transport. Saturations can range anywhere from zero to 100% inclusive. Condensation and evaporation are treated. Details of this model and examples of verification and validation are available in another Los Alamos report.[26]

Two calculations are considered. In the first, the tuff is uniform and the energy is deposited into a 2-m-tall by 6-m-radius room. In the second case, energy is deposited uniformly, reducing the problem to one space dimension. No allowances for ventilation are made in these computer computations. Also, no thermomechanical effects are included.

TABLE XI

MATERIAL PROPERTIES FOR HEAT LOAD STUDY

Material Property	Value
Permeability (darcy)	10^{-3}
Relative permeability (k_w,k_g)	$s^{3+2/\lambda}$,$(1-s^{1+2/\lambda})(1-s)^2$
Porosity	0.12
Saturation (%)	60
Thermal conductivity (ergs/°C•sec•cm)	1.6×10^5
Specific heat (erg/gm•°C)	10^7
Initial temperature (°C)	30
Grain density (g/cm^3)	2.6
Pore size index λ	0.2

Results of the simulations are presented in temperature and water saturation contour plots and velocity vector plots for water, vapor, and air. In Case 1 (Figs. 19 and 20), high temperatures are generated because of the small source volume and lack of ventilation. A dry region extends about 10 m around the repository. Limited convective circulation occurs. In Case 2, with lower energy density, the boiling would be somewhat slower to develop, but the lack of cylindrical divergence in this one-dimensional case results in a stronger push on the water and more rapid expansion of the dry region. Eventually, a region about 20 m above and 30 m below the repository dries out. Gravity is responsible for the differences in saturation above and below the repository. Water has boiled away, as illustrated by the centerline temperature and saturation profiles shown in Figs. 21 and 22. The results shown here are a very strong function of the material properties and of the heat load density distribution.

D. Conclusions

Several conclusions can be drawn. (1) Significant fracture flow can occur but only through large cracks (several 100 μm) or in a low-permeability, nearly saturated formation. (2) Diffusion, adsorption, and matrix suction have a profound effect on transport. Migration times to the water table for most of the important radionuclides are large (at least

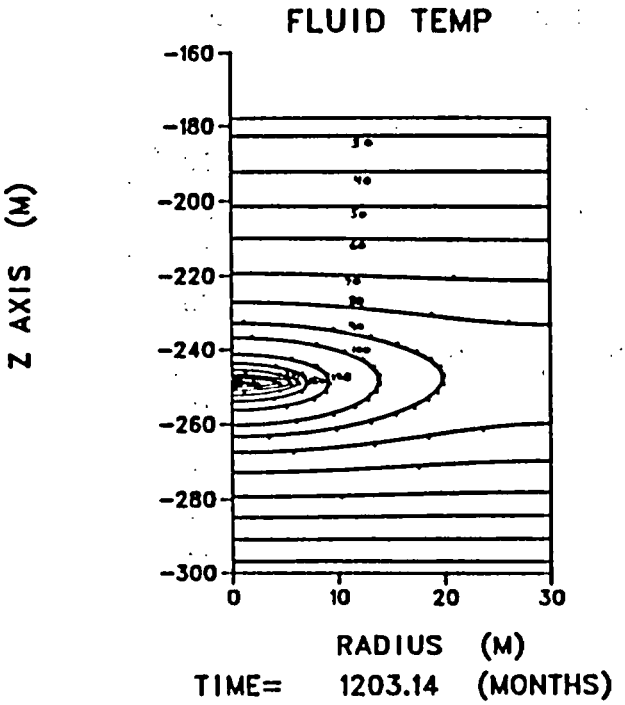

Fig. 19. Temperature contours 100 years after heat load emplacement.

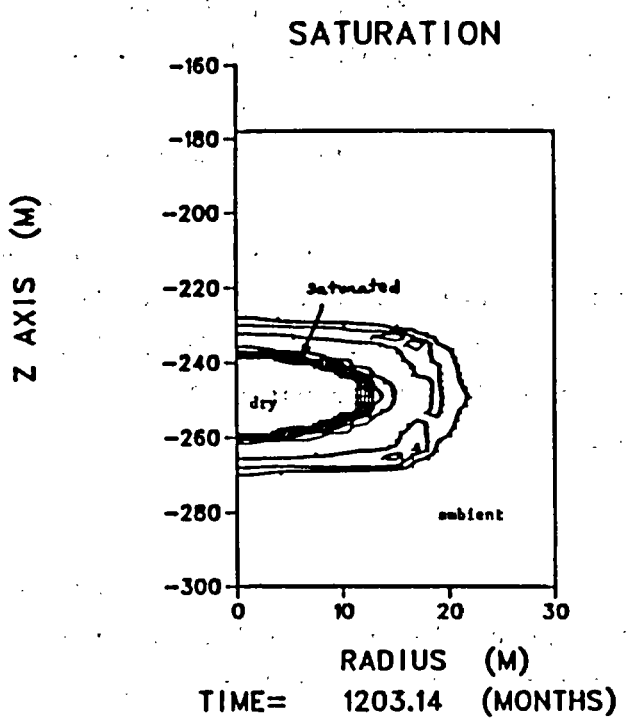

Fig. 20. Water saturation contours 100 years after heat load emplacement.

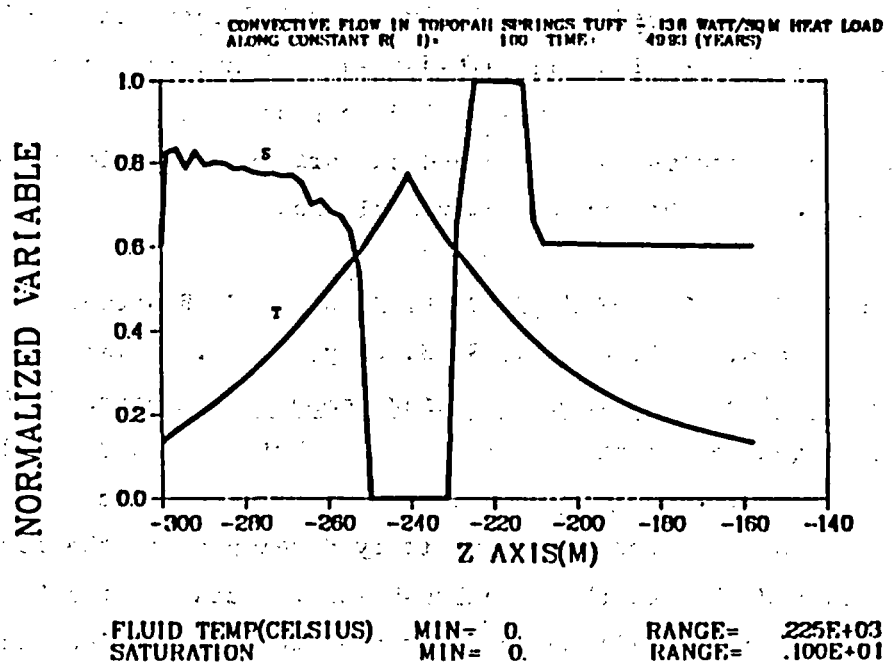

Fig. 21. Profiles of temperature (T) and saturation (S) vs depth on the centerline at 50 years.

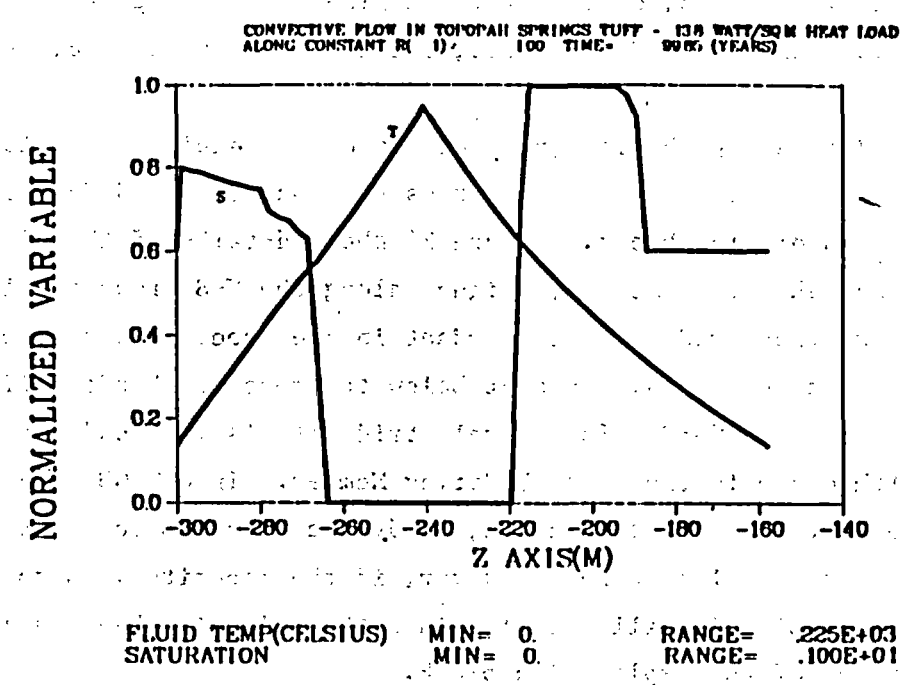

Fig. 22. Profiles of temperature (T) and saturation (S) vs depth on the centerline at 100 years.

10 000 years). (3) Heat load in partially saturated tuff can result in a dried out, steam-filled region that extends several meters above and below a repository, with recharge during the cool-down phase. It is important to remember that these conclusions are based on various assumptions and simplifications made in this preliminary analysis.

VIII. MINERALOGY-PETROLOGY OF TUFF (D. L. Bish, D. E. Broxton, F. M. Byers, Jr., F. A. Caporuscio, B. A. Carlos, S. S. Levy, and D. T. Vaniman)

A. Mineralogy of the Lower Topopah Spring Member, Paintbrush Tuff

During this quarter, cuttings samples from Drill Holes USW H-3, H-4, and H-5 were examined to improve our knowledge of the mineralogic variability within the potential host rock for repository development: the lower part of the Topopah Spring Member of the Paintbrush Tuff. Data for the host rock are now available from eight drill holes in or near the exploration block. Data derived from quantitative XRD analysis of the host rock (following the method outlined in Caporuscio et al.[33]) are summarized below.

The host rock includes the interval below the zone of abundant (>15%) lithophysal cavities in the upper Topopah Spring Member and above the basal vitrophyre of that member. Aside from sparse phenocrysts (less than 2%) and fracture-filling minerals, over 98% of the mineralogic content of the Topopah Spring host rock is composed of quartz, cristobalite, tridymite, and alkali feldspars.

Figure 23 is a map showing the location of the exploratory block at Yucca Mountain; the locations of two cross sections (N-S and E-W) are shown crossing the exploration block. Figure 24 shows details of the mineralogy within the Topopah Spring Member, aligned along the N-S cross section. Figure 24 shows that tridymite is abundant in the upper part of the Topopah Spring Member but is generally absent below the zone of abundant lithophysae, except at USW H-3 and GU-3. In general, tridymite is lost and quartz increases with depth in the Topopah Spring Member. In USW GU-3, at the southern end of the exploration block, tridymite persists to a depth only 70 m above the basal vitrophyre. However, if the repository is to be mined as level as possible, it will not rise into the tridymite-bearing levels at the southern end of the exploration block.

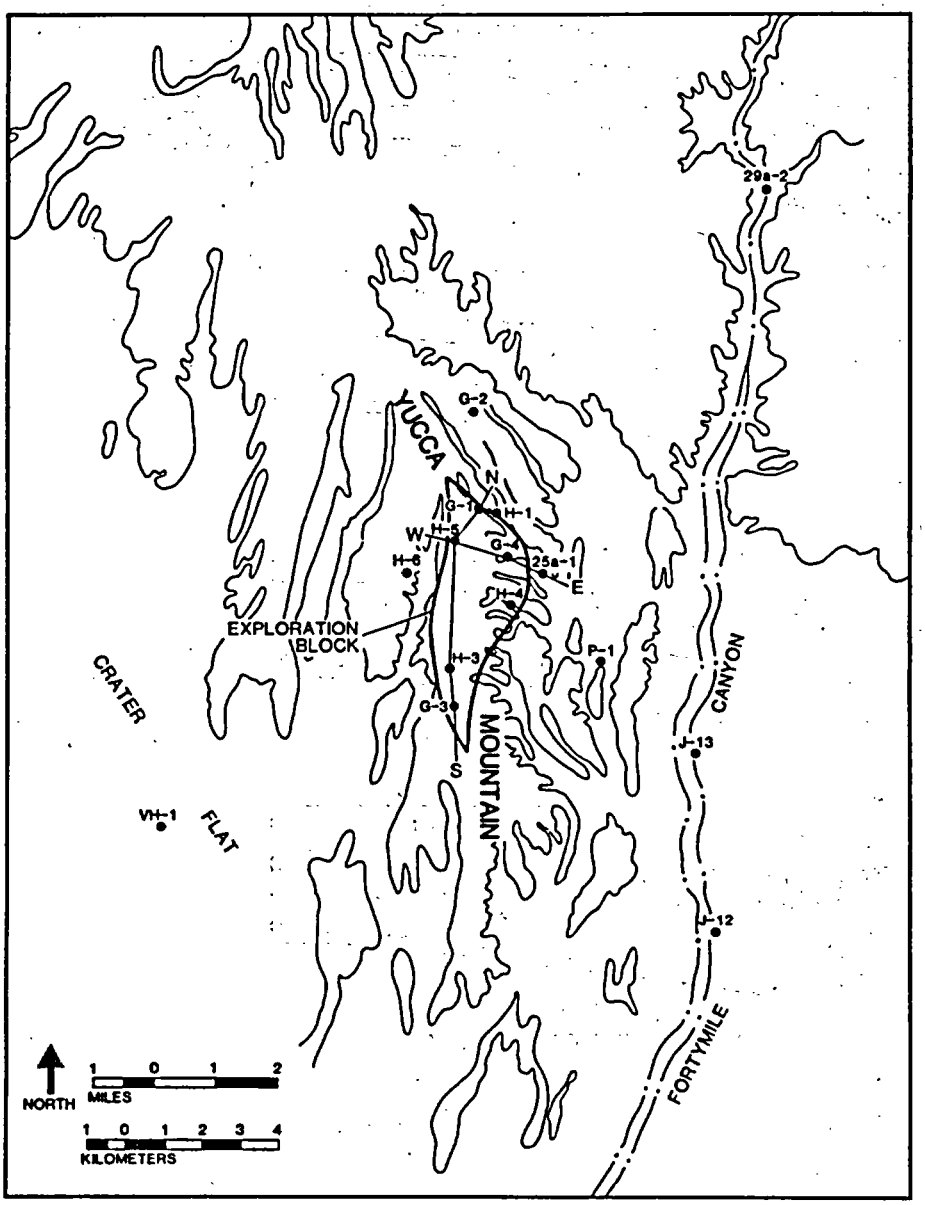

Fig. 23. Location map showing the exploration block at Yucca Mountain. Drill hole locations are indicated, as well as surface traces of west-to east (W-E) and north-to-south (N-S) cross sections used in Figs. 24-26.

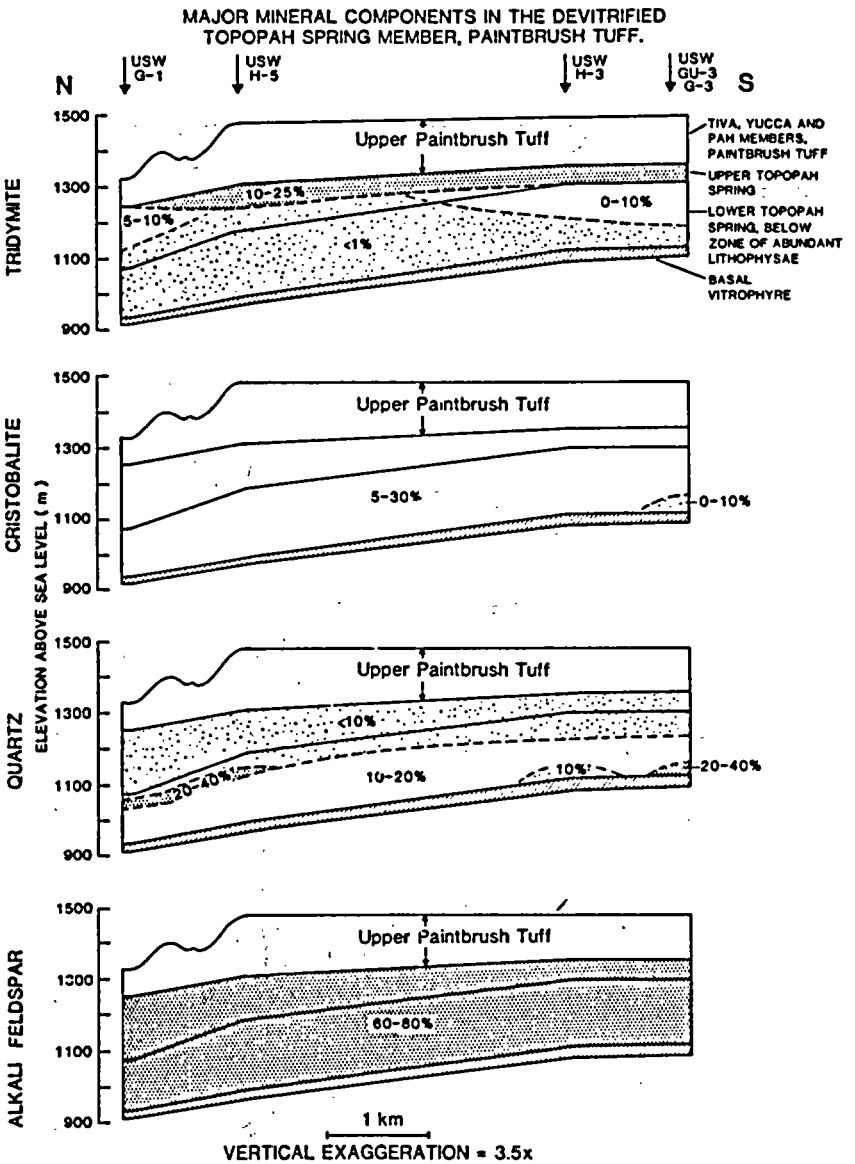

Fig. 24. North-to-south cross section through the Paintbrush Tuff, Yucca Mountain exploration block. Ranges of tridymite, cristobalite, quartz, and alkali feldspar abundance are indicated for the Topopah Spring Member of the Paintbrush Tuff; the lower Topopah Spring Member below the zone of abundant lithophysae and above the basal vitrophyre is the interval proposed for repository development. Note the transition from tridymite to quartz with increasing depth.

B. Mineralogy along Transport Pathways Away from the Repository

Intervals of sorptive zeolite formation were summarized in an earlier report.[5] The thicknesses and distributions of these and other petrologic zones beneath the host rock were refined during the review and revision of reports by Levy[34] and Vaniman et al.[35] As a result, it is possible to construct cross sections of the zeolitized intervals and other petrologic zones beneath the exploration block at Yucca Mountain.

Mineralogic variation within the host rock was discussed above. The variation in mineralogy beneath the host rock is discussed here. As mentioned above, the plain view in Fig. 23 shows the locations of two cross sections used to describe the variation in petrologic zones beneath the host rock. The two cross sections run generally N-S (Fig. 25) and E-W (Fig. 26). These cross sections show that the petrologic zones encountered are the same in all drill holes, although the thicknesses of these zones vary considerably across the exploration block. A listing of the major petrologic zones, in sequence of increasing depth, is given below.

(1) Host Rock.

(2) Zeolite Interval I. This is a zone containing up to 30% calcium-rich heulandite at the top of the basal vitrophyre within the Topopah Spring Member. This zone is commonly 2 to 3 m thick at Drill Hole Wash (USW G-1 and UE-25a#1) and along the eastern margin of the exploration block (solid lines in Figs. 25-26). The zeolite abundance in this zone decreases to trace amounts and minimal thickness (dashed lines in Figs. 25-26) to the south and at the ridge crest of Yucca Mountain.

(3) Basal Vitrophyre of the Topopah Spring Member. This zone consists predominantly of glass (40 to 90%) plus alkali feldspars, with some silica minerals and trace amounts of silicate and oxide phenocrysts. Perlitic fractures within the vitrophyre are commonly lined by trace amounts of smectite; zeolites occur in fractures at the top of the vitrophyre. The thickness of the basal vitrophyre ranges from 10 to 30 m; it is thinner toward the northeastern and eastern margins of the exploration block, where parts of the vitrophyre are altered, and thicker along the crest of Yucca Mountain, where the vitrophyre is relatively unaltered.

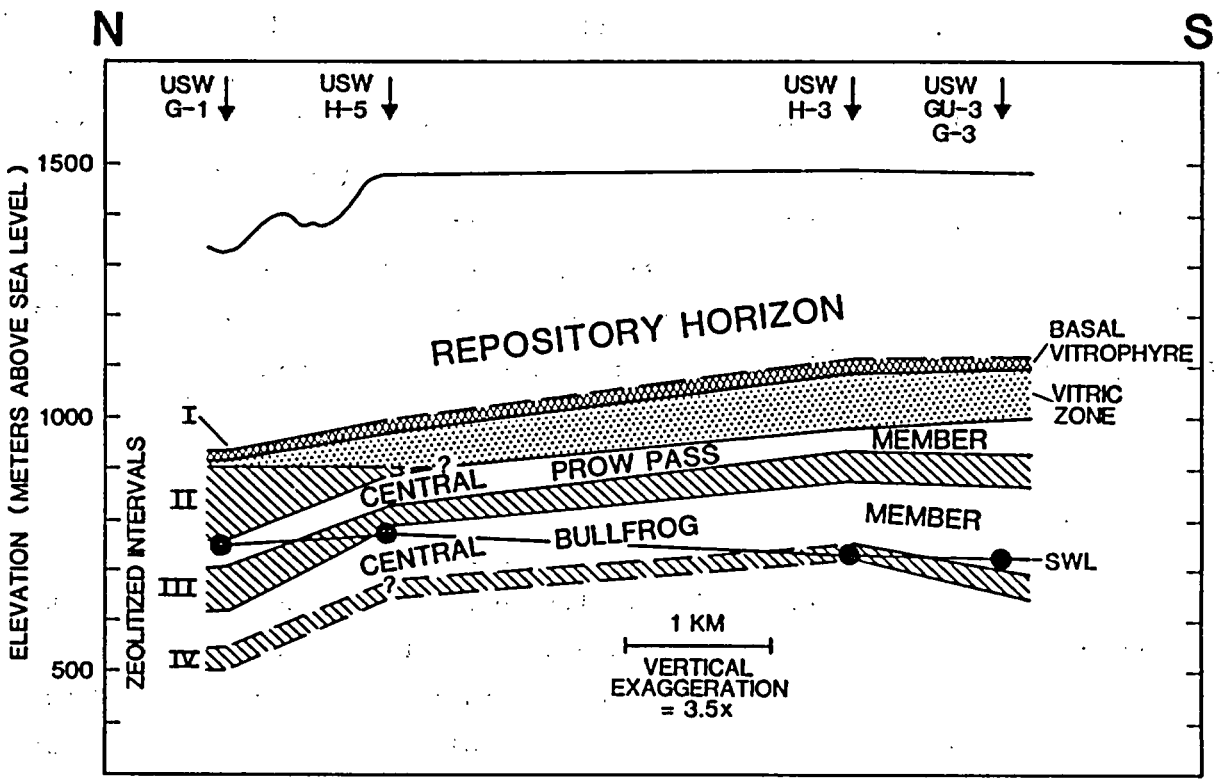

Fig. 25. The N-S cross section, which shows petrologic zones that occur below the repository horizon and their relations to the static water level (SWL).

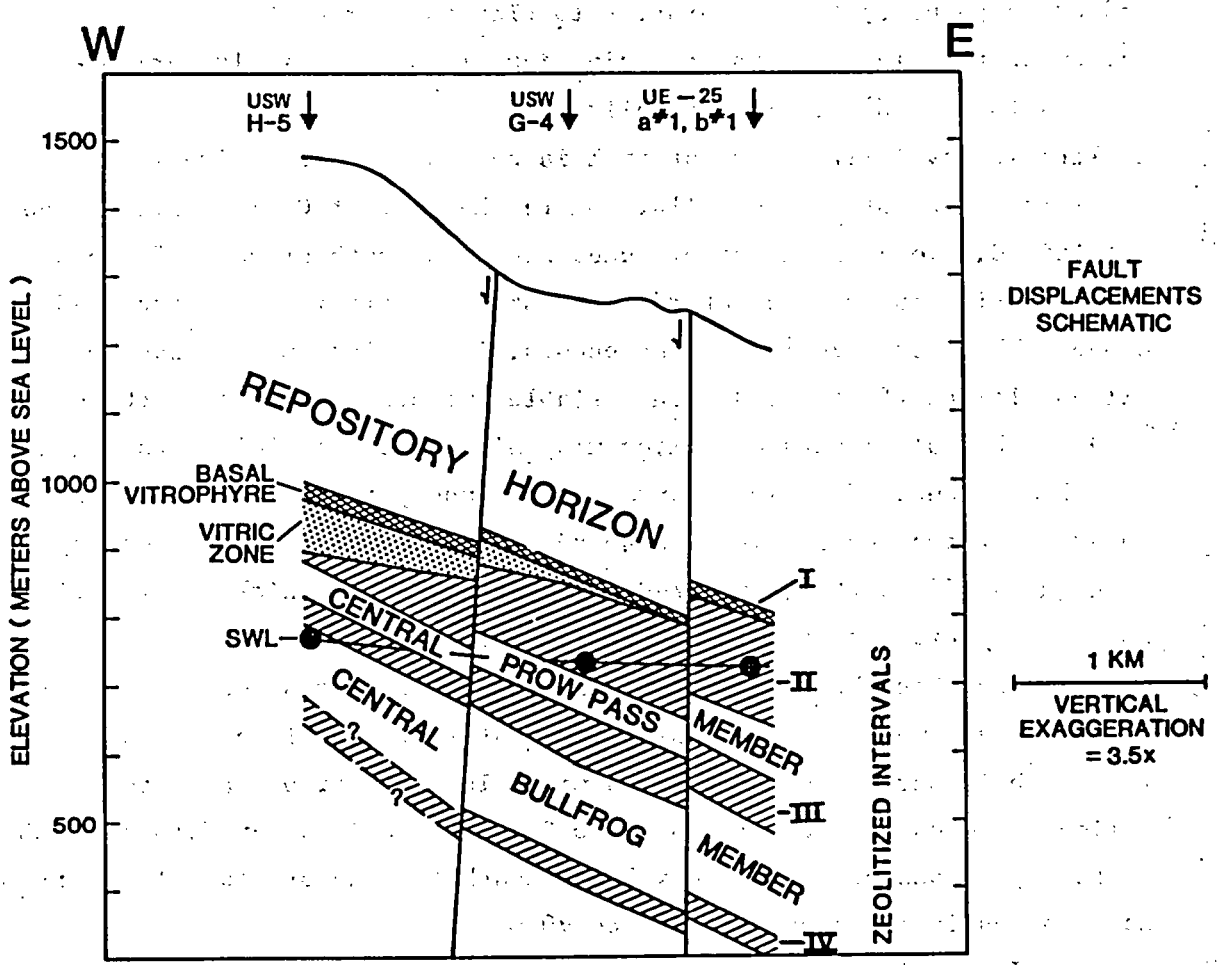

Fig. 26. The W-E cross section, which shows petrologic zones and the SWL below the repository horizon. Fault displacements are strictly schematic.

(4) Vitric Zone. This is an interval of moderately welded to nonwelded vitric tuffs, including the base of the Topopah Spring Member and, along the crest of Yucca Mountain, all or part of the underlying tuff of Calico Hills and parts of the upper Prow Pass Member, Crater Flat Tuff. This interval generally consists of about 40 to 80% glassy shards, with alkali feldspars and some silica minerals plus trace amounts of silicate and oxide phenocrysts. Alteration to clay is sparse; however, the bottom of this interval may contain significant but highly variable amounts (0 to 80%) of clinoptilolite.

(5) Zeolite Interval II. This interval is generally correlative with the zeolitized tuff of Calico Hills. Where the tuff of Calico Hills is not zeolitized, along the crest of Yucca Mountain south of USW H-5, this interval pinches out and interfingers with the vitric zone described above. Where this zeolitic zone occurs, it consists predominantly of clinoptilolite (50 to 70%) with variable amounts of mordenite (0 to 20%). Subequal amounts of silica minerals and alkali feldspars, with variable amounts of silicate and oxide phenocrysts (2 to 25%), make up the rest of the rock. Smectite abundances are generally low but may be as high as 15% in thin, interbedded layers. At its thickest, in Drill Hole Wash, this interval is 140 to 150 m thick.

(6) Central Prow Pass Member, Crater Flat Tuff. This is a zone of partially to moderately welded tuff, consisting mostly of alkali feldspars (60 to 70%) with lesser amounts of silica minerals and variable amounts of silicate and oxide phenocrysts (5 to 20%). Smectites may form up to 3% of some portions of this interval. Beneath the exploration block, this zone ranges in thickness from 45 to 90 m.

(7) Zeolite Interval III. This zone of zeolitization is continuous beneath the exploration block. At its thickest, 80 to 100 m in Drill Hole Wash and along the eastern margin of the exploration block, this zone consists mostly of clinoptilolite (30 to 50%) with lesser amounts of mordenite (~20%). Where this zone thins to ~30 to 60 m along the crest of Yucca Mountain, the only zeolite present is clinoptilolite (60 to 70%). The rest of the rock consists of alkali feldspars with smaller amounts of silica minerals and minor amounts of silicate and oxide phenocrysts. Smectite alteration is rare.

(8) Central Bullfrog Member, Crater Flat Tuff. The central Bullfrog Member varies from partially to densely welded and consists mostly of alkali feldspars (60 to 70%) with quartz (15 to 30%) and variable amounts of cristobalite (0 to 10%) and silicate and oxide phenocrysts (8 to 25%). Minor smectites (<1%) occur throughout this zone. This zone ranges in thickness from 70 to 160 m beneath the exploration block.

(9) Zeolite Interval IV. This zone, like Zeolite Interval III, is continuous beneath the exploration block. The thickness of this zone is relatively constant (30 to 45 m), but the zeolite composition ranges from mordenite dominant (35% mordenite and 10% clinoptilolite) to clinoptilolite only (35% clinoptilolite in USW G-3). Total zeolite abundance is 20 to 70% (lowest in Drill Hole Wash). The rest of this zone consists of alkali feldspar, quartz, and minor amounts of silicate and oxide phenocrysts. Smectite clays are locally abundant, forming up to 20% of some lenses within this interval.

(10) Deeper Petrologic Zones. Deeper petrologic zones are characterized by higher degrees of alteration. The sorptive zeolites (clinoptilolite and mordenite) are displaced by analcime and albite with increasing depth. The transition to abundant analcime occurs within a relatively consistent depth of 400 to 500 m below the present static water level (SWL). Discrete intervals of zeolitization begin to merge into the more thorough alteration at depth to clay, analcime, albite, calcite, and quartz, which affects phenocrysts and devitrification minerals as well as those portions of the tuff that were originally glassy.

All or part of the first nine zones described above, excluding (5), occur between the host rock and the SWL at the southern end of the exploration block. To the north and east in the exploration block, the SWL rises stratigraphically until only the first five zones intercede between host rock and SWL. This suite of petrologic zones includes the multiple zeolitic and nonwelded vitric zones that are important in overall retardation.

C. Petrofabric Constraints of the Age of Zeolitization at Yucca Mountain

This study uses indirect techniques to estimate the timing of zeolitization at Yucca Mountain. The principal technique is the examination of

geopetal structures in zeolitized tuffs. A geopetal structure is any rock feature whose form is influenced by gravity. The geopetal structures in tuffs at Yucca Mountain are pores (for example, bubbles in glass shards and cavities left by dissolved shards) that have been partly filled with opal, zeolite, clay, or any fine-grained detritus. The opal- and zeolite-filled pores are most useful for this study. Opal fillings commonly have very flat upper surfaces and may be visibly layered.

The opal geopetal structures are accumulations of opal particles that settled out of water in the pores, and the flat upper surfaces of the fillings were horizontal at the time of deposition. If the host rock were subjected to tectonic tilting while opal was being deposited, the upper surfaces of opal geopetal fillings might have differing orientations, and the angular difference would indicate the minimum amount of tilting that occurred. The tilting recorded by geopetal structures can be related to tectonic events of approximately known age. The timing of zeolitization, in turn, is indicated by textural relations between zeolites and geopetal pore fillings. For example, an accumulation of zeolite crystals at the bottom of a pore below an opal layer indicates that at least some zeolitization predated opal deposition. This relationship holds true for most of the samples studied. Additional textural criteria for relative dating of zeolites and geopetal pore fillings are described in Sec. VIII.C.5.

1. Methods. Standard thin sections that were cut approximately parallel to the drill core axis of the sample were mounted on a microscope mechanical stage. To measure the orientation of a geopetal structure, the flat upper surface of the structure was aligned with the horizontal (E-W) ocular cross-hair and the angle was read from the microscope stage vernier. Angle values are arbitrary and have meaning only with respect to each other; they are not comparable between samples. All measurements were made with a centered 20X microscope objective and 10X ocular; geopetal surfaces shorter than 0.13 mm were not measured.

The geopetal orientation measured in thin section is the orientation of the line of intersection between the planar geopetal surface and the plane of the thin section. Most measurements of opal geopetal surfaces are reproducible to 0.5°. Geopetal accumulations of coarser particles, such as zeolite crystals, may have more irregular upper surfaces; for these, measurements that could not be reproduced within 2° were rejected. For measurement

reproducibility in the 0.5 to 2° range, the plotted value is an average of two measurements. Experience has shown that a minimum of 15 experiments per thin section is necessary to delineate the distribution of geopetal orientations. The angle between any two measured geopetal orientations is an apparent angle less than or equal to the true angle; therefore, the amount of tectonic rotation measured from geopetal structure orientations in a sample is less than or equal to the true amount of rotation. It is important to emphasize that the evidence for tectonic rotation is the angular discordance between measured geopetal orientations.

2. Petrofabric Data. Geopetal orientation data are presented in Figs. 27 and 28 for the following samples; they are identified by drill hole, depth in feet, and stratigraphic unit. The samples are listed in approximate ascending stratigraphic order.

(1) USW G-1-2600: Bullfrog Member of the Crater Flat Tuff
(2) USW G-4-1438: tuff of Calico Hills
(3) USW H-5-1917: tuff of Calico Hills
(4) USW VH-1-1836: bedded tuff between the Prow Pass Member of the Crater Flat Tuff and the Topopah Spring Member of the Paintbrush Tuff
(5) USW G-4-1392: Topopah Spring Member of the Paintbrush Tuff

The USW prefix is omitted in subsequent references to these and other samples. Originally, all these samples were nonwelded glassy tuffs. The constitutents of measured geopetal structures are indicated in the figures.

3. Results. Most samples have two or more groupings of geopetal orientations. Such distributions can be attributed to tectonic tilting of the tuffs during or between periods of geopetal mineral deposition. A single grouping of measurements, as in sample H-5-1917, does not necessarily indicate that no tectonic displacement occurred during the period of geopetal mineral deposition; other factors, such as permeability changes and availability of pore-filling material, may limit geopetal deposition to a single episode.

4. Correlation with Structural History. Scott et al.[36] have determined that the major fault blocks of Yucca Mountain are bounded by N-NE-striking, commonly W-dipping, Basin and Range-style normal faults with displacement up to 100 m or more. Present day attitudes of the tilted Yucca

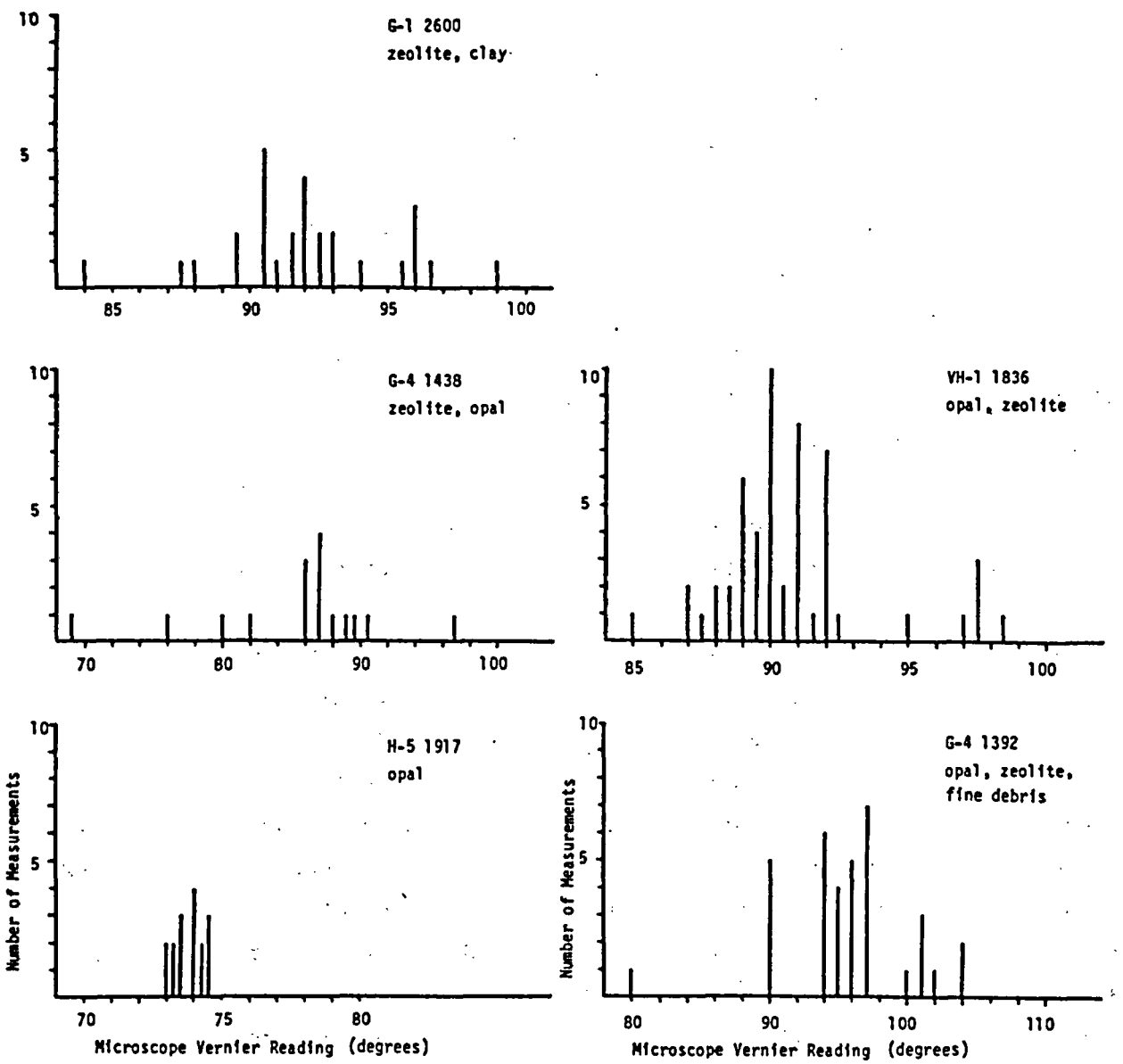

Fig. 27. Orientation of geopetal surfaces.

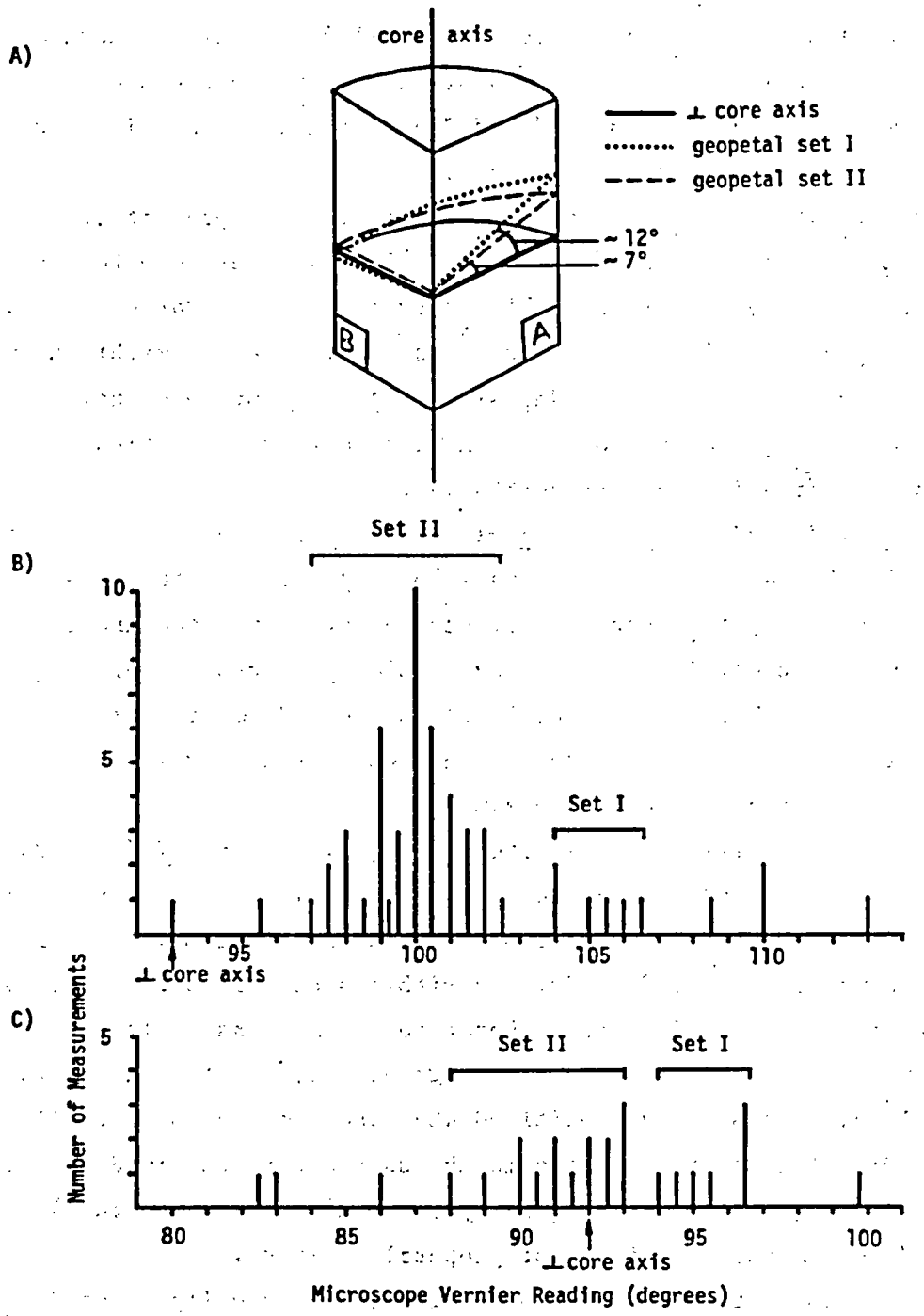

Fig. 28. Sample G-4-1392. (a) Orientation of thin sections G-4-1392A and B with respect to the drill core; reconstructed planar orientations of geopetal measurement sets I and II. (b) Relative orientations of geopetal surfaces and core axis, G-4-1392A. (c) Relative orientations of geopetal surfaces and core axis, G-4-1392B.

Mountain fault blocks are probably related to displacement along the bounding normal faults. Field evidence indicates that, with a few exceptions, tilting along these faults predated deposition of the 11.3-Myr Rainier Mesa Member of the Timber Mountain Tuff.[36,37] Scudies of faults in the Yucca Mountain area and vicinity by Swadley and Hoover[38] and Szabo et al.[39] show little or no evidence of major Quaternary displacement.

Textural relations in the samples examined for the present study indicate that substantial zeolitization had already occurred before the geopetal fillings were deposited. This means that zeolitization even in the youngest affected tuff (12.5 to 13 Myr)[40] was well advanced within about 1.2 to 1.7 Myr after the tuff was deposited. An attempt to quantify the amount of zeolitization contemporary with or predating deposition of geopetal fillings is presented in the next section.

5. Detailed Study of Sample G-4-1392. The abundant geopetal deposits in sample G-4-1392 were studied in detail to help estimate the alteration state of the tuff when the geopetal structures were deposited and to ascertain how much zeolitization, if any, could have occurred after geopetal deposition. This sample is from the basal, nonwelded portion of the Topopah Spring Member, very close to the top of the youngest interval that is extensively zeolitized at Yucca Mountain.

Examination of partially zeolitized tuffs, like H-4-1312 (Ref. 34), indicates that pumice and fine-grained ash are heavily to completely altered before shards have undergone appreciable alteration. The majority of geopetal deposits in sample G-4-1392 are within secondary pores created by the complete dissolution of shards; therefore, it is reasonable to assume that the pumice and ash in this sample, together representing about 75% of the rock volume, were already zeolitized when the geopetal pore fillings were deposited. Dissolved shard cavities in the sample were examined to estimate what proportion of the shards (originally about 25 vol% of the tuff) may have been altered before the deposition of geopetal fillings.

There are two parts to this study. First, two mutually perpendicular thin sections were cut from a portion of drill core in such a way that the position of the core axis (long axis of the cylindrical core) could be located on each thin section (Fig. 28a). Upper surface orientations of suitable geopetal fillings and the orientation of the core axis were measured for each section, using the technique described in Sec. VIII.C.1. The

results are plotted in Figs. 28b and c. In both thin sections, at least two sets of geopetal orientations have been tentatively identified and are labelled sets I and II. The correlation of sets between thin sections is uncertain and is based on assumed correspondence of the largest and next largest sets of measurements from one thin section to the other. Approximate reconstructed planar orientations of both sets are shown in Fig. 28a.

The rationale for constraining the time of zeolitic alteration has been discussed in a previous section. If any of the geopetal filling surfaces in an altered tuff are horizontal, then those fillings could have been deposited any time after the last period of most active local tectonism (before 11.3 Myr); therefore, the horizontal fillings place no minimum age constraint on shard dissolution or zeolitization. To identify horizontal geopetal fillings would provide a means of estimating what proportión of filled shard cavities could represent shards that were altered after the tectonic activity.

The measured drill hole deviation at the 1400-ft-depth (426.7 m) in drill hole USW G-4, which indicates the deviation of the core axis from vertical, is 6 to 6.5° in the approximate direction S50°W.[41] The drill core itself is unoriented and the dip direction of the geopetal surfaces in samples G-4-1392A and G-4-1392B cannot be determined. The dip directions measured in oriented core from other segments of the Topopah Spring tuff mostly lie between N53°E and S80°E (Ref. 42). If the dip directions of the geopetal surfaces were within this range, none of the measured geopetal surfaces could be horizontal because rotation of the orientation data to bring the core axis to its true position would increase the dip of the geopetal surfaces. For any of the geopetal surfaces to be horizontal, their dip directions would have to be close to the drill hole deviation direction. This case seems unlikely, but it merits evaluation to help estimate the maximum possible proportion of geopetal surfaces that could be horizontal. The number of potentially horizontal surfaces in proportion to all measured geopetal surfaces can be estimated from the data from the thin section for G-4-1392A (Fig. 28b), which is an approximate dip section through the geopetal surfaces (the section is about parallel to the dip directions of the geopetal surfaces). Geopetal surface measurements that lie within 6 to 6.5° of the perpendicular to the core axis could be horizontal; such measurements represent 27 to 34% of all geopetal measurements for this thin section.

These percentage values are overestimates of the possible proportion of horizontal geopetal surfaces because a single rotation could not bring all the values to a horizontal position; however, further refinement of the values is not practical.

The second part of this study involved a survey of dissolved shard cavities in sample G-4-1392 to determine what proportion of cavities contain geopetal fillings. Cavities with no fillings represent alteration whose timing cannot be constrained by the tectonism-geopetal filling association. Similarly, any zeolites that crystallized within shard cavities after geopetal fillings were deposited would be of younger, but indeterminable, age than the fillings.

The most common type of shard alteration is replacement of the shard boundary by a zeolite rind of variable thickness and dissolution of the remainder of the shard. Geopetal fillings were then deposited in the secondary pores created by shard dissolution. The principal geopetal fillings are zeolite and opal-cristobalite. In nearly all geopetal fillings containing both materials, the zeolite is the earlier pore filling and is overlain by opal-cristobalite. It is assumed that these geopetal fillings were deposited at about the same times as the fillings whose upper surface orientations were measured and plotted in Fig. 27. Textural evidence indicates little or no zeolite crystallization within shard cavities following deposition of geopetal fillings. Zeolite crystals at the upper surfaces of geopetal deposits tend to be slightly coarser than underlying crystals and may project into the shard cavities. This texture may indicate postdepositional crystal growth.

The information recorded for each dissolved shard cavity examined in thin section includes the geopetal filling (if any), other alteration products, and the apparent long dimension of the relict shard. Proportions of shard cavities with geopetal fillings, by size class, are listed in Table XII. This study has shown that very small dissolved shard cavities (<0.3 mm) and the thinnest parts of larger shard cavities are unlikely to contain geopetal fillings because the zeolite rind fills most of the relict shard, leaving little or no pore space. For this reason, data for larger shards (>0.3 mm) are considered to be more reliable indicators of geopetal filling abundance. The emphasis on data for larger shards is also justified

TABLE XII

ABUNDANCE OF GEOPETAL FILLINGS IN DISSOLVED SHARD CAVITIES (SAMPLE G-4-1392)

Long Dimension of Dissolved Shard (mm)	Dissolved Shards with Fillings/Total Shards	Abundance (%)
<0.1	10/33	30
0.1 - 0.19	46/83	55
0.2 - 0.29	38/64	59
0.3 - 0.39	16/18	89
0.4 - 0.49	8/8	100
0.5 - 0.59	15/16	94
0.6 - 0.69	5/7	71
0.7 - 0.79	2/2	100
0.8 - 0.89	2/2	100
0.9 - 0.99	0/0	—
>1.0	7/7	100
>0.3	55/60	92

Total Measurements: 240

because the larger shards should have been among the last vitric components to be completely altered.

Results of the survey for shard cavities >0.3 mm across show that 92% of such cavities have geopetal fillings. This figure can be combined with values obtained in the first part of this study according to the following relationship:

vol% of pumice and ash in original tuff
+ [(vol% shards in original tuff) x (minimum fraction of measured geopetal fillings with nonhorizontal surfaces) x (fraction of shard cavities with geopetal fillings)]
= minimum vol% of vitric material altered before or during tectonism (before 11.3 Myr ago)
= 75% + [(25%) x (0.66 to 1.0) x (0.92)]
= 90 to 98%.

These results suggest that the tuff was almost completely altered by the time most geopetal fillings were deposited, earlier than 11.3 Myr ago. With so little unaltered glass remaining in the rock, zeolitic alteration rates since then must have been close to zero.

6. Paleohydrologic Evidence from Geopetal Structures. Some geopetal fillings show signs of disruption by moving water (for example, ripped-up layers of opal in G-1-2166). Water probably cannot move through saturated tuff rapidly enough to cause such erosion. The disrupted geopetal fillings may indicate that at some time during the period of alteration water was moving rapidly through incompletely saturated rock. The rapid water movement must have been episodic because geopetal accumulations of fine opal particles must be deposited from still water. This textural evidence suggests that some zeolitization may have occurred around or above the SWL. At 2166-ft-depth (660.2 m), the zeolitic tuff in USW G-1 is below the present SWL and must therefore have been altered before the present hydrologic regime was established.

7. Possibility of Future Alteration. Zeolitic alteration of volcanic glass, whether above or below the SWL, requires large amounts of groundwater. The major zeolite features at Yucca Mountain were formed before the Quaternary Period, and zeolitization should remain essentially inoperative during the next 100 000 years because of the near absence of volcanic glass below the present SWL and for several hundred feet above the SWL as well. Remaining unaltered glass below the SWL is almost all within vitrophyres that are highly resistant to alteration because of their low porosity and permeability.[3,43] Thus, the rate of zeolitization that results from natural causes should remain close to zero, barring climatic changes that would increase the local groundwater recharge or significantly raise the SWL at Yucca Mountain above the highest level reached during Pleistocene time.[44]

D. Effects of Composition on Thermal Expansion/Contraction Behavior of Clinoptilolite

Six natural and three cation-exchanged (sodium, potassium, and calcium) clinoptilolites have been examined by XRD at temperatures from 20 to 300°C in a heated sample holder. Unit cell parameters were refined from x-ray data every 50°C to determine the compositional effects on thermal expansion/contraction. The effects of exchangeable cation were very pronounced;

sodium-saturated clinoptilolite contracted about 8.5% between 20 and 300°C, calcium-saturated clinoptilolite contracted about 3.5%, and potassium-saturated clinoptilolite contracted about 1.6%. The bulk of the contraction in the potassium-saturated material occurred upon evacuating at 20°C (0.1 torr), and the sodium-saturated clinoptilolite contracted between 50 and 100°C, reaching a relatively constant volume by 150°C. Calcium-saturated clinoptilolite continued to contract up to 300°C. Natural samples with mixed exchangeable-cation compositions exhibited intermediate amounts of thermal contraction but generally continued to contract up to 300°C. Samples of clinoptilolite from the basal Topoaph Spring Member in USW G-4 exhibited intermediate amounts of collapse, similar to calcium-exchanged clinoptilolite. Clinoptilolite from above the basal Topopah vitrophyre in USW G-4 behaved like heulandite, reversibly forming a highly collapsed "B phase" at 200°C. In all samples, cation-exchange and natural, a reduction in the b cell dimension was primarily responsible for the decrease in volume. This is probably the result of collapse of the channels parallel to c and a. Expansion behavior upon cooling in a vacuum was variable, but most samples rapidly reexpanded and the calcium-rich samples completely expanded to the preheating in-vacuo volume. Sodium-rich samples reexpanded completely in a few minutes in the room atmosphere. These data provide information on the nature of the channels at elevated temperatures and they explain the variability in macroscopic thermal expansion data obtained for zeolitic tuffs from the NTS.

IX. VOLCANISM (B. M. Crowe, D. T. Vaniman, D. B. Curtis, and N. Bower)

Volcanism studies are being conducted for the NNWSI to evaluate the relative hazards of future volcanism, with respect to storage of high-level radioactive waste. The required work for volcanism is almost complete; work during this quarter concentrated on continuing updates of the SCP and on geochemistry studies needed to resolve data uncertainties identified in an earlier report.[45]

Review comments of volcanism sections of the SCP were examined and incorporated in revisions of the document. These comments were received from consultants of the DOE, ERTEC Associates, SAI, and by personnel of the USGS who are not associated with the NNWSI. Responses were made to all review

comments either through changes in the text of the SCP or through written comments sent to M. Carr of the USGS.

Areas of uncertainty identified in the volcanism status report include (1) mechanism and conditions of formation of shallow basalt intrusions; (2) geochemical patterns of basalt geochemistry through time; (3) possible recurrence of bimodal volcanism; and (4) origin of the trace-element enrichment in younger rift basalts. Work during the quarter focused on the latter three topics.

The major- and trace-element geochemistry of the basalts of the NTS region shows distinct compositional variations through time. These variations correlate closely with the three defined basalt episodes: the basalts of the silicic episode, the older rift basalts, and the younger rift basalts.[46] Basalts of the silicic episode are classified into three groups, based on normative compositions projected onto the basalt tetrahedron (Ne-Ol-Di-Hy-SiO, Fig. 29): (1) Straddle-type hawaiites that cluster near the Di-Hy join. These rocks, which are similar to the basalts of Crater Flat,[47] show an inverse variation between normative nepheline or hypersthene composition and magnesium number. Rocks with higher magnesium numbers (less fractionated from parental compositions) cluster near the Di-Hy join. Those with lower magnesium numbers plot away from this join and within the hyperstene or nepheline fields of the basalt tetrahedron. (2) Hypersthene-hawaiites that show a direct covariation between magnesium number and normative hypersthene composition. These rocks plot in the center of the Ol-Di-Hy portion of the basalt tetrahedron and show increasing normative hypersthene with increasing magnesium number. (3) Basalts and basaltic andesites that cluster near the Di-Hy join and project into the field of quartz saturation. The older rift basalts (Fig. 30) show a limited range of compositional variation, and all samples analyzed exhibit the straddle-type association. Rocks of this suite contain normative nepheline, with one exception: the basalt of Silent Canyon. Some of the samples from Paiute Ridge are classified as basanites (Ne > 5%). The younger rift basalts follow the same three groups as the basalts of the silicic episode, with minor differences (Fig. 31). First, the majority of the younger rift basalts are straddle-type basalts; only a few samples are hypersthene-hawaiites or show quartz saturation. Second, all samples that make up the quartz-saturation

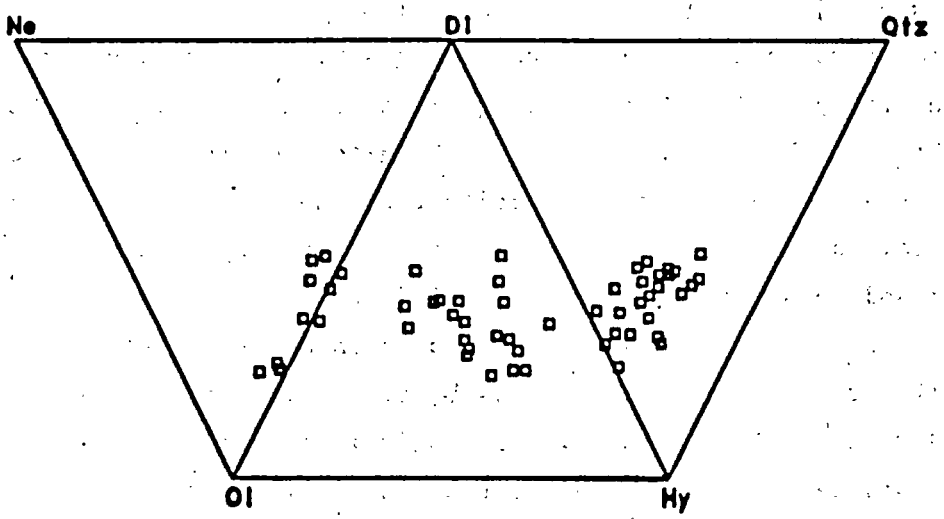

Fig. 29. Normative compositions for the system nepheline-olivine-diopside-hypersthene-quartz; basalts of the silicic episode.

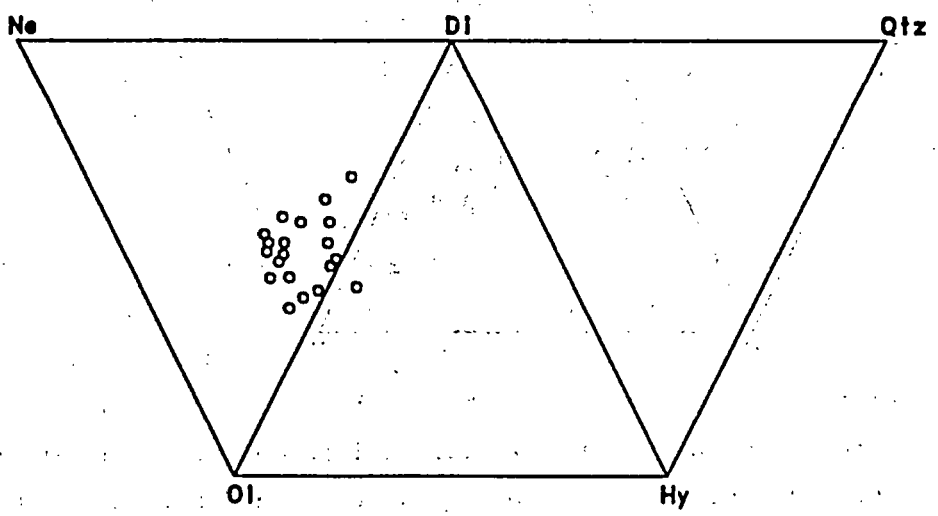

Fig. 30. Normative compositions for the system nepheline-olivine-diopside-hypersthene-quartz; older rift basalts.

group show very small contents of normative diopside (diopside-poor hawaiites of Buckboard Mesa).

There are major changes in the trace-element contents of the three basalt cycles through time. As noted previously,[45,47] the younger rift basalts are highly enriched in incompatible trace elements, with the exception of rubidium, whereas the older rift basalts exhibit trace-element contents that are more typical of basalts throughout the Great Basin. Newly obtained data, mostly for the basalts of the silicic episode, show that each volcanic episode has differing patterns of trace-element abundances. Potassium, a minor element that behaves as an incompatible element in basalt systems, illustrates the divergence of the older rift basalts from the silicic and younger rift episodes. Figure 32 is a plot of K_2O vs Na_2O for all basalt episodes. This plot shows the generally lower K_2O content of the older rift basalts. The basalt regression line, from Chayes,[48] is based on Hawaiian samples but is appropriate for illustrating K_2O-Na_2O covariation in

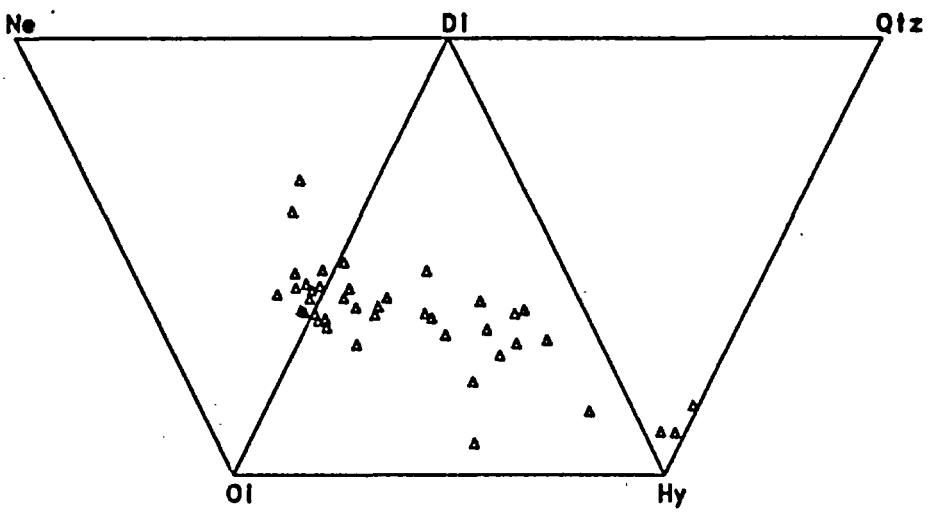

Fig. 31. Normative compositions for the system nepheline-olivine-diopside-hypersthene-quartz; younger rift basalts.

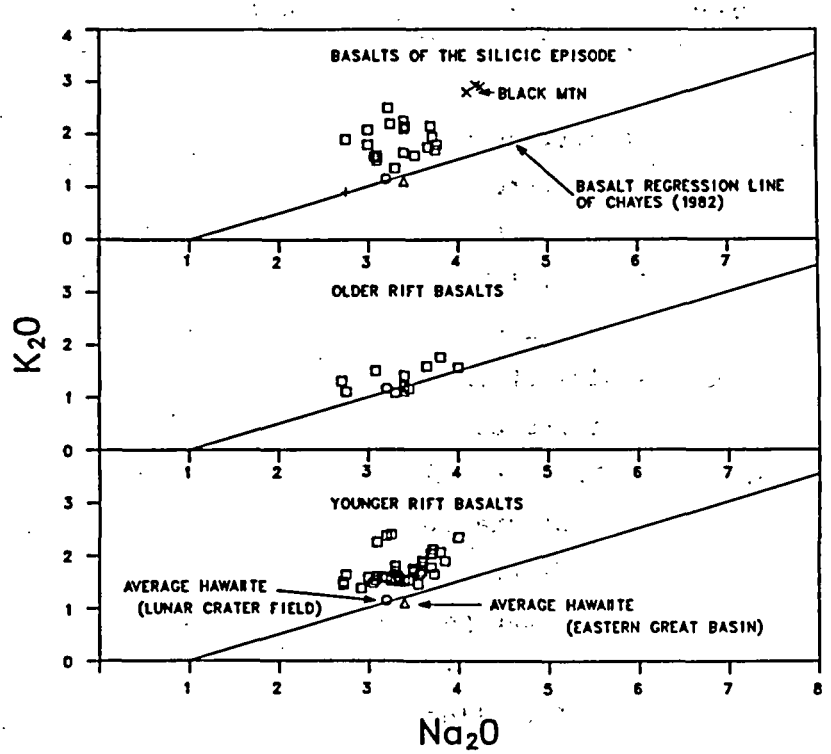

Fig. 32. The K_2O vs Na_2O diagram for the basaltic episodes of the NTS region.

continental basalts of tholeiitic and hawaiite affinity. The older rift basalts are similar to most other basalts of the world, whereas the basalts of the silicic and younger rift episodes are atypically enriched in potassium. It is important to understand the origins of the two trace-element-enriched basaltic episodes of the NTS region.

Figures 33, 34, and 35, respectively, show the variation of lanthanum, strontium, and thorium with time in hawaiite basalts of the NTS region. These elements represent three major groups of incompatible elements: lanthanides, alkaline earths, and actinides. Lanthanum concentration is lowest in the older rift basalts, intermediate in the basalts of the silicic episode, and highest in the younger rift basalts. The 3.7-Myr basalt of southeastern Crater Flat are more similar in composition to the basalts of the silicic episode. This pattern of chemical variation with time is repeated in the alkaline earth elements (Fig. 34) and the actinide elements (Fig. 35).

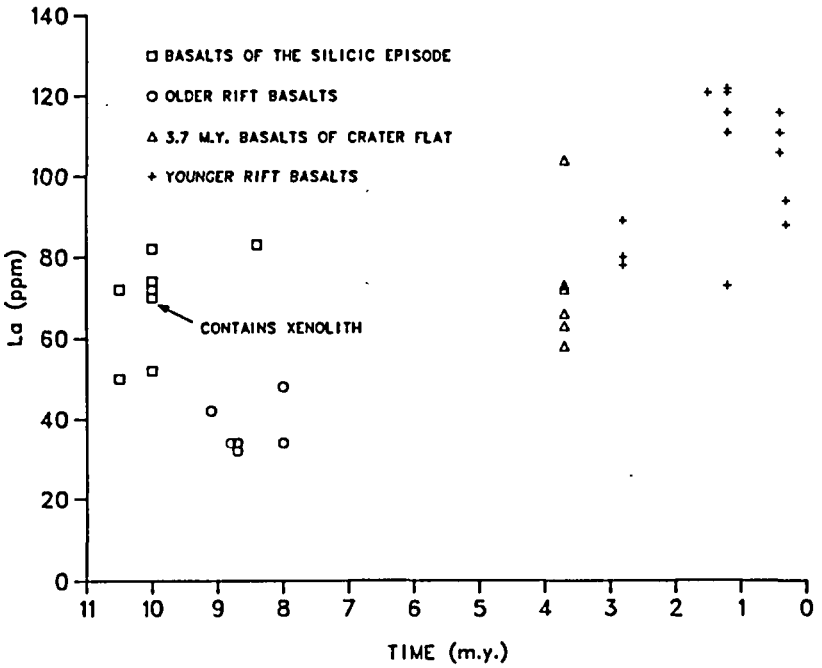

Fig. 33. Lanthanum vs time diagram for basaltic episodes of the NTS region. Plotted points are restricted to basalts (SiO_2 < 54%).

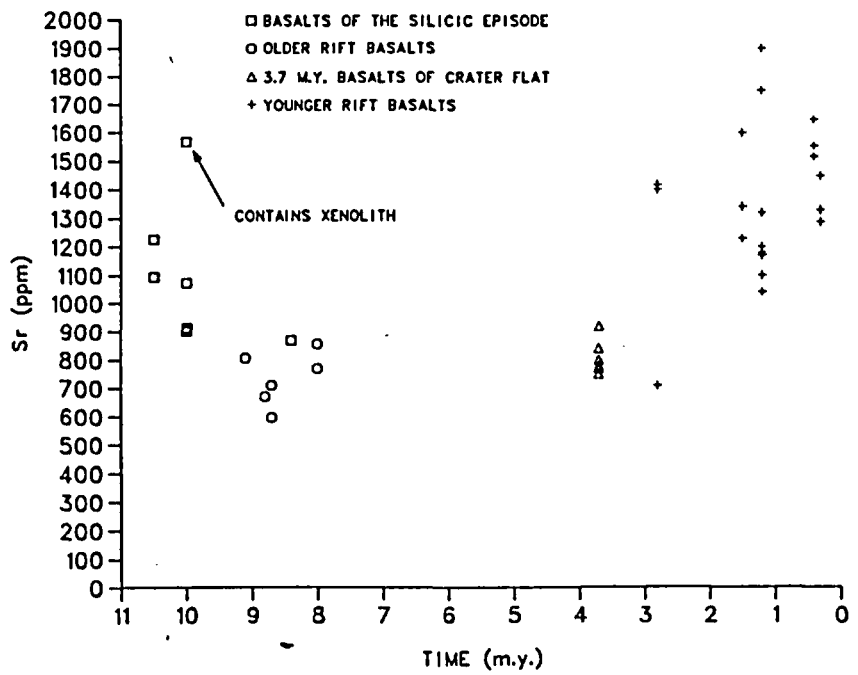

Fig. 34. Strontium vs time diagram for basaltic episodes of the NTS region. Plotted points are restricted to basalts (SiO_2 < 54%).

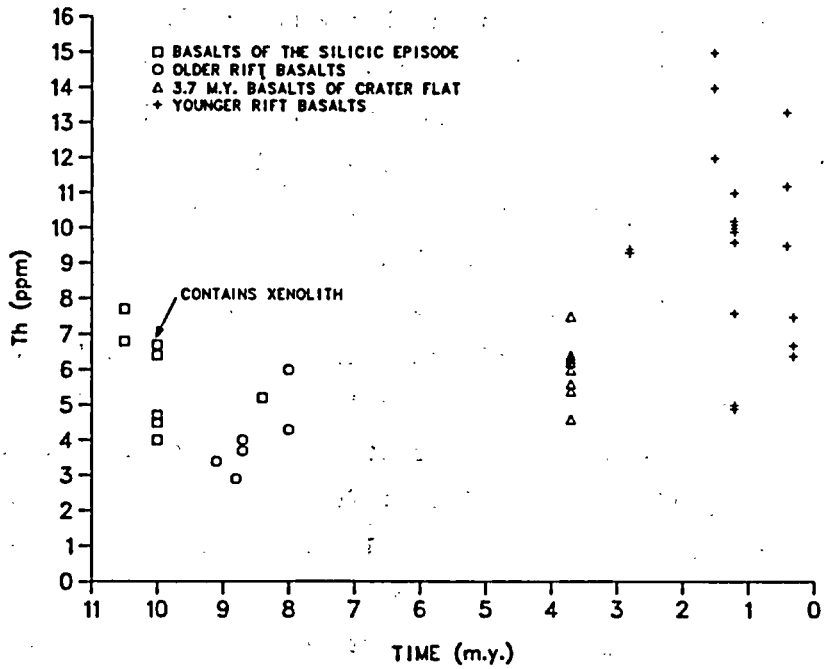

Fig. 35. Thorium vs time diagram for basaltic episodes of the NTS region. Plotted points are restricted to basalts (SiO_2 < 54%).

Although the patterns of trace-element enrichment are consistent for each group of incompatible elements, the relative magnitude of variation is different for each incompatible element. If the average trace-element contents of the basalt episodes are normalized to the average concentration of respective elements in the older rift basalts, enrichment factors can be calculated as follows:

	Silicic Episode		Older Rift		Younger Rift
Lanthanum	2	:	1	:	2.9
Strontium	1.4	:	1	:	2.1
Thorium	1.5	:	1	:	2.6

These enrichment factors show an overall incompatible-element enrichment in both the basalts of the silicic episode and the younger rift basalts; the greatest degree of enrichment is in basalts younger than 3.7 Myr.

The processes that are likely to account for the incompatible-element enrichments can be classified into three categories: (1) mantle metasomatic processes, (2) decreases in the degree of partial melting in the mantle source regions, and (3) contamination of basalts during ascent by trace-element enriched crustal rocks. One test of the third possibility, crustal contamination, is shown in Figs. 33-35. These figures highlight an analyzed sample from the basalts of the silicic episode, which contain an inclusion of sillimanite-plagioclase-spinel-monazite mineralogy, a possible lithology of the lower crust. Only the strontium content of this sample (Fig. 34) appears significantly different for the representative incompatible elements, which suggests that this possible contaminant cannot account for the overall patterns of incompatible-element enrichment. Other types of contamination may operate in both the crust and the mantle, and these possibilities are being investigated through isotopic studies of strontium and neodymium by S. Semken of Massachussets Institute of Technology. However, these two isotopic systems only define a mantle line from which crustal contaminants may deviate. A more rigorous test is provided by the mantle plane for the neodymium-strontium-lead isotopic systems.[49] Work is under way to add lead isotopic data to the neodymium and strontium isotopic data, and results of this work will be presented in the next quarterly report.

Considerable progress has been made toward resolving the question of future bimodal volcanism. Drill Hole VH-2, drilled in the central part of Crater Flat, penetrated a sequence of basaltic lavas at about 1100 ft beneath the surface. These lavas overlie the Timber Mountain Tuff and are overlain in turn by alluvial deposits and slide breccia deposits of Paleozoic rocks that were probably emplaced during the uplift of Bare Mountain. The basaltic lavas have been analyzed for their major- and trace-element contents. They are similar to a sequence of reversely magnetized lavas and cone scoria that were exposed at the southern end of Crater Flat and dated at about 10.5 Myr. The lavas of Drill Hole VH-2 yielded a potassium-argon age of about 11 Myr, and they are also reversely magnetized. This suggests that the two lavas are related and that basalt flows of this general age probably underlie much of

the western and southwestern part of Crater Flat. Further, the reversed aeromagnetic anomalies of Crater Flat[50] could reasonably be attributed to the presence of these flows and not to the presence of buried silicic domes. This theory is supported by the absence of silicic debris in the alluvial deposits of Crater Flat above the lava flow. If buried rhyolite domes younger than 10 Myr are present in Crater Flat, eroded dome debris of pyroclastic deposits related to the domes should be present in the alluvial sections of Drill Hole VH-2 or VH-1. The absence of these deposits suggests that there has not been any major silicic volcanic activity younger than 10 Myr in the Crater Flat area.

The 134 major-element chemical analyses of basalt samples in the NTS region have been entered and edited in the DATATRIEVE data base management system of the VAX 11/780. This includes all available chemical data for basalts of this region that have been obtained through the volcanism studies for the NNWSI or from published sources. The data base system is being used to selectively sort and report geochemical data for an evaluation of time-petrological patterns of volcanism in the NTS region. The data base system also provides a documented source of data generated by the volcanism studies, which can be used to satisfy quality assurance requirements. The 58 major-element analyses of volcanic rocks of the Death Valley-Pancake Range volcanic belt have been entered but have not yet been edited in the DATATRIEVE system.

Geochemical procedures using wavelength dispersive x-ray fluoresence analyses were developed for analyses of nickel, chromium, strontium, and rubidium in basalt samples of the NTS region. This makes it possible to obtain better data for these elements than can be obtained through techniques of INAA. Seventy samples of selected basalts were analyzed for these elements during the quarter. This trace-element data, in addition to data from rapid INAA and radiochemical INAA, will also be entered into the data base management system. The structure for this data base has been developed, but the data have not yet been entered.

Recently published geologic papers on hydrovolcanic eruptions and ongoing research concerned with vapor explosions that result from interaction of fuel and coolant systems in nuclear reactors have both been reviewed. The 1980 eruption of Mount St. Helens (the opening eruption) had a significant hydrovolcanic component, and as a result, increased attention has been given

to magma/water interactions as a mechanism for producing explosive volcanism. This new work and the recent discovery of two additional sites of past hydrovolcanic volcanism (basalts of Nye Canyon) have raised questions about the effects of hydrovolcanic activity associated with possible future volcanism at Yucca Mountain. This possibility was not considered in past volcanic-consequence analyses for a number of reasons:

- the considerable depth to groundwater at Yucca Mountain,
- the absence of surface or perched groundwater at Yucca Mountain, and
- the low flux of moisture in the unsaturated zone.

A current inconsistency exists between field studies of past sites of hydrovolcanic eruptions and new theoretical data on the effects of pressure on vapor explosions. Field studies invariably indicate a relatively shallow source of water for hydrovolcanic explosions, whereas theoretical calculations indicate that depth (pressure effect) may not be a critical factor. Under some conditions, basalt may intermix at depth with water in a supercritical state. With further ascent of basalt, a pressure release could cause this supercritical water to flash into steam that drives vapor explosions. Further work will be undertaken on the question of future hydrovolcanic activity at Yucca Mountain.

X. ROCK PHYSICS (J. D. Blacic)

This quarter long-term creep tests have continued on zeolitized Calico Hills tuff from USW G-4 for borehole sealing and other applications. Tests have ranged from about 5 to 30 days. During these tests, steady-strain rates as low as 6×10^{-10}/second were measured. Because these tests are of long duration, sufficient data has not been accumulated to characterize the mechanical response of Calico Hills tuff in the form of a constitutive equation. However, there have been several interesting and unexpected phenomena in tests.

First, unexpectedly long pore saturation times have been encountered, ranging up to 5 weeks (sample volume is about 250 cm^3). These long saturation times appear to be the result of continued high porosity and low permeability, typically 25% and 0.5 microdarcy, respectively, in the samples.

This implies that equilibrium pore pressure of effective stress conditions in large volumes of tuff, characterized by combined high porosity and low permeability, will be difficult to achieve in any reasonable time. This problem could impact interpretation of the heated block or other in situ tests.

Second, in one experiment performed at low deviatoric stress, the sample slowly lengthened against the stress. This is apparently the result of slow swelling during rehydration of the sample, which is analogous to the clay swelling-induced stresses that are well known in engineering practice. The implication is that stresses at least as high as 20 MPa might result from changes in hydration of zeolitized tuff. The altered vitrophyre layer below the candidate host rock zone in the Topopah Spring would be a possible location where these effects could occur. The induced stresses could be either compressive or tensile, depending on whether the zeolites were hydrating or dehydrating, respectively, and could therefore change rock mass permeability during postclosure or could cause other changes. Further work is necessary to determine if the net effect of this change would be favorable or adverse.

XI. SHAFT AND BOREHOLE SEALING (D. M. Roy, C. J. Duffy, and R. J. Vidale)

A. CON-14 Studies

A significant portion of this quarter's activities has been devoted to data analysis and preparation of the topical report dealing with evaluation of the accelerated stability of a proposed tuff sealing material, highlights of which are outlined below.

Reactivity of the concrete CL-40 CON-14, prepared from a shrinkage-compensating cement and indigenous aggregate (crushed tuff, coarse aggregate, and local sands) was investigated. The 2.5-cm-diam-disk samples and fine powders were chemically reacted under a variety of conditions that were designed to represent (1) an extremely accelerated, static condition, (2) an accelerated reaction with a concrete monolith, and (3) exposure of a concrete to elevated-temperature aqueous vapors to simulate possible exposure conditions when sealing a nuclear-waste repository located in tuff. These three represent different end-member conditions that might arise in an unsaturated hydrogeological repository environment; the conditions are accelerated by temperature to simulate prolonged time exposure.

Disks of CON-14 exposed to the vapor phase at 200°C exhibited similar but much less intense alteration reactions, contrasted to those exposed to liquid. Large, glassy, poorly welded tuff aggregate particles revealed deep weathering at 1-month exposure with extensive surface scaling and crystalline alteration products developing at all times greater than or equal to 2 months. The scale material consisted of very fine calcium silicate phases with varied morphologies and euhedral crystals of calcium sulfate, presumably from the thermal decomposition and dissolution of ettringite.

Parallel studies, in which powders of CON-14 were reacted with a 10-fold excess of groundwater from the Well J-13, supported the observation that ettringite is unstable at these test conditions. In addition, smectite formed as the solution in contact with the concrete became saturated.

Hydrothermal solutions at 200°C produced extensive alteration of the vitrophyric tuff aggregates in the concrete disks, whereas the more crystalline, densely welded tuff aggregates were much less altered. Quartz xenoliths in the vitrophyric tuff grains apparently resisted alteration. The cementitious matrix material exhibited an intermediate degree of resistance to hydrothermal alteration; preexisting cracks exhibited the majority of the alteration along edges that formed the crack. No surface scaling or development of individual crystalline material was observed on the surfaces of the monolith. These observations suggest that the groundwater solution used as a mineralizer in the hydrothermal reactions was unsaturated.

B. Reactions of Simulated Concrete with Topopah Spring Tuff

With the completion of the CON-14 studies, studies on accelerated curing and reactivity of potential tuff repository sealing materials will concentrate on the evaluation of the behavior of a silica-rich cementitious mixture PSU/MRL #82-22 and a tuff from the Topopah Spring Member. Samples were prepared with a prism of tuff cast into a cylindrical specimen, surrounded by the mortar 82-22. Disks cut perpendicular to the cylinder axis were exposed to accelerated reaction by immersion in hydrothermal fluids (Well J-13 groundwater) and, in other experiments, to the vapor phase above Well J-13 water. Replicate experiments involving a mechanical mixture of tuff and #82-22 cured cement mortar that was ground to -20+30 sieve size were completed in a rocking autoclave at similar temperature/pressure conditions.

Finally, static hydrothermal experiments in cold-seal hydrothermal vessels have been carried out at a series of temperatures.

In general, all the solids that remained in the reaction products develop a scale on the surface, the extent of which depends on the severity of the elevated temperature test. The samples that were recovered from the vapor phase study, in contrast to those from the CON-14 experiments, show only limited scaling. Samples immersed in Well J-13 water exhibited extensive scaling. The SEM/EDX characterization of the scale shows that it is a mat consisting of very fine needle crystals. The chemical composition of the scale is dominantly a calcium silicate with subordinate amounts of potassium and aluminum. Sulfur can only be recognized in those portions of the sample with very thin coating, which suggests that the sulfur contribution is from the bulk sample beneath. No calcium sulfate phases were noted. The XRD studies of these separate scales are in progress.

Both sets of powders from the rocking autoclave studies were also coated with a similar white scale; in some instances the scale appeared to act as a cement binding the powders into a ridged mass. The scales that were observed in these experiments appear to have developed at-temperature and not as a result of a thermal quench associated with sampling of the vessel. This statement is supported principally from the rocking autoclave studies, where the solid charge was contained in a stainless steel mesh during the course of the experiment. The scale developed uniformly throughout the solid charge, as would be anticipated for an at-temperature reaction. Further, in the disk experiments, no scaling was noted on the interior of the pressure vessels, as would be the case if quench precipitation was the observed phenomenon.

Partial chemical analyses for the aqueous phase in contact with the cementitious material are completed. Table XIII is a list of the carbon analyses for the first rocking autoclave experiment and a partial listing of the replicate run; it also provides values for the initial Well J-13 water in which replicate samples showed a 15% variation. The rocking autoclave samples were all sampled at-temperature and stabilized until testing by storage at ~6°C. The fourth set of results is from the first week of immersed hydrothermal treatment. Sample P1 represents a sample recovered at-temperature, and P2 represents the room-temperature-solution data. Major differences are apparent: first, the total carbon and total organic carbon content are nearly 14 times larger than those of any rocking autoclave

TABLE XIII

CARBON ANALYSES FOR 8222/TUFF ACCELERATED EXPERIMENTS

Rocking Autoclave

Run #1

Sample		Experimental Duration (hour)	Total Carbon (ppm)	Total Organic Carbon (ppm)	Carbonate Carbon (by difference) (ppm)
8230	1	.5	66.4	45.7	20.7
	2	1	65.0	48.9	16.1
	4	4	67.5	56.7	10.8
	5	16	72.4	56.3	16.1
	6	26	69.4	52.7	16.7
	8	62	82.9	63.6	19.3
	9	138	insufficient sample (<0.2 cc)		
	10[a]	258	105.8	79.2	26.6
	11[b]	258	82.5	69.3	13.2

[a] 5 to 10% higher; insufficient sample for accurate determination.

[b] Sample 10 collected at-temperature; sample 11 collected at room temperature.

Run #2

Sample		Experimental Duration (hour)	Total Carbon (ppm)	Total Organic Carbon (ppm)	Carbonate Carbon (by difference) (ppm)
8222-2	1	1	60.9	49.0	11.9
	2	2	39.8	26.4	13.4
	3	4	57.1	39.3	17.8
	4	8	53.6	31.9	21.7
	5	22	55.9	35.7	20.2
	6	57	59.4	43.1	16.3
	12	—	48.7	14.3	34.4
	13	—	63.7	20.9	42.8

Parr Vessel Agitated

P1	168	851.3	684.5	166.8
P2	168	152.6	122.6	30.0

samples, and second, there appears to be a significant removal of carbonate from solution during the quenching process. Two possible sources for the high carbon content are (1) appreciable contamination of the vessel during preparation for the experiment (although only acetone was used to rinse the interior) and (2) the teflon main seal of the Parr vessel. Nevertheless, as expected, the carbonate is higher at elevated temperature than at room temperature.

Table XIV details the recorded pH values from the rocking autoclave and Parr vessel studies. Of particular interest are the relatively high pH values of 6.5 observed here in contrast to the 4.5 values recorded for the CON-14 concrete.

XII. EXPLORATORY SHAFT

A. Design (D. C. Nelson and D. A. York)

Two ES Project Status Meetings were held at DOE/NTSSO during the report period. At the meeting on August 4, 1983, the Title II design status of the ES surface and subsurface facilities was discussed. The back-up power for the Integrated Data System (IDS), the status of items being procured, the schedule, and quality assurance (QA) were also dicusssed. At the meeting on September 15, 1983, it was stated that the Title II design was essentially completed and approved by Los Alamos. The DOE has approved some, but not all, of the design. There are several items that were not included in the Title II design because of incomplete criteria. Those items include the downhole power system, the downhole instrumentation system, and the final layout of the underground openings. Complete criteria for these items are not expected until after the ESTP has been reviewed. All future changes to the approved portion of the design will be handled as revisions.

The status meeting held on September 15, 1983, was the last scheduled monthly status meeting. Until further notice, such meetings will only be held on an as-needed basis.

Except for pressure testing of the water line up to the NTS boundary, all construction activity has ceased.

Procurement of the long-lead items has continued; many of these items have been received and are in storage. However, the two refurbished hoists, the head frame, and the shaft conveyances will not be delivered during this report period.

TABLE XIV

THE pH VALUES FOR 8222/TUFF ROCKING AUTOCLAVE ACCELERATED EXPERIMENTS

Sample		Experimental Duration (hour)	pH
		Run #1	
8230	1	0.5	8.80
	2	1	9.10
	4	4	9.13
	5	16	8.94
	6	26	9.03
	8	62	9.11
	9	138	8.89
	10	258	8.86
	11	258	8.86
		Run #2	
8222	1	1	8.79
	2	2	8.80
	3	4	8.74
	4	8	8.48
	5	22	8.68
	6	57	8.68
	8	143	8.58
	9	276	8.49
	10	505	8.65
	11	985	6.8
	12	985	6.95

A Title II design package was compiled, printed, and delivered to DOE/NV. This package represents the status of design as of August 5, 1983, and contains all the Title II drawings and specifications (approved or not approved), all past design criteria letters, the minutes of all past ES Project Status Meetings, and a cost estimate.

It now appears that shaft construction will not start before the spring or summer of 1985, based on an assumed Presidential site recommendation in January 1985. Following the recommendation, time will be required for site preparation and contractor mobilization.

B. Test Plan (C. W. Myers and J. C. Rowley)

The ESTP activity continued at a very high level this quarter. About 75% of the final draft of the ESTP was prepared. However, delivery of some of the individual test plans was slower than planned. A sufficiently complete "working draft" of the ESTP was prepared and reproduced for the ESTP Committee meeting September 22-23, 1983. The Committee proposed major revisions for the summary, introduction, rationale, and other sections of the ESTP. As a result, it was apparent at the end of the quarter that the September 30, 1983, delivery of a complete draft to WMPO could not be met. A revised schedule was proposed, as follows:

(1)	Committee members deliver outstanding items to C. W. Myers.	10/11/83
(2)	Committee meeting. Working session to review and revise draft based on 10/11/83 input.	10/20-21/83
(3)	Committee meeting. Final review and wrap-up for delivery of ESTP to WMPO and TPOs.	11/17-18/83
(4)	Delivery draft to WMPO and TPOs.	11/23/83
(5)	Presentation of ESTP at TPO meeting (1/2 day minimum).	11/30-12/1/83

Meeting this schedule is contingent upon receipt of drafts as indicated. D. Vieth was asked to request that TPOs support ESTP Committee members and minimize non-ESTP assignments during the comming weeks. A decision was made to prepare cost and schedule estimates for individual test plans on a uniform basis.

Several technical issues of concern to the planning and implementation of the ESTP were considered, discussed, and reviewed by the Committee:

(1) The Committee discussed the potential contamination of the ES site by drilling fluids. A quantitative assessment of the effects of fluids on ES tests was begun and is due for completion in November 1983.

(2) C. Garvin, SAI, visited all the ESTP participant organizations in August. A detailed review and update were performed; many contributions were made to the ESTP scheduling network during these visits and at the ESTP Committee meetings held during the quarter.

(3) The issue of the depth, nature, and purpose for the penetration of the ES into the Calico Hills below the Topopah Spring Member was reviewed. The potential for lessened groundwater travel time was the predominant concern. Testing of the Calico Hills is primarily aimed at the very important evaluation of characteristics of the hydrology and zeolitization of the Calico Hills and the nature of the contact with the Topopah Spring Member. Revisions were made to the tests to be conducted from the ES in the Calico Hills to minimize the required penetration depth. This subject will be further reviewed when the performance assessment aspects and trade-offs are analyzed.

4) The problems of "dry" drilling and coring in the installation, test, instrumentation, and site exploration activities required of the individual test plans remain unresolved. A proposal to conduct a development drilling/coring program to provide techniques for the ES needs is still under review and revision.

C. IDS (C. W. Myers and J. C. Rowley)

Instrumentation requirements and needs were included in the IDS as the draft test plans evolved. At present, only a data acquisition system is planned. The IDS equipment prototype laboratory has been set up and initial tests of the typical sensors and equipment have commenced.

XIII. QUALITY ASSURANCE (R. R. Geoffrion)

A. Los Alamos

The QA staff reviewed comments on the SCP.

A records survey of NNWSI records was made by J. A. Beaton. He estimated 10 000 documents on hand and a growth rate of 2000 documents per year. The QA staff reviewed and wrote comments for the "NNWSI Records Management Study." A draft for handling NNWSI records was prepared and circulated for comment.

R. D. Michels observed shaft sinking techniques at a mine near Prescott, Arizona.

An archive was established for the volcanism study basalt rock samples. The samples were catalogued and placed in permanent storage.

The Test Plan for the Integrated Data System was reviewed, and comments were prepared.

The QA review was completed for 42 Title II drawings and 12 specifications for the ES. Revised QA requirements for the ES were prepared. Comments were written on QA manuals from REECo and Holmes and Narver. Five test plans prepared by R. Scott of USGS for the ES were reviewed, and comments were written.

A. H. Davis met with Pennsylvania State University personnel to discuss QA requirements for work being performed on the geochemistry of shaft and borehole sealing materials contract.

The NRC Technical Position Paper on Design Information Requirements was reviewed, and comments were prepared.

J. A. Beaton toured the Records Center at GA Technologies in San Diego, California.

R. D. Michels attended a computer software QA seminar in San Diego, and R. R. Geoffrion attended a software QA meeting sponsored by DOE/AL in Albuquerque.

R. D. Michels met with Hewlett-Packard personnel in Denver to discuss QA requirements for the IDS for the ES.

R. R. Geoffrion attended the American Society for Quality Control in San Diego and served on a committee preparing a QA handbook for research and development.

B. USGS

Two audits were performed at Fluke Manufacturing, Inc. and the Colorado Department of Agriculture to qualify calibration services supplied to the USGS.

Opening and closing meetings for the DOE Salt Investigations audit were attended by P. L. Bussolini and F. L. Kerstiens, who represented the USGS.

QA indoctrination and training session was given to J. Willmon of the USGS Denver Office. In a planning session with P. L. Bussolini and R. R. Geoffrion, work for USGS QA activities for the next 6 months was laid out.

Five USGS ESTPs were reviewed and comments were prepared.

Surveillance activities were performed and documented for the insertion of heat dissipation probes and psychrometers at UZ-1.

R. D. Michels toured the Yucca Mountain site with R. Scott of the USGS.

F. L. Kerstiens attended a National Bureau of Standards symposium on calibration in Boulder, Colorado.

ACKNOWLEDGMENTS

The following Los Alamos National Laboratory personnel are acknowledged for their efforts: P. A. Elder, M. E. Lark, and S. Lermuseaux (sample counting and gamma-spectra analyses); and L. M. Mitchell (typing of manuscript).

REFERENCES

1. Hans C. Claassen, "Water Quality and Physical Characteristics of Nevada Test Site Water - Supply Wells," USGS-474-158 (1973).

2. A. E. Ogard, K. Wolfsberg, and D. T. Vaniman, Comps., "Research and Development Related to the Nevada Nuclear Waste Storage Investigations, April 1--June 30, 1983," Los Alamos National Laboratory report LA-9846-PR (December 1983).

3. W. R. Daniels, K. Wolfsberg, R. S. Rundberg, A. E. Ogard, J. F. Kerrisk, C. J. Duffy, et al., "Summary Report on the Geochemistry of Yucca Mountain and Environs," Los Alamos National Laboratory report LA-9328-MS (December 1982).

4. A. E. Ogard, W. R. Daniels, and D. T. Vaniman, Comps., "Research and Development Related to the Nevada Nuclear Waste Storage Investigations, October-December, 1982," Los Alamos National Laboratory report LA-9666-PR (May 1983).

5. K. Wolfsberg, D. T. Vaniman, and A. E. Ogard, Comps., "Research and Development Related to the Nevada Nuclear Waste Storage Investigations, January-March, 1983," Los Alamos National Laboratory report LA-9793-PR (June 1983).

6. W. R. Daniels, B. R. Erdal, and D. T. Vaniman, Comps., "Research and Development Related to the Nevada Nuclear Waste Storage Investigations, July-September, 1982," Los Alamos National Laboratory LA-9577-PR (March 1983).

7. G. Bidoglio, "Characterization of Am(III) Complexes with Bicarbonate and Carbonate at Groundwater Concentration Levels," Radiochem. Radioanal. Lett. 53, 45-60 (1982).

8. R. Lundqvist, "Hydrophilic Complexes of the Actinides, I. Carbonates of Trivalent Americium and Europium," Acta Chem. Scand. A36, 741-750 (1982).

9. M. Shiloh, M. Givon, and Y. Marcus, "A Spectrophotometric Study of Trivalent Actinide Complexes in Solution - III Americium with Bromide, Iodide, Nitrate and Carbonate Ligands," Jour. of Inorg. Nucl. Chem. 31, 1807-1814 (1969).

10. W. W. Schulz, "The Chemistry of Americium," Technical Information Center, Energy Research and Development Administration report TID-2671 (October 1976).

11. N. Edelstein, J. Bucher, R. Silva, and H. Nitsche, "Thermodynamic Properties of Chemical Species in Nuclear Waste," Lawrence Berkeley Laboratory report LBL-14325 (January 1983).

12. D. Rai, G. Strickert, D. A. Moore, and R. J. Serne, "Influence of an Americium Solid Phase on Americium Concentrations in Solution," Geochem. Cosmochem. Acta 45, 2257-2265 (1981).

13. P. L. Chambre, S. J. Zavoshy, and T. H. Pigford, "Solubility-Limited Fractional Dissolution Rate of Vitrified Waste in Groundwater," Trans. Am. Nucl. Soc. 43, 111-112 (1982).

14. C. Keller and D. Fang, "Uber Karbonatokomplexe des dreiwertigen Americiums sowie des vier- und sechswertigen Urans und Plutoniums," Radiochim. Acta 11, 123-127 (1969).

15. J. I. Kim, Ch. Lierse, and F. Baumgartner, "Complexation of the Plutonium(IV) Ion in Carbonate-Bicarbonate Solutions," in Plutonium Chemistry, W. T. Carnall and G. R. Choppin, Eds., ACS Symposium Series No. 216. (American Chemical Society, Washington, DC, 1983), pp. 317-334.

16. D. Rai and J. L. Swanson, "Properties of Plutonium(IV) Polymer of Environmental Importance," Nucl. Technol. 54, 107-112 (1981).

17. D. S. Coombs and J. T. Whetten, "Composition of Analcime from Sedimentry and Burial Metamorphic Rocks," Geol. Soc. Amer. Bull. 78, 269-282 (1967).

18. G. K. Johnson, H. E. Flotow, P. A. G. O'Hare, and W. S. Wise, "Thermodynamic Studies of Zeolites: Analcime and Dehydrated Analcime," Am. Mineral. 67, 736-748 (1982).

19. J. J. Hemley, unpublished data, cited in Ref. 2.

20. H. C. Helgeson, J. M. Delany, H. W. Nesbitt, and D. K. Bird, "Summary and Critique of the Thermodynamic Properties of Rock Forming Minerals," Am. J. Sci. 278-A, 229 (1978).

21. J. V. Walther and H. C. Helgeson, "Calculation of the Thermodynamic Properties of Aqueous Silica and the Solubility of Quartz and its Polymorphs at High Pressures and Temperatures," Am. J. Sci. 277, 1315-1351 (1977).

22. H. C. Helgeson and D. H. Kirkham, "Theoretical Prediction of the Thermodynamic Behavior of Aqueous Electrolytes at High Pressures and Temperatures, I. Summary of the Thermodynamic/electrostatic Properties of the Solvent," Am. J. Sci. 274, 1089-1198 (1974).

23. A. Iijima and M. Utada, "Present Day Zeolitic Diagensis of the Neogene Geosynclinal Deposits in the Niigata Oil Field, Japan," Am. Chem. Soc. Adv. in Chem. Series 101, Molecular Sieve Zeolites-1, 342-349 (1971).

24 A. Iijima and R. L. Hay, "Analcime Composition in Tuffs of the Green River Formation of Wyoming," Am. Mineral. 53, 184-201 (1968).

25. B. J. Travis, "TRACR3D: A Model of Flow and Transport in Porous/Fractured Media," Los Alamos National Laboratory report LA-9667-MS (May 1984).

26. B. J. Travis, "WAFE: A Model for Two-Phase, Multicomponent Mass and Heat Transport in Porous, Sorptive Media," Los Alamos National Laboratory report (in preparation).

27. H. E. Nuttall and A. K. Ray, "A Combined Fracture-Porous Media Model for Contaminant Transport of Radioactive Ions," in Scientific Basis for Nuclear Waste Management, Vol. 3 (Plenum Press, New York, 1980), pp. 577-590.

28. H. E. Nuttall and A. K. Ray, "A Combined Fracture-Porous Media Model for Contaminant Transport," J. Energy 5, 376-380 (1981).

29. D. H. Tang, E. O. Frind, and E. A. Sudicky, "Contaminant Transport in Fractured Porous Media: Analytical Solution for a Single Fracture," Water Resour. Res. 17 No. 3, 555-564 (1981).

30. E. A. Sudicky and E. O. Frind, "Contaminant Transport in Fractured Porous Media: Analytical Solutions for a System of Parallel Fractures," Water Resour. Res. 18 No. 6., 1634-1642 (1982).

31. B. J. Travis et al., "Preliminary Estimates of Water Flow and Radionuclide Transport in Yucca Mountain," Los Alamos National Laboratory report (in preparation).

32. R. Waddell, from minutes of NNWSI Performance Assessment Working Group Meeting, April 21-22, 1983.

33. F. A. Caporuscio, D. T. Vaniman, D. L. Bish, D. E. Broxton, B. H. Arney, G. H. Heiken, et al., "Petrologic Studies of Drill Core USW-G2 and UE25b-1H, Yucca Mountain, Nevada," Los Alamos National Laboratory report LA-9255-MS (July 1982).

34. S. S. Levy, "Petrology of Samples from Drill Holes USW-H3, H4, and H5, Yucca Mountain, Nevada," Los Alamos National Laboratory report LA-9706-MS (July 1984).

35. D. Vaniman, D. Bish, D. Broxton, F. Byers, G. Heiken, B. Carlos, E. Semarge, F. Caporuscio, and R. Gooley, "Variations in Authegenic Mineralogy and Sorption Zeolite Abundance at Yucca Mountain, Nevada, Based on Studies of Drill Cores USW GU-3 and G-3," Los Alamos National Laboratory report LA-9707-MS (June 1984).

36. R. B. Scott, R. W. Spengler, S. Diehl, A. R. Lappin, and M. P. Chornack, "Geologic Character of Tuffs in the Unsaturated Zone at Yucca Mountain, Southern Nevada," in Role of the Unsaturated Zone in Radioactive and Hazardous Waste Disposal, J. W. Mercer, P. S. C. Rao, and I. W. Marine, Eds. (Ann Arbor, Ann Arbor Science Publishers, 1983), pp. 289-335.

37. E. B. Ekren, C. L. Rogers, R. E. Anderson, and P. P. Orkild, "Age of Basin and Range Normal Faults in Nevada Test Site and Nellis Air Force Range, Nevada," Geol. Soc. Am. Mem. 110, 247-250 (1968).

38. W. C. Swadley and D. L. Hoover, "Geology of Faults Exposed in Trenches in Crater Flat, Nye County, Nevada," US Geol. Surv. Open-File report 83-608 (1983).

39. B. J. Szabo, W. J. Carr, and W. C. Gottschall, "Uranium-Thorium Dating of Quaternary Carbonate Accumulations in the Nevada Test Site Region, Southern Nevada," US Geol. Surv. Open-File report 81-119 (1981).

40. R. W. Kistler, "Potassium-Argon Ages of Volcanic Rocks in Nye and Esmeralda Counties, Nevada," Geol. Soc. Am. Mem. 110, 251-262 (1968).

41. "Report of Sub-surface Directional Survey, ISW G-4, Nevada Test Site, Nevada," Eastman Whipstock Job number P1182-G-1208 (November 7, 1982).

42. R. W. Spengler and D. C. Muller, "Preliminary Geologic and Geophysical Data Derived from USW-G4, Yucca Mountain, Nevada," US Geol. Surv. administrative report (April 1983).

43. A. R. Lappin, R. G. VanBuskirk, D. O. Enniss, S. W. Butters, F. M. Prater, C. B. Muller, and J. L. Bergosh, "Thermal Conductivity, Bulk Properties, and Thermal Stratigraphy of Silicic Tuffs From the Upper Portion of Hole USW-G1, Yucca Muntain, Nye County, Nevada," Sandia National Laboratories report SAND81-1873 (March 1982).

44. D. L. Hoover, "Genesis of Zeolites, Nevada Test Site," Geol. Soc. Am. Mem. 110, 275-284 (1968).

45. B. M. Crowe, D. T. Vaniman, and W. J. Carr, "Status of Volcanic Hazard Studies for the Nevada Nuclear Waste Storage Investigations," Los Alamos National Laboratory report LA-9325-MS (March 1983).

46. B. M Crowe, R. Amos, F. Perry, S. Self, and D. T. Vaniman, "Aspects of Possible Magmatic Disruption of a High-Level Radioactive Waste Repository in Southern Nevada," Los Alamos National Laboratory report LA-9326-MS (October 1982).

47. D. T. Vaniman, B. M. Crowe, and E. S. Gladney, "Petrology and Geochemistry of Hawaiite Lavas from Crater Flat, Nevada," Contrib. Mineral. Petrol. 80, 341-357 (1982).

48. H. S. Yoder, Jr., and F. Chayes, "Alkali Correlation in Some Alkali Basalts," in Carnegie Institution Annual Report of the Director, Yearbook No. 81 (1982), pp. 309-314.

49. A. Zindler, E. Jagoutz, and S. Goldstein, "Nd, Sr, and Pb Isotopic Systematics in a Three-Component Mantle: A New Perspective," Nature 298 No. 5A, 519-523 (1982).

50. B. M. Crowe and W. J. Carr, "Preliminary Assessment of the Risk of Volcanism at a Proposed Nuclear Waste Repository in the Southern Great Basin," US Geologic Survey Open File report 80-357 (1980).

☆U.S. GOVERNMENT PRINTING OFFICE:1984—776-026 / 4131

Printed in the United States of America
Available from
National Technical Information Service
US Department of Commerce
5285 Port Royal Road
Springfield, VA 22161

Microfiche (A01)

Page Range	NTIS Price Code
001-025	A02
026-050	A03
051-075	A04
076-100	A05
101-125	A06
126-150	A07
151-175	A08
176-200	A09
201-225	A10
226-250	A11
251-275	A12
276-300	A13
301-325	A14
326-350	A15
351-375	A16
376-400	A17
401-425	A18
426-450	A19
451-475	A20
476-500	A21
501-525	A22
526-550	A23
551-575	A24
576-600	A25
601-up*	A99

*Contact NTIS for a price quote.

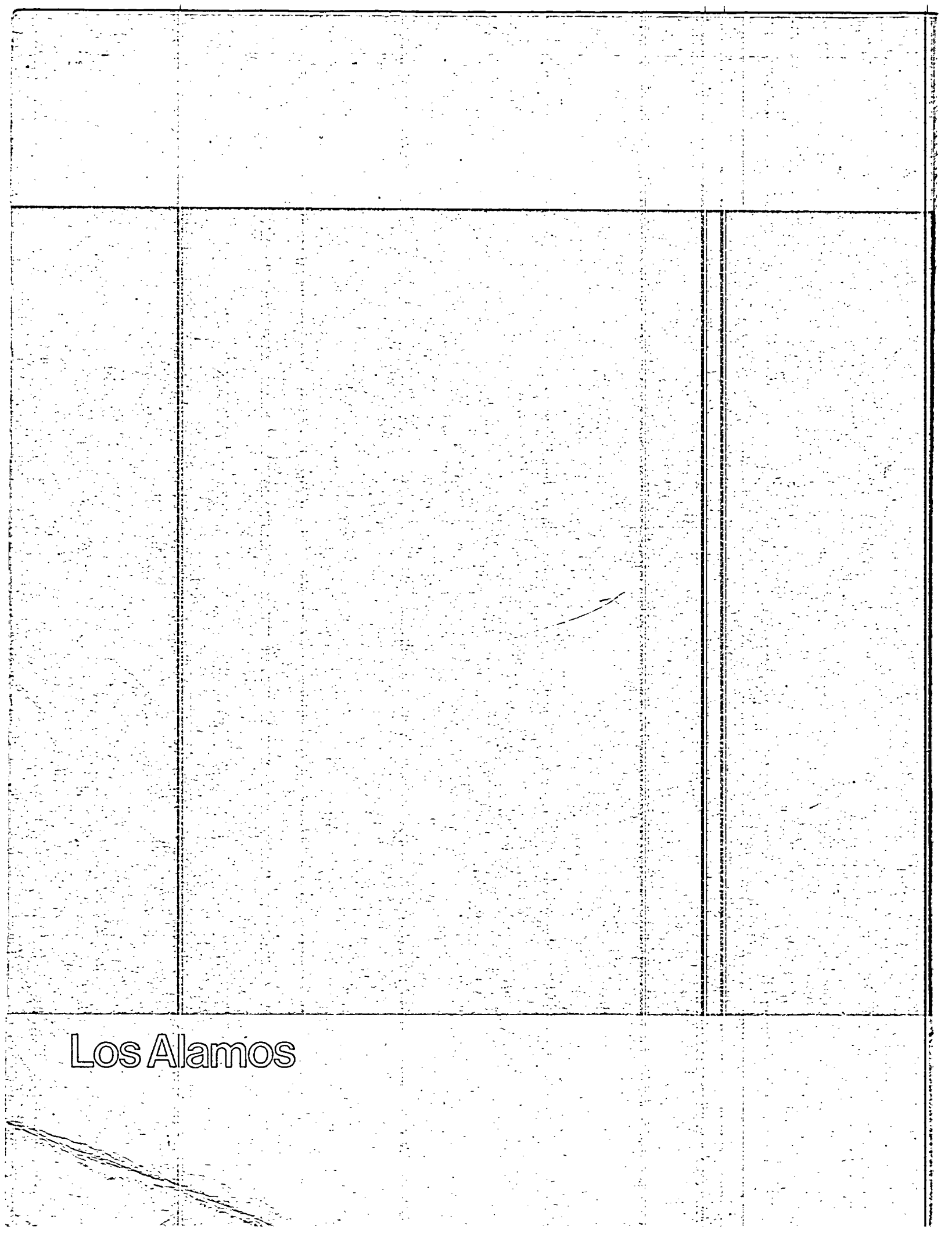
Los Alamos